Feasibility Study for Rapid Evaluation of Bridge Decks

Final Report

Prepared by:

Dr. Paul Ziehl
Professor, Civil and Environmental Engineering
University of South Carolina

Dr. Nathan Huynh
Associate Professor, Civil and Environmental Engineering
University of South Carolina

Rafal Anay
Research Assistant, Civil and Environmental Engineering
University of South Carolina

Rawya Abduljabbar
Research Assistant, Civil and Environmental Engineering
University of South Carolina

Bhavya Padmanabhan
Research Assistant, Civil and Environmental Engineering
University of South Carolina

Vafa Soltangharaei
Research Assistant, Civil and Environmental Engineering
University of South Carolina

FHWA-SC-18-09

December 2018

Sponsoring Agencies:

South Carolina Department of Transportation
Office of Materials and Research
1406 Shop Road
Columbia, SC 29201

Federal Highway Administration
South Carolina Division
Strom Thurmond Federal Building
1835 Assembly Street, Suite 1270
Columbia, SC 29201

Technical Report Documentation Page

1. Report No FHWA-SC-18-09	2. Government Accession No.	3. Recipient's Catalog No.	
4. Title and Subtitle Feasibility Study for Rapid Evaluation of Bridge Decks		5. Report Date December 2018 6. Performing Organization Code	
7. Author/s Dr. Paul Ziehl, Dr. Nathan Huynh, Rafal Anay, Rawya Abduljabbar, Bhavya Padmanabhan, and Vafa Soltangharaei		8. Performing Organization Report No.	
9. Performing Organization Name and Address University of South Carolina Dept. of Civil and Environmental Engineering 300 Main Street, Columbia, SC 29208		10. Work Unit No. (TRAIS) 11. Contract or Grant No. SPR No. 724	
12. Sponsoring Organization Name and Address South Carolina Department of Transportation Office of Materials and Research 1406 Shop Road Columbia, SC 29201		13. Type of Report and Period Covered Final Report 14. Sponsoring Agency Code	
15. Supplementary Notes			

16. Abstract

The South Carolina Department of Transportation utilizes different methods for concrete bridge deck evaluation including visual inspection and chain dragging. The current methods for concrete bridge deck evaluation are effective, but they require traffic control and many operators. To address these limitations, this project investigates rapid evaluation methods including vehicle mounted scanning (utilizing ground penetrating radar, infrared sensing, and high definition video scanning), pole mounted scanning (utilizing ultra-time domain infrared sensing), and deck acoustic response to identify which method, or combination of methods, is well suited for the evaluation of concrete bridge decks in South Carolina. Four in-service bridge decks with differing damage levels were selected to serve as testbeds. Chloride sampling, chain dragging, and coring were performed to verify results. In addition, bridge deck specimens (removed from a bridge in South Carolina) were investigated in a laboratory and sensors were embedded in a newly constructed concrete bridge deck. Among the methods, deck acoustic response was found to be the most suitable for detection of delamination, with infrared and ultra-time domain imaging also providing good results. Ground penetrating radar was less effective for detection of delamination but showed promise for detection of chlorides and moisture intrusion. Benefit-cost analysis was performed to better understand the potential for implementation. Recommendations for implementation are provided for both local evaluation and asset management of concrete bridge decks in South Carolina.

17. Key Words	18. Distribution Statement		
	No restrictions. This document is available to the public through the National Technical Information Service, Springfield, VA 22161.		
19. Security Classification (of this report) Unclassified	20. Security Classification (of this page) Unclassified	21. No. Of Pages 107	22. Price $5.04

Form DOT F 1700.7 (8-72) Reproduction of form and completed page is authorized

DISCLAIMER

The contents of this report reflect the views of the authors who are responsible for the facts and the accuracy of the data presented herein. The contents do not necessarily reflect the official views or policies of the South Carolina Department of Transportation or the Federal Highway Administration. This report does not constitute a standard, specification, or regulation.

The State of South Carolina and the United States Government do not endorse products or manufacturers. Trade or manufacturer's names appear herein solely because they are considered essential to the object of this report.

ACKNOWLEDGMENTS

The authors wish to acknowledge the co-Chairs of the Steering Committee, Lee Floyd and David Rister, and all members of the committee: Mark Hunter, Chad Hawkins, Caleb Gunter, Aly Hussein, Jim McCabe, Jason Thompson, and Ken Johnson (FHWA), as well as Merrill Zwanka, Terry Swygert, Judy Hundley, and Meredith Heaps.

We would also like to acknowledge the support of Wil Pointer who was instrumental to the field evaluation portion of the project, and Russell Inglett and the technical staff at the University of South Carolina Structures and Materials Laboratory.

EXECUTIVE SUMMARY

Degradation of concrete bridge decks is an ongoing challenge facing the South Carolina Department of Transportation (SCDOT). When a bridge deck exhibits a significant percentage of degraded area decisions must be made regarding approaches to repair of the degraded areas, hydro-blasting with subsequent partial depth overlay, or replacement of the entire deck. To aid in decision making, different methods for bridge deck evaluation have been employed by the South Carolina Department of Transportation including visual inspection, chain dragging, and chloride sampling. While these methods are informative, they have the drawback of requiring traffic control, thereby increasing the cost of the evaluation and decreasing safety of the workers during the evaluation.

The ideal bridge deck evaluation method would provide information that is as informative (or more informative) as the current methods used by SCDOT and does not require traffic control. The motivation for this project is to identify the availability of such methods and to assess the associated reliability of interpretation. Many approaches to this issue have recently become commercially available and others are under development. These approaches vary in terms of traffic control requirements, cost, and fidelity of the results. Among the different approaches are a) vehicle mounted scanning (commonly utilizing ground penetrating radar, infrared sensing, and high definition video scanning); b) pole mounted scanning (utilizing ultra-time domain infrared sensing and high definition video scanning); and c) acoustic response enabled by a trailed device, referred to here as deck acoustic response (utilizing trailed impactors in combination with acoustic detectors).

To assess the feasibility of different evaluation methods for South Carolina bridge decks, in-service decks with differing damage levels were selected to serve as testbeds. Chloride sampling, chain dragging, and coring were performed in addition to the more rapid evaluation methods to enable assessment of the results. Bridge deck specimens (removed from a bridge in South Carolina) were also investigated under an accelerated aging protocol in the laboratory. Instrumentation was added to a new bridge deck during construction to aid in assessment of conditions potentially related to early degradation.

One finding of the research is that the methods investigated did not provide a clear and definitive means for interpretation. Rather, contour plots were provided by the service providers that were generally representative of differing parameters (for example, permittivity in the case of ground penetrating radar). Therefore, interpretation of the contour plots is generally required on the part of the decision maker. With consideration to this potential complication, it was found that many of the rapid evaluation methods can offer levels of accuracy in a similar range to existing evaluation methods. Furthermore, vehicle mounted scanning is amenable to evaluation on a widespread basis (asset management). The benefits and costs of different approaches to rapid evaluation are discussed and recommendations for implementation are provided.

Contents

LIST OF FIGURES

LIST OF TABLES

LIST OF APPENDICES

LIST OF ABBREVIATIONS

AADT	Annual Average Daily Traffic
BDI	Bridge Diagnostics Inc.
Cl-	Chloride Ion Concentration
DAR	Deck Acoustic Response
DOT	Department of Transportation
E_{corr}	Corrosion Potential
FHWA	Federal Highway Administration
GPR	Ground Penetrating Radar
HCP	Half Cell Potential
HDV	High Definition Video
HRV	High Resolution Video
IE	Impact Echo
IR	Infrared
IR-UTD	Infrared-Ultra Time Domain
LCC	Life Cycle Cost
LPR	Linear Polarization Resistance
NDE	Nondestructive Evaluation
NPV	Net Present Value
OCP	Open Circuit Potential
PUNDIT	Portable Ultrasonic Nondestructive Indication Tester
UPV	Ultrasonic Pulse Velocity
VTI	Virginia Technologies Inc.

CHAPTER 1: INTRODUCTION

The deterioration of concrete bridge decks presents a maintenance challenge for most transportation agencies and bridge owners. Different evaluation methods such as visual inspection, half-cell potential, chain dragging, and chloride sampling have been utilized in damage evaluation for bridge decks. These methods require traffic control and many operators; therefore, they are generally time consuming and costly. Rapid evaluation methods such as ground penetrating radar (GPR) and infrared (IR) imaging are developing for the evaluation of damage in bridge decks. These methods generally do not require traffic control and can be performed by one or two operators.

Delamination is one of the primary causes for concern in concrete bridge decks as this can lead to spalling and corrosion of the reinforcement. The mechanism for delamination is complex, but two main causes have been identified:

- Bleed water (upward flow of mixing water) and bleed air trapped below the prematurely closed (densified) mortar surface. Delaminations form when finishing the surface before bleeding has occurred (NRMCA, 2004).
- Corrosion of steel reinforcement may initiate delamination due to expansive corrosion products on the upper layer of reinforcing steel, breaking the bond between the steel and the surrounding concrete (NRMCA, 2004).

Depending on the deterioration mechanism of interest (e.g., delamination and corrosion), one technology may be more suitable than another. For example, impact echo (IE) and IR are recommended to detect delamination (Robison and Tanner, 2011). Recommended methods for detecting corrosion include electrical resistivity, half-cell potential, and GPR (Robison and Tanner, 2011).

The primary objective of this study is to assess the effectiveness of rapid evaluation methods for bridge decks, thereby improving worker safety and reducing costs associated with repairs. More specifically, the goal is to identify which rapid evaluation method, or combination of methods, is best suited for the evaluation of concrete bridge decks in South Carolina. To achieve this goal, the following research tasks were performed:

- A literature review of current rapid evaluation methods applied to concrete bridge decks.
- A survey of state transportation agencies to identify current practices related to bridge deck evaluation using nondestructive evaluation methods in different state highway agencies.
- Damage evaluation of selected bridge decks using promising rapid evaluation techniques with comparisons to traditional evaluation methods.
- Evaluation of laboratory test specimens for validation.
- Evaluation of results to determine the most efficient and accurate techniques.
- Benefit-cost analysis for potential adoption of optimal rapid evaluation techniques.

Chapter 2: LITERATURE REVIEW AND SURVEY

The literature review is focused on studies that examine the use of traditional and rapid evaluation methods with an emphasis on examination of concrete bridge decks. This review is divided into three sections. Sections 2.1 and 2.2 provide a brief description of the most common damage evaluation methods and their advantages and limitations, and section 2.3 addresses comparisons between traditional and rapid evaluation techniques that have been implemented in other studies.

2.1 Traditional Evaluation Methods

Different traditional evaluation methods such as chain dragging, visual inspection, coring, permeability assessment, and chloride sampling have been used by the South Carolina Department of Transportation (SCDOT). A brief explanation of these methods is presented below:

Chain dragging is one of the most commonly used methods for detecting delamination in concrete bridge decks. This method involves moving a row of chains back and forth across a bridge deck (Robison and Tanner, 2011) and listening to the resulting sound. A clear ringing sound represents a sound deck while a dull or hollow sound represents a delaminated deck. Delaminated areas are then outlined on the deck surface. A common chain drag configuration consists of four or five segments of 1 in. link chain of 1⁄4 in. diameter steel approximately 18 in. (45.7 cm) long, (ASTM D4580, 2012). The advantages of this method are simplicity and direct interpretation of results. In addition, it does not require costly instrumentation and highly-trained operators. However, it is limited to surface damage detection and traffic control is required. Operator experience can play a significant role and damage identification is subjective (Graybeal et al., 2011; Gucunski et al., 2005; Parrillo et al., 2006; Huston et al. 2007).

Visual inspection is an essential task performed at the beginning of the structural evaluation process to identify surface distress types such as cracks, spalling, scaling, efflorescence, rust on stay-in-place forms, and concrete discoloration. This method does not require specialized equipment or traffic disruption (Sketchley, 2014). It is subjective and depends on the experience of the inspector (Moore et al. 2001) and is limited to surface or near-surface damage.

Chloride concentration testing is a common method for evaluation of damage in reinforced concrete structures in relation to corrosion. This method involves taking concrete powder samples from specific structure depths to measure chloride concentrations (Montgomery, 2014). The procedure is simple. However, traffic control is needed and the method is time consuming. Moreover, the procedure only addresses chloride content of the concrete and does not directly assess damage. The sampling locations are often randomly selected and may not represent the condition of the entire bridge deck.

Half-cell potential (HCP) is the measurement of electrical potential in the reinforcement that provides an indicator of the level of corrosion (ASTM C876, 2017). The HCP measurement system includes (Jaquez, 2013):

- A half-cell which consists of a copper rod immersed in a saturated solution of copper sulfate dissolved in distilled water. The rod is placed in a rigid container made from a dielectric material which does not react with the copper or the solution.

- An electrical junction device, which consists of a sponge wetted with a contact solution to provide low electrical continuity between the concrete surface and the half cell.
- A voltmeter, which is a small, battery operated device with ± 3% accuracy at the voltage range and a potential of less than 0.02 Volts. The reinforcing bar is connected to the positive terminal of the voltmeter, and the negative terminal is connected to the reference electrode.

According to ASTM C876 (2017), **Table 2.1** presents the likelihood of corrosion activity based on the electrical potential measurement.

Table 2.1: ASTM corrosion ranges for Cu-CuSO4 reference electrode (ASTM C876, 2017)

Potential Against Cu-CuSO4 Electrode	Corrosion Condition
> – 200 mV	Low Risk (10% probability of corrosion)
– 200 to – 350 mV	Intermediate corrosion risk
< – 350 mV	High corrosion risk (90% probability)
< – 500 mV	Severe corrosion damage

This method is simple to apply and does not require complicated instrumentation. It is invasive as it requires a direct connection with the steel for reliable measurements. It provides only an estimate for the probability of corrosion at local positions. In addition, traffic control is generally required.

Coring is an important method for evaluating the condition of concrete structures (NYDOT, 1992). This method involves taking cores from different locations and performing laboratory tests such as carbonation, compression, air content, permeability, petrographic examination, and chloride determination. Visual analysis is sufficient for most cores, especially if distress is clearly identifiable. Cores should be taken with a core drill using thin-walled, diamond-bit core barrels.

Coring can be considered as a benchmark for other methods as it represents the actual condition of concrete. The method is destructive and there is always a risk of cutting reinforcement and/or prestressing strands. It is also time-consuming and requires traffic control. Furthermore, coring locations are discrete and do not represent the condition of the entire bridge deck.

2.2 Rapid Evaluation Methods

In this section, rapid methods for bridge deck assessment are discussed.

Ground Penetrating Radar (GPR) is an electromagnetic reflection method used to assess deterioration and/or rebar depth in bridge decks. This method involves moving an antenna across a test surface while periodically pulsing electromagnetic waves from the antenna and measuring the return strength (ASTM D6087, 2015). Different types of antennae emit and record different ranges of frequencies. For bridge inspection, an antenna with frequency more than one GHz is recommended. If there is a change or discontinuity in the propagation medium, such as air-concrete or asphalt-concrete, the pulses are reflected to the antenna. The amplitudes of reflected waves depend on the difference between the dielectric properties of the material (Penetradar Corporation, 2017). The reflected energy is recorded as radar signals and analyzed to indicate structural

deterioration. These signals contain a record of the properties and thickness of the layers within the deck (BDI and Infrasense Inc., 2017). **Figure 2.1** shows a schematic GPR signal. The test method and equipment used for this technique is described in ASTM D6087 (2015) and is further discussed in Chapter 3.

Two parameters may serve to indicate the deterioration of bridge decks; large variations in dielectric constant and attenuation of GPR signals (loss of signal strength). The dielectric constant is a measure of density, chlorides, and moisture content. Large variations in the dielectric constant can indicate concrete degradation. For example, areas with higher chloride ion concentration levels have lower reflection amplitudes in the GPR data, indicating a higher likelihood of deterioration. Moreover, the attenuation of the signal as measured from the top rebar reflection and/or the bottom of the deck may be used as a measure of concrete delamination (BDI and Infrasense Inc., 2017).

Figure 2.2 presents examples of GPR data used for mapping rebar-depth, evidence of moisture at the rebar-level, and deterioration. The advantages of this method include versatility, portability, applicability to decks with asphalt overlays, and minimal traffic control. On the other hand, the interpretation of results may be complex.

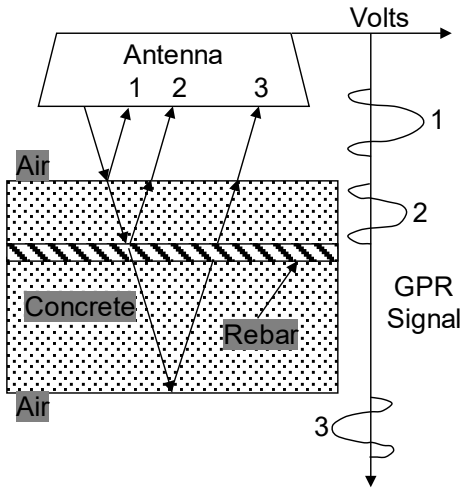

Figure 2.1: GPR signal for concrete bridge deck

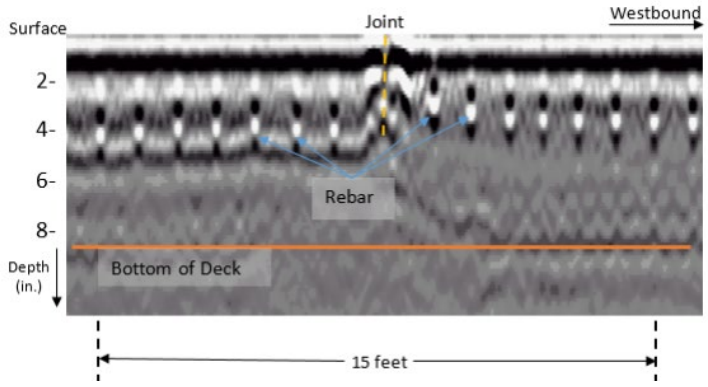

(a) Consistent rebar reflections and varying depths

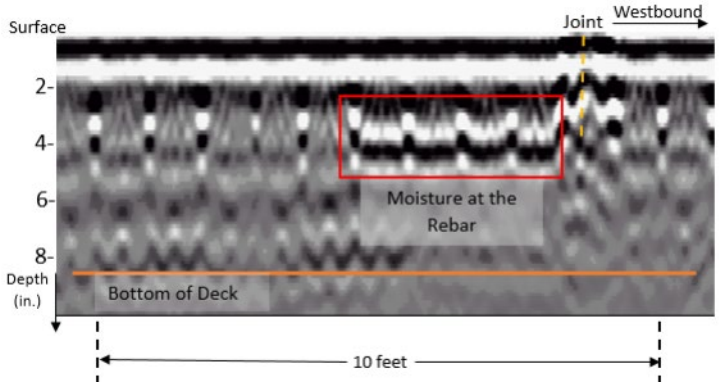

(b) Evidence of moisture at the bottom of the overlay

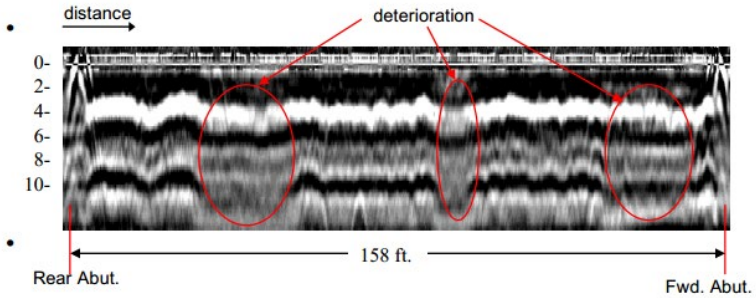

c) Bridge deterioration data

Figure 2.2: Sample of GPR data (BDI and Infrasense Inc., 2017),
(figures a, b and c reproduced with permission)

Infrared (IR) imaging is a non-contact method for detection of delamination and de-bonded areas on a bridge deck. The technique involves a high-resolution digital camera that may be held on an elevated platform attached to a truck or survey vehicle. IR is sensitive to the temperature differences between concrete layers where delamination interrupts the heat transfer through the concrete. IR thermography transforms the thermal energy emitted by objects in the infrared band of the electromagnetic spectrum into a visible image (Meola and Carlomagno, 2004). The test method and equipment used for this technique are described in ASTM D4788 (2013).

Many factors affect IR measurements such as emissivity (which depends on the amount of energy emitted from the material), moisture content, and environmental conditions. The higher the thermal conductivity coefficient and density of the concrete, the more accurate the defect detection may be (Farrag et al. 2015). This method generally does not require traffic control. On the other hand, shadows and reflections can lead to incorrect interpretations. In response to these challenges, a system based on Infrared Ultra-Time Domain (IR-UTD) has been developed. The system collects time-lapse measurements that reveal subsurface damage caused by corrosion, debonding, and other damage and is pole mounted so that thermal images may be obtained without affecting traffic (ThermalStare, LLC., 2017). This approach minimizes the impact of environmental conditions.

Impact-Echo (IE) is an acoustic method used to detect flaws and estimate the thickness of concrete structures such as bridge decks, slabs, and pavement. IE can also be used to detect areas of localized damage, crack propagation, and stiffness loss (Gassman and Tawhed, 2004). This method involves an impact source that generates stress waves which propagate through a structure and reflect discontinuities such as flaws and voids. The stress waves are detected by a transducer attached to the same surface and create a resonant condition that can be seen in the frequency content of the waveforms. Two test procedures are proposed according to ASTM C1383 (2015): procedure A measures P-wave speed and procedure B measures the frequency at which a P-wave is reflected between the parallel (opposite) surface of a plate as shown schematically in **Figure 2.3**. The P-wave speed and frequency obtained from procedures A and B are used to calculate the thickness using ASTM C1383 (2015):

$$T = \frac{0.96\ Cp}{2f} \tag{2.1}$$

where T is slab thickness; C_p is P-wave speed, and f is frequency of the p-wave thickness mode of the plate obtained from the amplitude spectrum (Hz).

If the deck is in good condition, the input wave is reflected from the bottom of the concrete deck at a low frequency, while in a flawed area (cracks, voids, and delamination) the energy is reflected from the concrete-air interface. Therefore, the amplitude spectrum will show many frequency peaks corresponding to the frequencies from de-bonded areas (Sneed et al., 2014).

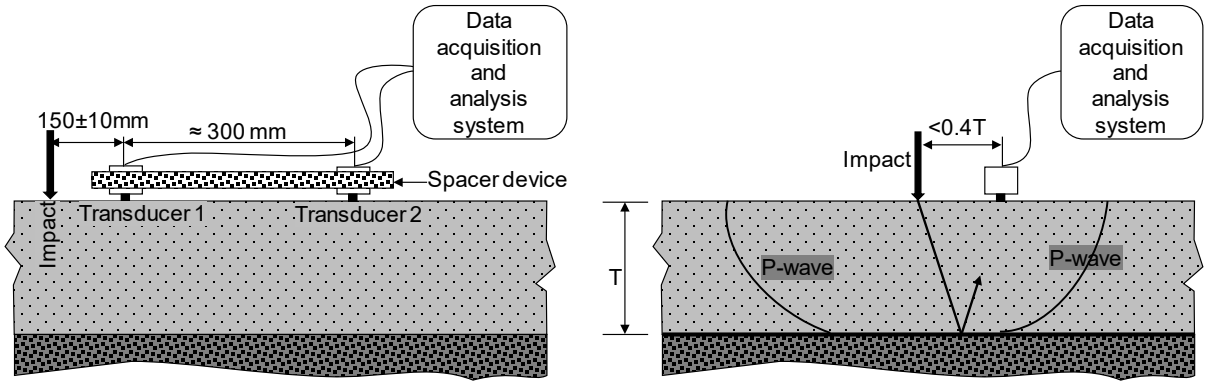

(a) P-wave speed measurement (b) Impact echo

Figure 2.3: Schematic of testing configuration for impact-echo test

This method is widely used for assessment of bridge decks because it can be operated by accessing only one surface. In addition, data analysis is straightforward. However, the size of detected flaws is dependent on the impact duration and it is less reliable in the presence of asphalt overlays.

Ultra-sonic pulse velocity (UPV) is a nondestructive technique used to detect damage in a structure (Song and Saraswathy, 2007) and/or to estimate mechanical properties such as Poisson's ratio and modulus of elasticity (Petro and Kim, 2012). This method involves longitudinal elastic stress wave pulses generated by the electro-acoustical transducer directly attached to the structure surface. These waves travel through the concrete and are received by another transducer at the opposite surface. To calculate the concrete wave velocity, equation 2.2 is used as follows:

$$V = \frac{L}{t} \tag{2.2}$$

where V is velocity, L is the distance between the transducers, and t is the travel time required for a pulse to be emitted by a sender transducer and received by another transducer.

According to ASTM C597 (2016), the P-wave velocity can be calculated as follows:

$$Cp = \sqrt{\frac{E\,(1-v)}{(1+v)(1-2v)\rho}} \tag{2.3}$$

Where C_p is the longitudinal pulse velocity, E is the modulus of elasticity, v is Poisson's ratio, and ρ is density.

Wave behavior based on condition is described schematically in **Figure 2.4**. At the top, the path between the two transducers is through solid concrete, therefore the travel time is the shortest. Below that is the case where there is an area of porous concrete; the pulse is scattered as it travels through this area resulting in longer pulse travel time and reduction in the pulse velocity. In the next case, the direct travel path is near the edge of a crack, therefore the travel path is longer than the distance between the transducers, so the pulse velocity is lower than through sound concrete. In the last case, the pulse is reflected by the crack and the travel time cannot be measured. This method is straightforward and does not require costly instrumentation. However, the method requires traffic control and access to both sides, which is not usually available for bridge decks.

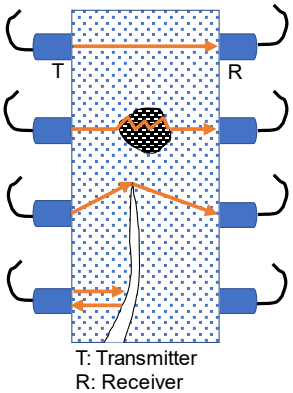

Figure 2.4: Wave behavior according to condition

Sound deck acoustic response (SoundDar) is an automated type of chain dragging used to detect delamination in bridge decks. This method involves ball-chains for continual impact excitation and multi-channel microphones for acoustic sensing. A ball-chain is formed by multiple metal or plastic balls connected by flexible ropes and is dragged on a concrete surface to excite vibration of delaminated regions (Sun et al., 2017). The microphones record sound and vibration amplitude as a function of time, and this data is transferred into the frequency domain for analysis. Rather than depending on the human ear, the device utilizes a machine learning algorithm that identifies changes in the acoustic response and identifies them as intact concrete or degraded concrete (BDI and Infrasense Inc., 2018). This method is vehicle mounted and requires minimal traffic control. Furthermore, using this method, acoustic signals with higher signal-to-noise ratios (S/N) compared to traditional chain dragging are generated (Sun et al., 2017). However, traffic noise may affect the results.

2.3 Review of Traditional and Rapid Evaluation Methods Applied to Bridge Decks

Parrillo et al. (2006) used the BridgeScan GPR system for evaluating the condition of an asphalt overlaid bridge deck located in Lewiston, Maine. A color-coded deterioration map of the bridge deck was produced, and the deterioration map from the GPR data was compared with the visual data from the top and bottom. The results showed a good correlation. The Maine Department of Transportation (DOT) then removed the asphalt overlay and conducted chain dragging. Comparing the results with the GPR data provided confirmation of the results obtained.

Washer et al. (2015) performed a study to develop and implement infrared thermography for the condition assessment of concrete bridges using hand-held infrared cameras. The goal was to develop new technologies to ensure bridge safety and improve the effectiveness of maintenance and repair. Capability and reliability were demonstrated through field testing of the technology and comparison with a traditional inspection technique (e.g. hammer sounding, coring, and/or drilling). Results showed that the new technology provided suitable conditions for detection of subsurface damage in concrete.

Robison and Tanner (2011) performed an exploratory study on three bridge decks in Wyoming using standard Wyoming DOT (WYDOT) practices for chain dragging and half-cell potential, along with impact echo, thermal imaging, and ground penetrating radar (GPR). The goal was to consider alternative practical solutions that WYDOT could implement for evaluating bridge decks to save time while increasing safety, efficiency, and accuracy. Cores were taken from each bridge. The results can be summarized as follows:

- Impact echo, thermal imaging, and GPR methods investigated minimally improved the safety or efficiency of the bridge deck evaluation process because they required personnel on the bridge. They did increase accuracy by removing the bias that can occur with chain dragging.
- Using the impact echo method, immediate results were provided instead of waiting to analyze the data in the office.
- Thermal imaging was not recommended for bridge investigations in Wyoming as the time to perform this test is much longer than other methods, and it requires additional analysis to interpret the output.

- Corrosion in the deck can be quantified using GPR, which can remove the necessity for collecting half-cell potential readings. If a GPR vehicle mounted system provided the same level of accuracy, this would be the preferred method of evaluating bridge decks.
- Damage locations indicated by impact echo, thermal imaging, and GPR generally correlated well. A combination of impact echo with GPR testing provided the most accurate predictions of delamination, debonding, and active corrosion.

Gucunski et al. (2013) conducted a project in Haymarket, Virginia with four objectives: a) to identify and characterize nondestructive technologies that can detect deterioration in concrete bridge decks, b) to assess the strengths and limitations of each nondestructive technology through accuracy, ease of use, speed, and cost; c) to recommend procedures and protocols for application of the technologies; and d) to summarize the information gathered with each technology that would be helpful for an electronic repository. Ground penetrating radar, impact echo, ultrasonic surface waves, impulse response, half-cell potential, electrical resistivity, galvanostatic pulse, infrared thermography, ultrasonic pulse echo, chain dragging, and hammer sounding were the technologies investigated. The results are summarized as follows:

1. Four technologies were identified as having fair-to-good potential for delamination detection and characterization. These were impact echo, chain dragging/hammer sounding, infrared thermography, and ground-penetrating radar.
2. Four technologies were identified as having fair-to-good potential for corrosion detection or characterization. These include half-cell potential, electrical resistivity, galvanostatic pulse measurement, and ground-penetrating radar.
3. Only one technology, surface wave testing, was validated as a fair technology for vertical crack characterization.

Sneed et al. (2014) examined nondestructive techniques on eleven bridge decks to determine the most cost-effective, efficient, and accurate technique for evaluating the condition of Missouri Department of Transportation (MoDOT) bridge decks. The bridge decks were evaluated through visual inspection, ground-coupled/ground penetrating radar, Portable Seismic Property Analyzer (PSPA), core extractions, and chloride ion concentration measurements. The authors recommended GPR to evaluate the condition of bridge decks because it is simple to use and relatively accurate when compared with the core results, whereas PSPA had a slow data collection speed, requires expertise, and should be combined with other nondestructive methods.

A summary of the bridge deck damage evaluation techniques with their applications, advantages and disadvantages is presented in **Table 2.2**.

Table 2.2: Bridge deck damage evaluation techniques

Method	Method classification	Applications	Advantages	Disadvantages
Visual inspection	Traditional	Visual Surface distress identification	Convenient inspection without instrumentation	Human error, traffic control
Half-Cell potentials		Measurement of probability of active rebar corrosion	Easy to apply	Direct connection with reinforcement is required, traffic control
Chloride sampling		Measurement of Chloride content of bridge deck	Simple instrumentation, benchmark for other methods like GPR	Time-consuming, traffic control, not showing condition of whole structure, not directly showing damage
Coring		Determining the extent of the distress and mechanical properties, verifying findings of other evaluation methods	Showing real condition of structure	Destructive testing, traffic control, time-consuming, not showing condition of whole structure
Chain dragging		Delamination detection	Simple field method, direct interpretation of results, cheap instrumentation, limited training	Surface damage detection, traffic control, traffic noise effects on accuracy, subjective
Ground penetration radar (GPR)	Rapid	Detection of deterioration caused by corrosion	Versatility, portability, good with overlays, minimum traffic control	Complexity of interpretation of results
Impact Echo (IE)		Detection of delamination, voids, and cracks Determining thickness	Requires only one surface of tested structure, independent of the geometry of the structure, less susceptible to steel reinforcement	Size of detected flaws is highly dependent on the impact duration, less reliable in the presence of asphalt overlays
Infrared (IR)		Detection of delamination defects	Non-contact method, no traffic control	Shadows and reflections can lead to incorrect interpretation
Ultra-sonic pulse velocity (UPV)		Detection of cracks, voids, internal flaws and other damage	Easy to apply, direct interpretation of results	Requires access to both sides of the tested material, for structural members containing large voids, signal transmission may be completely lost
Deck Acoustic Response (DAR)		Detection of delamination defects	Vehicle mounted (minimal traffic control), high signal-to-noise ratio	Traffic noise may affect the results

2.4 Summary of Survey Results

To identify current practices related to bridge deck evaluation using nondestructive evaluation methods in different state highway agencies, a six-question survey was prepared using Survey Monkey for nine state DOTs (i.e. FL, OH, IA, OR, IN, LA, MO, VA and PA) which are involved in the Strategic Highway Research Program (SHRP) study related to Nondestructive Evaluation methods for bridge decks. The following questions were posed:

1. What types of technologies are you considering for bridge deck evaluation at the asset management level?
2. What types of technologies are you considering for bridge deck evaluation at the local level?
3. How do you intend to incorporate the findings from these evaluations into your maintenance procedures?
4. How do you intend to incorporate the findings from these evaluations into your asset management procedures?
5. How did you know that the results were accurate or that they made sense?
6. Have you conducted a benefit/cost analysis? If so, what were the results?

Representatives of the Iowa DOT, Florida DOT, and Louisiana Department of Transportation and Development (LaDOTD) responded to the survey. Iowa DOT investigated impact echo and infrared thermography in bridge deck evaluations on the local level. Findings will be used to localize areas for repair and to determine quantities related to different deck conditions. Hammer sounding was used to verify the accuracy of the results. Benefit/cost analysis has not been conducted. Florida DOT utilized visual inspection, ground penetrating radar, and infrared technologies for the asset management level. Findings are reported by condition status to inform maintenance procedures, and it was found that rapid technologies are not always accurate. Benefit/cost analysis has not been conducted and is anticipated only for large bridges with known deck problems. The Louisiana Department of Transportation and Development employed ground penetrating radar and infrared thermography for both the local and asset management levels. Deficiencies noted are addressed through maintenance work orders and will also be used for deterioration modeling in asset management procedures. Core samples have been taken to verify the accuracy of the technologies. Benefit/cost analysis has not been conducted.

CHAPTER 3: METHODOLOGY

3.1 Site Selection

The bridge sites were based in consultation with the steering committee. To provide for an evaluation of the differing technologies bridge decks in good, medium, and poor condition were included in the study and it was also desired to select bridges with differing superstructure types. As mobilization is a primary cost for all of the evalution methods it was desired to have all bridges within a one hour drive from the Columbia Metropolitan Airport (CAE). All bridge decks were bare concrete.

3.2 Site Description

Four in-service bridge decks were selected for evaluation. The decks were evaluated using different methods including GPR, IR, high definition video scanning, and DAR (in one instance). **Table 3.1** provides information about each bridge.

Table 3.1: Summary of selected bridges

Structure No.	Location	Year of Construction	Condition
3270003400300	S-34, Pond Branch Road over I-20	1970	good with no significant damage
4040055510210	SC 555, Farrow Road over I-77	1976	medium with spalls
4020002100300	US-21, Wilson Blvd over I-20	1966	poor with significant damage
3270010600200	S-106, Mineral Springs Road over I-20	1964	poor with significant damage

S-34, Pond Branch Road over I-20: This bridge is at the intersection of Pond Branch Road and I-20 and was constructed in 1970. The bridge has a length of 300 feet with three pourable joints. It has four main spans, two at 102 feet and two at 48 feet. The bridge is on a skew of 45 degrees with two lanes on and four lanes under the bridge. The out-to-out dimension is 48 feet, and the curb-to-curb dimension is 44 feet. This bridge deck is in good condition with very minor spalls and has no overlays. **Figure 3.1** shows a satellite view of the bridge and a photograph to describe the existing condition.

(a) Satellite view (b) Deck with no patches

Figure 3.1: S-34, Pond Branch Road over I-20 (good condition)

SC 555, Farrow Road over I-77: This bridge is located at the intersection of Farrow Road and I-77 and was constructed in 1976. The bridge has two separate lanes (each lane is a bridge). One bridge is SC 555 North Bound Lane (NBL) and the other is SC 555 South Bound Lane (SBL). SC 555 NBL has a length of 446 feet with two pourable joints and two compression joints. It has four main spans, two at 138 feet and two at 85 feet. The bridge is on a skew of 20 degrees and has an out-to-out width of 42.6 feet. The SC 555 SBL bridge has a length of 480 feet with two pourable joints and two compression joints. It has four main spans, two at 138 feet and two at 102 feet. The bridge is also on a 20-degree skew and has out-to-out width of 50.5 feet. This bridge deck was in medium condition with 40-45% deck spalls and delamination prior to deck rehabilitation. **Figure 3.2** shows a satellite view of the bridges and photographs that describe the condition prior to deck rehabilitation.

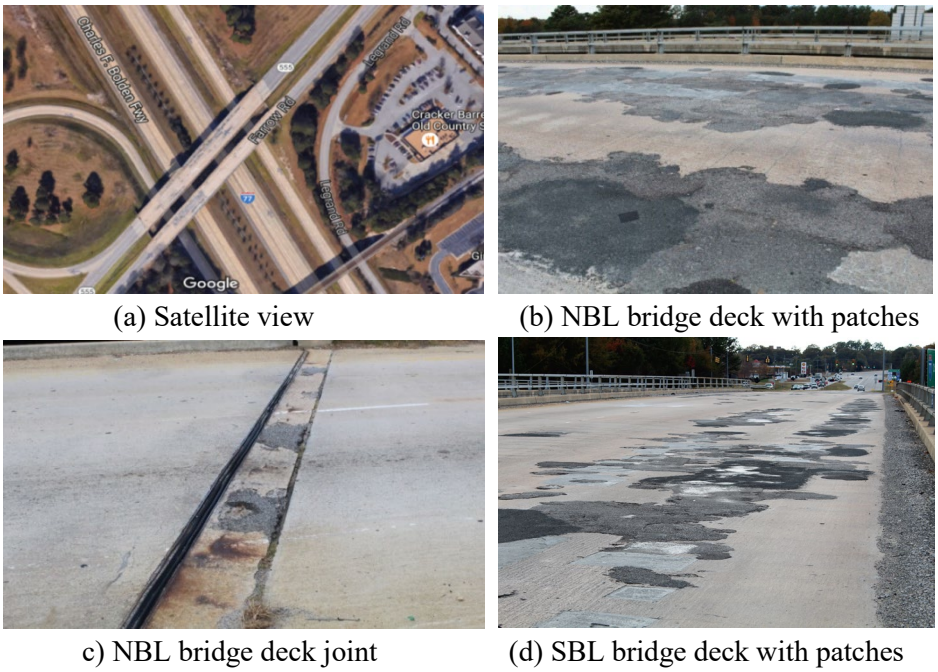

(a) Satellite view (b) NBL bridge deck with patches

c) NBL bridge deck joint (d) SBL bridge deck with patches

Figure 3.2: SC 555, Farrow Road over I-77 (medium condition)

US-21, Wilson Boulevard over I-20: This concrete bridge is located at the intersection of Wilson Boulevard and I-20. It was constructed in 1966, and it has a length of 275 feet with three pourable

joints. It has four main spans, two at 67.5 feet and two at 70 feet. The bridge is on a skew of 25 degrees and has four lanes on the bridge and eight lanes under the bridge. The bridge has two sidewalks (each four feet wide). The out-to-out dimension is 67 feet and the curb-to-curb dimension is 56 feet. The bridge deck has no overlay and temperature patching. **Figure 3.3** shows a satellite view and photographs of the deck with patches.

(a) satellite view (b) deck with patches

Figure 3.3: US-21, Wilson Blvd. over I-20 (poor condition)

S-106, Mineral Springs Road over I-20: This concrete bridge is located at the intersection of Mineral Springs road and I-20. It was constructed in 1964 and has a length of 254 feet with three pourable joints. It has four main spans, two at 66 feet and two at 61 feet. The bridge is on a skew of 25 degrees with two lanes on the bridge and four lanes under the bridge. The out-to-out dimension is 30 feet, and the curb-to-curb dimension is 26 feet. The bridge deck has no overlay and temporary patching. **Figure 3.4** shows a satellite view and a photograph that describes the existing condition of the deck.

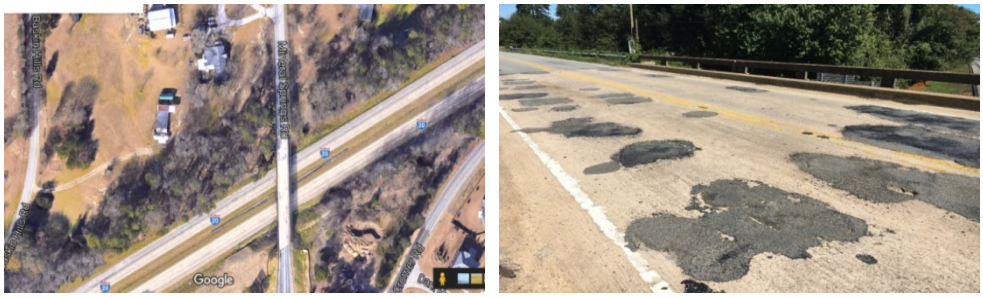

(a) satellite view (b) deck with patches

Figure 3.4: S-106, Mineral Springs Road over I-20 (poor condition)

3.3 Rapid Evaluation Methods

The rapid evaluation methods used for scanning the selected bridges included high-speed GPR, IR, High Resolution Video (HRV) scanning, and DAR (in one instance).

3.3.1 Mobile scanning

On May 26, 2017, rapid evaluation of the four bridge decks was performed by Bridge Diagnostic Incorporation (BDI)/Infrasense using vehicle mounted GPR, IR, and HRV scanning. Ultra-time

Domain Infrared (IR-UTD) scanning was carried out on two bridges by Thermal Stare. Additionally, DAR testing was carried out on one bridge by BDI/Infrasense. Test procedures were as follows:

Ground penetrating radar (GPR): GPR surveys were carried out on all four bridges in accordance with ASTM D 6087 (2015) using twin air-coupled 2 GHz horn antennas attached to a vehicle as shown in **Figure 3.5**. The GPR data was collected in a series of lines spaced 3 feet transversely across the width of each deck at a vehicle speed of approximately 55 mph. Using a rotary encoder (Distance Measurement Instrument, DMI), the distance data was continuously recorded into each GPR record so that each GPR data scan had an associated distance. The GPR analysis was conducted with Geophysical Survey System, Inc. (GSSI) commercial software, Radan 7, along with proprietary software.

Figure 3.5: GPR survey equipment (BDI and Infrasense Inc., 2017),
(figure reproduced with permission)

Infrared (IR) thermography and HDV scanning: Vehicle mounted infrared thermography scanning was carried out on all four bridge decks in accordance with ASTM D4788 (2013) using a 640*480-pixel FLIR System Model A655sc infrared camera in combination with a Sony-Alpha 74K HRV camera. Both were mounted on an elevated platform on a vehicle as shown in **Figure 3.6**. The infrared and video data were collected across each deck at approximately 55 mph. The infrared data is analyzed simultaneously with HRV data to differentiate delaminated areas from surface features such as oil stains and discolorations.

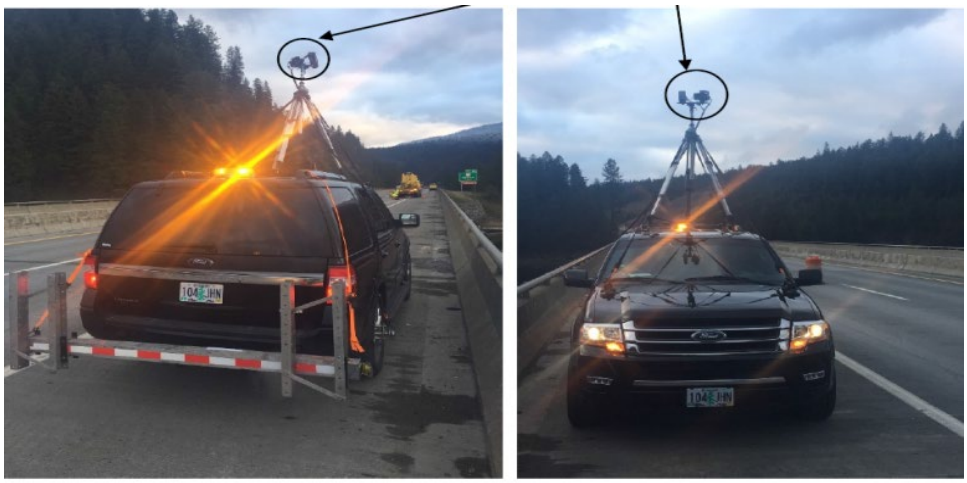

Figure 3.6: Infrared and video survey equipment (BDI and Infrasense Inc., 2017),
(figure reproduced with permission)

3.3.2 Pole mounted scanning (IR-UTD)

Ultra-Time Domain Infrared sensing was deployed on two of the four subject bridges as described below.

S-34, Pond Branch Road over I-20: The Infrared Ultra-Time Domain (IR-UTD) system was positioned at the middle of the bridge on the north side. The system was installed using a parapet mount system. **Figure 3.7** shows the system mounted on the bridge (ThermalStare, LLC., 2017).

(a) view from I-20

(b) view from bridge deck

Figure 3.7: IR-UTD setup at S-34, Pond Branch Road over I-20 (ThermalStare, LLC., 2017)
(figures reproduced with permission)

Measurements were collected from three areas, as shown in **Figure 3.8**. The image on the left shows a view looking east from the position of the IR-UTD, the middle image is looking downward, and the right image is looking west from the position of the IR-UTD. **Figure 3.8** shows that the IR-UTD images were optimized to display the structural features supporting the bridge deck. The girder lines are visible (except the girders hidden by the parapets) as well as the joints between the spans. **Figure 3.9** shows visual images of the bridge deck associated with the IR-UTD images shown in **Figure 3.8**.

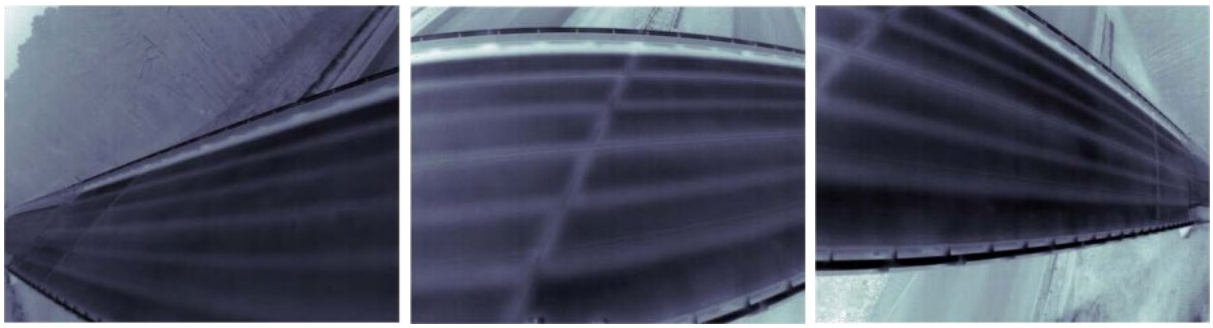

Figure 3.8: IR-UTD data showing structural features at S-34, Pond Branch Road over I-20 (ThermalStare, LLC., 2017) *(figure reproduced with permission)*

Figure 3.9: IR-UTD visual images at S-34, Pond Branch Road over I-20 (ThermalStare, LLC., 2017) *(figure reproduced with permission)*

US-21, Wilson Boulevard over I-20: The IR-UTD system was positioned at the middle of the bridge on the west side as shown in **Figure 3.10**. The system was again installed using a parapet mount system.

(a) view from deck

(b) view from I-20

Figure 3.10: IR-UTD setup at US-21, Wilson Blvd. over I-20 (ThermalStare, LLC., 2017)
(figures reproduced with permission)

Measurements were collected at three areas as shown in **Figure 3.11**. The image on the left shows a view looking north from the position of the IR-UTD, the middle image is looking downward, and the right image is looking south. **Figure 3.11** shows IR-UTD images optimized to display the structural features supporting the bridge deck. The beam lines are visible (except the beams hidden by the parapet and median berm) as well as the joints between the spans and diaphragms. **Figure 3.12** shows the visual images of the bridge deck corresponding to the IR-UTD data shown in **Figure 3.11**.

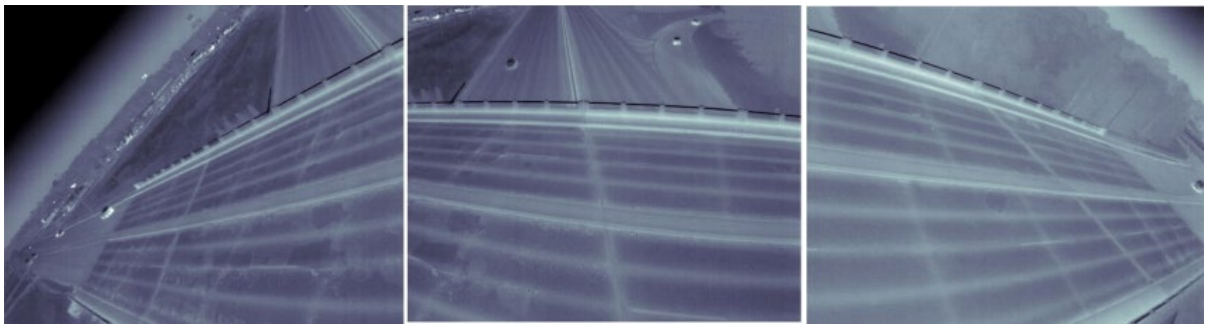

Figure 3.11: IR-UTD data showing structural features at US-21 Wilson Blvd. over I-20 (ThermalStare, LLC., 2017) *(figures reproduced with permission)*

Figure 3.12: IR-UTD visual images at US-21, Wilson Blvd. over I-20 (ThermalStare, LLC., 2017) *(figures reproduced with permission)*

3.4 Field Validation

3.4.1 Chain Dragging and DAR

Manual chain dragging using a 3/8 in. galvanized chain was conducted only on the east bound lane and shoulder between bents 4 and 5 of the S-34 Pond Branch Road bridge (structure no. 3270003400300), the south bound right lane between bents 2 and 3 of US-21 Wilson Blvd bridge (structure no. 4020002100300), and the south bound lane and shoulder between bents 3 and 4 of S-106 Mineral Springs Road bridge (structure no. 3270010600200). **Figure 3.13** shows chain dragging conducted on the S-106 Mineral Springs Road bridge.

Figure 3.13: Chain dragging on S-106, Mineral Springs Road bridge over I-20

An automated Deck Acoustic Response (DAR) device was used for rapid detection of delamination. This method includes ball-chain assemblies for continual impact excitation and multi-channel microphones for acoustic sensing mounted on a vehicle. The device is designed for individual impacts like hammer sounding (**Figure 3.14**) or ball-chain assemblies may be attached as shown in **Figure 3.15**.

Figure 3.14: Deck acoustic response for individual solenoid impactors (BDI/Infrasense, Phase II Report, 2018) *(figure reproduced with permission)*

Figure 3.15: DAR ball-chain assembly in use on US-21, Wilson Blvd. over I-20

3.4.2 Coring

Cores locations were selected based on the GPR results (discussed in more detail in chapter 4) provided by BDI/Infrasense as shown in **Figure 3.16**. Three different regions were marked on each bridge deck and labeled as severe, medium, and no damage as shown in **Figure 3.17**. A Profoscope rebar locator was used to select core locations in each region and to avoid cutting reinforcement during coring (see **Figure 3.18**).

A total of 49 cores were extracted from three of the four bridge decks. The number of cores extracted is summarized in **Table 3.2.** Thirteen cores were taken by the U. South Carolina team using a deck-mounted, wet coring device and the remainder were extracted by BDI using a truck-mounted wet coring device. Coring devices are shown in **Figure 3.19**. Each core was labeled and stored in sealed plastic bags after extraction. Severe damage, medium damage, and no damage regions are indicated by "S", "M", and "N" in the core labels, respectively. Core holes were cleaned and filled with a repair material as shown in **Figure 3.20**. SikaQuick 2500, a very rapid hardening and repair mortar, was used to fill the holes after coring. According to the SikaQuick manufacturer recommendations 3/8 in. coarse aggregate was added.

Table 3.2: Number of cores extracted

	Bridge name		
	S-34, Pond Branch Road over I-20	S-106, Mineral Springs Road over I-20	US-21, Wilson Blvd. over I-20
Severe damage region	4	5	6
Medium damage region	4	7	6
No damage region	6	6	5
Total	**14**	**18**	**17**

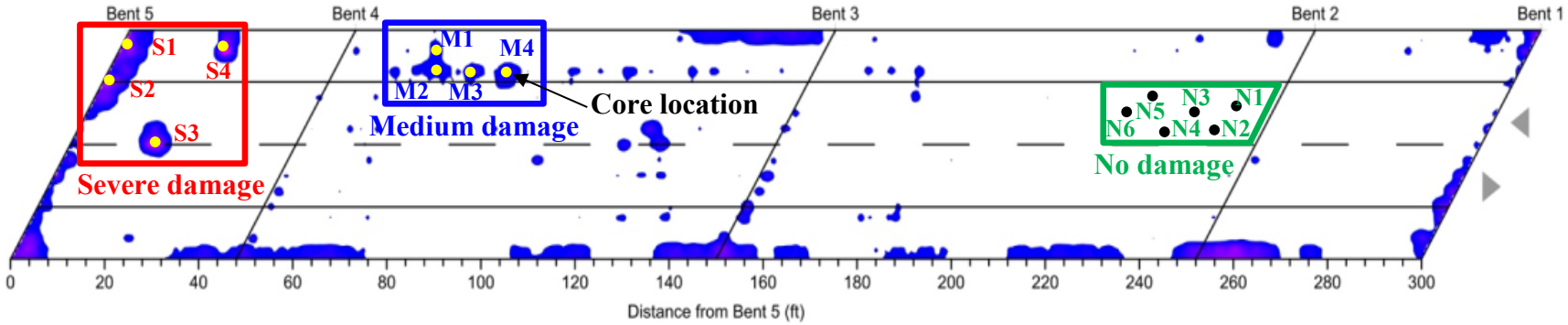

(a) S-34, Pond Branch Road over I-20

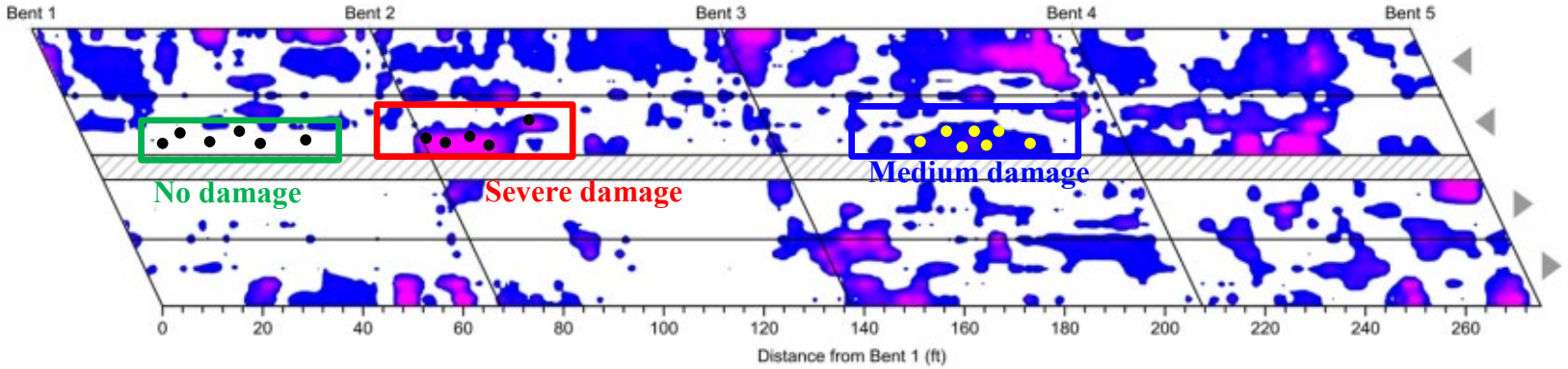

(b) US-21, Wilson Blvd over I-20

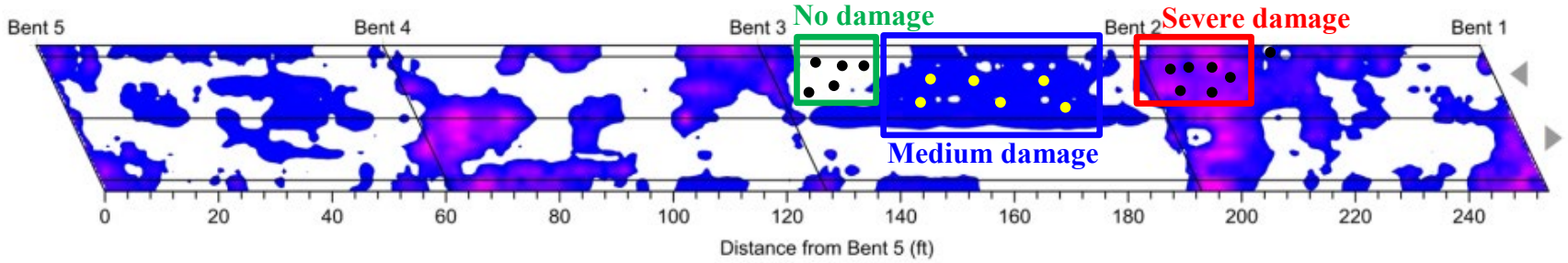

(c) S-106, Mineral Springs Road over I-20

Figure 3.16: Core locations (marked as yellow or black circles) (BDI/Infrasense Inc., 2017)

(a) severe damage (b) medium damage (c) no damage

Figure 3.17: Mapping of damaged regions on S-106, Mineral Springs Road over I-20

Figure 3.18: Profoscope rebar locator

(a) deck-mounted (b) truck-mounted

Figure 3.19: Coring devices

(a) cleaned core location (b) SikaQuick 2500

Figure 3.20: Repairing of core locations

3.4.3 Chloride concentration testing

Locations for chloride sampling were selected based on the GPR results (**Figure 3.17**). Locations were selected in proximity to the core locations.

Two site visits were made to each bridge to obtain concrete powder samples for chloride concentration testing. A hole was drilled for each sample location using different bit sizes for different penetration depths. Powder samples were taken at depths of 1, 2 and 3 inches in each location. First, a 1 in. deep hole was drilled by a 1.5 in. diameter drill bit and a powder sample was taken. Then the hole was drilled to a depth of 2 in. by a 1 in. drill bit and a second powder sample was taken. Finally, the hole was drilled down to 3 in. by a 0.5 in. drill bit and a third sample was taken. This technique was utilized to limit contamination from one sample to the next. In the first site visit 10 samples were obtained by BDI and in the second site visit 33 samples were taken by the U. South Carolina team as described in **Table 3.3. Figure 3.21** shows concrete powder sampling. SikaQuick 2500 was again used to fill the holes.

Table 3.3: Number of concrete powder samples taken

		Bridge name		
	S-34, Pond Branch Road over I-20	SC 555, Farrow road over I-77	S-106, Mineral Springs Road over I-20	US-21, Wilson Blvd. over I-20
Severe damage region	5	-	5	5
Medium damage region	5	1	5	5
No damage region	1	1	5	5
Total	**11**	**2**	**15**	**15**

Figure 3.21: Drilling holes to collect concrete powder samples on US-21, Wilson Blvd. over I-20 bridge deck

3.4.4 Evaluation of field samples

Evaluation of Cores: Upon arrival at the U. South Carolina Structures and Materials Laboratory the cores were visually inspected for determination of visible cracks and delamination. Physical characteristics of the cores such as average diameter, average length, and weight were also determined. Carbonation depth and absorption tests were then conducted.

Carbonation occurs when carbon dioxide penetrates through the surface and reacts with alkaline in the concrete thereby reducing the pH level. In carbonation depth testing, the pH level of a specimen is evaluated with an indicator solution. Hardened cement generally has a high pH value and turns purple when exposed to an indicator solution while carbonated regions remain colorless. The depth of the colorless region is then measured. A solution of 1% phenolphthalein in 70% ethyl alcohol was utilized as an indicator and sprayed on the cores. The colorless depth was measured after 24 hours for each core. This depth is referred to as the depth of carbonation (ASTM C642, 2006).

Density, absorption, and void tests were conducted according to ASTM C642 (2006). First, cores with weight exceeding 800 grams were selected. Three cores from each bridge exceeded 800 grams. The cores were weighed before being placing in an oven and then dried in the oven at a temperature of 100 to 110^{o} C for 24 hours. A specimen is considered dry if its weight has not changed after 24 hours in the oven. If the specimen remains wet, it remains in the oven for another 24 hours. This procedure is continued until the difference between two successive values of mass does not exceed 0.5% of the lowest value. The dry mass of the cores is then recorded.

Once the dry mass for each core had been measured, the cores were immersed in water at a temperature of 21^{o}C for not less than 48 hours. A minimum of two mass measurements at intervals of 24 hours were taken. The surface moisture on the cores was removed and the specimens were

weighed. This procedure was continued until the difference between two successful measurements was less than 0.5% of the larger value. The final mass was reported as saturated mass after immersion.

The cores were then placed in a container with water and boiled for five hours. After boiling, the container was left to cool naturally for at least 14 hours to a final temperature of 20 to 25ºC. The surface moisture of the cores was removed, and the specimens weighed. The measurements at this stage were designated as the soaked, boiled, surface-dried mass.

The specimens in the previous stage were then suspended in a water container by a wire and their weights were measured (referred to as apparent mass). Absorption after immersion and after immersion and boiling, dry bulk density, and volume of permeable pore space (voids) were then calculated in general conformance with ASTM C642 (2006).

Chloride concentration testing: A chlorimeter (C-CL-3000) from James Instruments was used to measure chloride concentration of concrete powder samples. An accurately weighed three-gram sample was dissolved in 20 ml of extraction liquid consisting of a precisely measured acid concentration. The chloride ions in the sample then reacted with the acid in the digestive solution (James Instruments, 2018). An electrode, with an integral temperature sensor, was inserted into the liquid solution and the electrochemical reaction measured. The instrument converts the voltage generated by the chloride concentration and automatically applies a temperature correction factor. The percentage of chloride by weight of the three-gram sample can then be viewed on the LCD display. The CL unit displays the free CL ions in an acid solution (**Figure 3.22**).

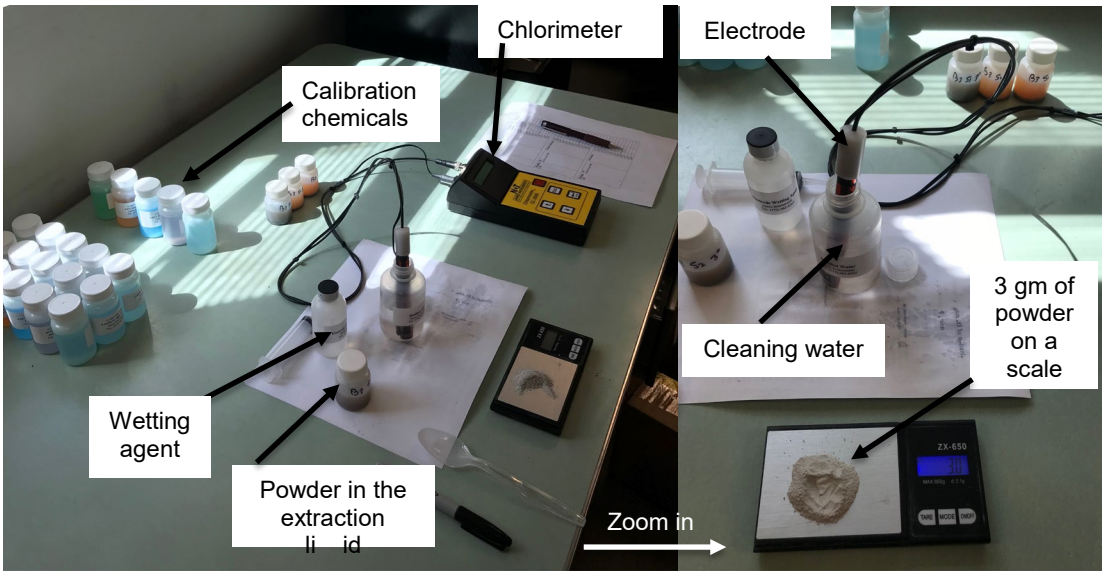

Figure 3.22: Chloride concentration test using C-CL-3000 chlorimeter (James Instruments)

3.5 Decommissioned Laboratory Deck Specimens

3.5.1 Preparation of specimens

Since the corrosion process takes years to affect performance an accelerated investigation was performed. Two bridge deck specimens recovered from an SCDOT bridge were used for this study. The bridge was constructed in 1953 and it is now out of service. The slabs are 15 ft. long, 5 ft. wide and 8 in. thick. The asphalt layer overlay was removed as shown in **Figure 3.23**. Scanning using a rebar locator was done to indicate the rebar position (**Figure 3.24**). The specimens were then moved outside the laboratory for preliminary testing by BDI/Infrasense.

Figure 3.23: Removing the asphalt layer

Figure 3.24: Marking positions of reinforcement

3.5.2 Preliminary testing

BDI/Infrasense performed visual inspection, ground penetrating radar, infrared thermography, impact echo, and half-cell potential on the bridge deck specimen after establishing a 1 ft.×1 ft. testing grid. For the GPR scanning, a 2.6 GHz GSSI antenna was used to send electromagnetic waves through the concrete deck (**Figure 3.25)**. Infrared thermography testing was carried out using a 640 × 480-pixel FLIR System Model A-655sc infrared camera and a high-resolution visual camera as shown in **Figure 3.26**. For IE testing, an Olson Instruments NDE-360 unit was used on the testing grid (**Figure 3.27**) while half-cell potential testing was conducted with a James Instruments Cor-Map II HCP device (**Figure 3.28**).

Figure 3.25: GPR scanning

Figure 3.26: Infrared thermography scanning

Figure 3.27: IE testing

Figure 3.28: Half-cell potential testing

3.5.3 Accelerated corrosion

After the initial assessment, an accelerated test was conducted to corrode eight different areas. Eight concrete cores were drilled (4 in. diameter x 6 in. deep) to access the rebar as shown in **Figure 3.29**. The deck was set vertically to provide access to both sides which is needed for the ultrasonic pulse velocity test (**Figure 3.30**). Wet/dry cycles were conducted (three days wet/four days dry) with 3% NaCl Chloride solution to accelerate the corrosion process. To monitor the corrosion process, half-cell potential and linear polarization resistance measurements were recorded at the end of the wet period to ensure better concrete conductivity. The objective of these measurements was to provide insight related to the corrosion process of the reinforcement at the selected locations.

Figure 3.29: Extraction of cores

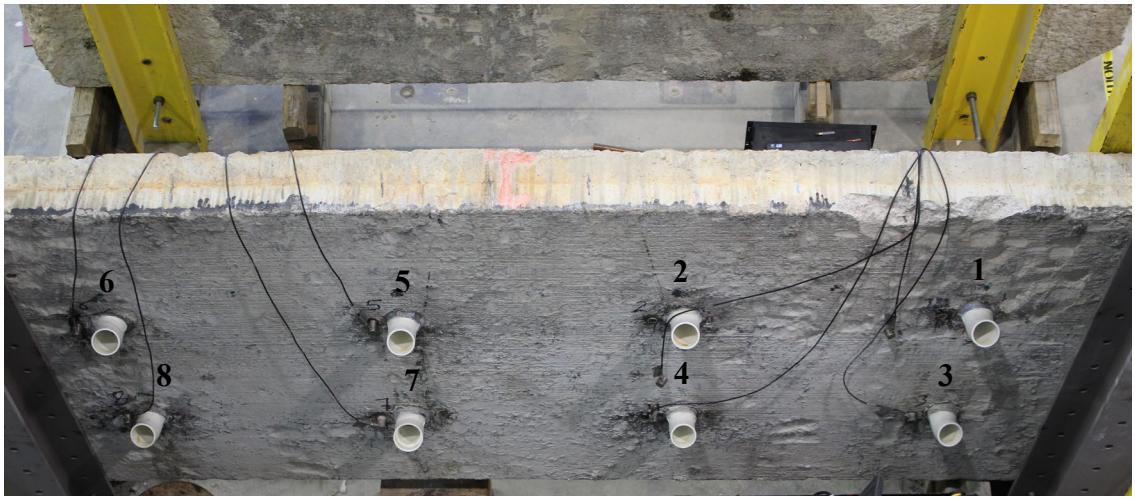

Figure 3.30: Bridge deck test setup

The Half-Cell Potential (HCP) method was utilized in general conformance with ASTM C876 (2015) to determine the likelihood of corrosion activity. The test includes measuring the potential of the embedded steel rebar relative to the known potential of a reference electrode attached on the concrete surface. An electrical junction device (a sponge wetted with a contact solution) was used between the concrete surface and a reference electrode to provide low electrical continuity as shown in **Figure 3.31**. The HCP measurements were recorded using a voltmeter which has a ± 3% accuracy at the voltage range and a potential of less than 0.02 Volts. The reinforcing bar is connected to the positive terminal of the voltmeter, and the negative terminal is connected to the reference electrode (see **Figure 3.31**).

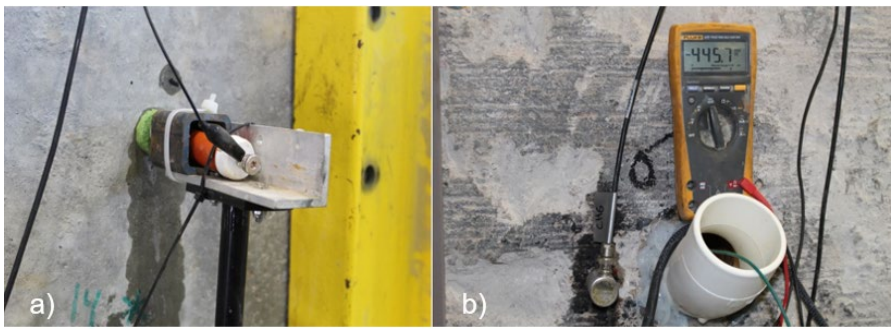

(a) half-cell (b) voltmeter

Figure 3.31: HCP apparatus

Linear Polarization Resistance (LPR) was also used to assess the corrosion activity in the reinforcement using a potentiostat/galvanostat (Model 263A, Princeton Applied Research, New Jersey, USA). The working electrode is connected to the steel reinforcement and a Cu/CuSO4 (reference electrode) is then applied to the concrete surface to measure the corrosion potential with a copper plate immersed in the water inside the opening as a counter electrode. The reference electrode was placed about 2 in. from the rebar level and attached with a sponge wetted with a contact solution to provide low electrical continuity between the concrete surface and the half cell. According to ASTM C876 (2015), a mixture consisting of 95 ml of the commercially available wetting agent with five gallons of potable water was used as a contact solution. The method is based on polarizing the reinforcement cathodically and anodically by ± 20 mV to obtain the potential-current curve. The polarization resistance, Rp, is the slope of the curve at current = 0 calculated using the following equation, (O'Reilly et al., 2011; Vélez et al., 2014; Andrade and Alonso, 2004).

$$Rp = \frac{\Delta E}{\Delta I} \tag{3.1}$$

where ΔE is the concrete potential in volts and ΔI is the concrete current in amperes. Rp can be used to calculate the corrosion current (I_{corr}) and corrosion current density (i_{corr}). These parameters are then used to estimate the corrosion rate (CR).

Ultrasonic Pulse Velocity (UPV) testing was conducted in general conformance with ASTM C597 (2016) using a PUNDIT Plus system (Portable Ultrasonic Nondestructive Indicating Tester). PUNDIT Plus is a portable device for field testing and can be used for many methods by switching the instrument modes as shown in **Figure 3.32**. The pulse mode creates an ultrasonic pulse using 50-mm diameter transducers. The deck was placed vertically to access both sides so that the two transducers were located opposite each other. Coupling grease was applied between the deck surface and the transducers to reduce signal loss (Petro and Kim, 2012). This test is nondestructive, and it is possible to repeat at the same point many times to determine changes of UPV over time (Germann Instruments. Inc., 2016). The test was conducted every two months throughout the 21 testing grid points along the deck. The testing grid points were selected to be adjacent to the accelerated corrosion locations where damage is expected to occur. Points 1, 3, 5, 7, 15, 17, 19, and 21 are two in. above the holes filled with the chloride solution. **Figure 3.33** shows the testing grid points.

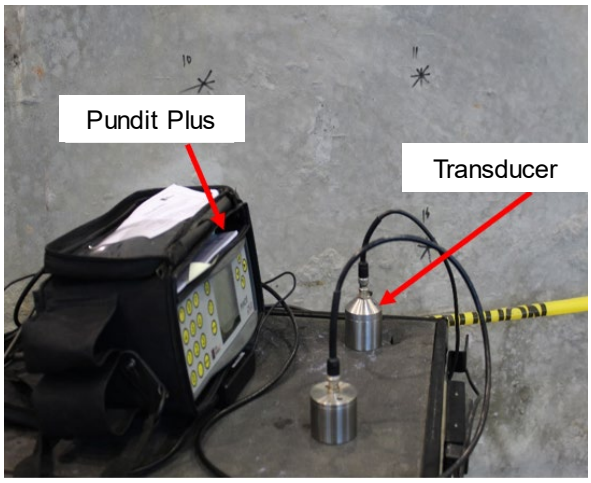

Figure 3.32: PUNDIT Plus device

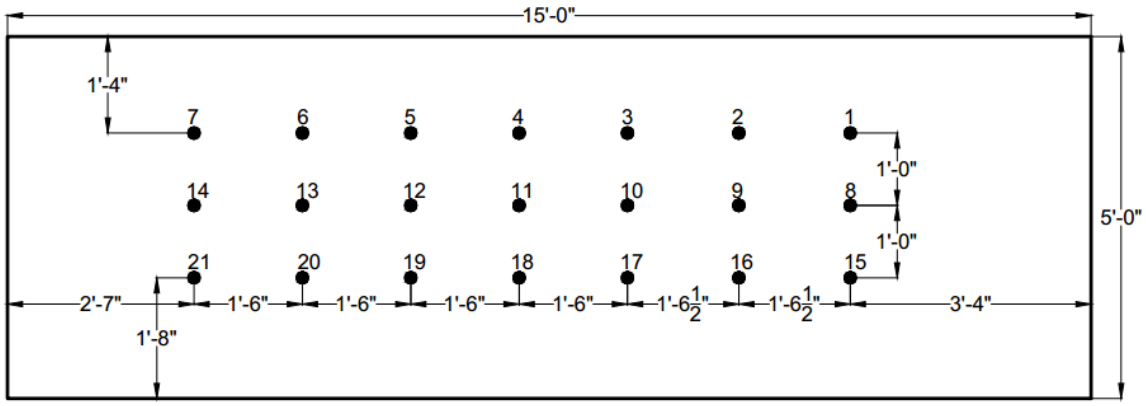

Figure 3.33: UPV and IE testing grid points

Impact echo (IE) testing was conducted at 21 grid points along the slab to measure the resonant frequency associated with the thickness. The change in the frequency is the key for detecting the presence of a flaw (Hsiao et al. 2008). The peak of the reflected wave from the bottom of the deck occurs at a lower frequency because the path length increases. The test was performed using a Data Physics SignalCalc ACE Dynamic Signal Analyzer (**Figure 3.34**). SignalCalc ACE is a small portable board that can be connected to a computer to form a powerful and comprehensive signal analyzer with a wide range of measurements in the time, frequency, and amplitude domain (Data Physics Corporation, 2017). An accelerometer with a frequency range of 0-10 Khz was connected to the SignalCalc board, and a stress wave was generated using a ball bearing. The wave traveled through the slab thickness and reflected to be captured by the accelerometer. The time required for the wave to travel and reflect was recorded. Fast Fourier Transform (FFT), one of the fundamentals of digital signal processing, was used to convert time domain signals to the frequency domain. The recorded signal was displayed in both time and frequency domains.

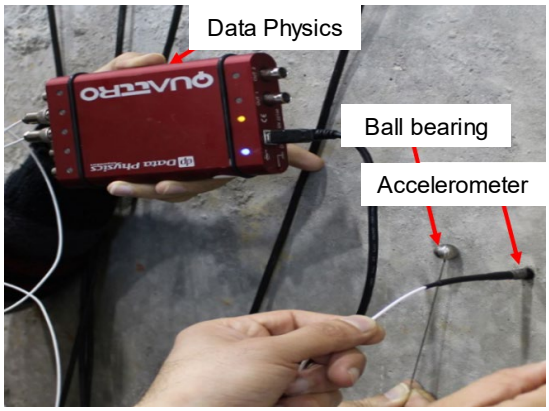

Figure 3.34: IE test apparatus

3.6 Monitoring of the Leaphart Road Bridge over I-26

A portion of the deck of the Leaphart Road Bridge over I-26 was monitored to better understand conditions that may contribute to durability of bridge decks in South Carolina. Instruments were embedded prior to casting of the bridge deck.

Embedded corrosion monitoring (ECI-2): Corrosion of reinforcement in concrete occurs in the presence of chlorides and moisture. The Corrosion Instrument (ECI-2) is an embedded nondestructive evaluation (NDE) monitoring device developed by Virginia Technologies, Incorporated (VTI) (**Figure 3.35**). The ECI-2 embeddable corrosion instrument incorporates five sensors into one package that is installed and placed wherever needed during construction (**Figure 3.36**). The ECI-2 monitors five parameters related to corrosion of steel reinforcement in concrete including linear polarization resistance (LPR), open circuit potential (OCP), chloride ion concentration (Cl-), resistivity, and temperature. These parameters are important for long-term corrosion monitoring. More details are provided in Appendix A. Each ECI-2 instrument is a digital peripheral device that can be communicated with through an external datalogger using SDI-12 industry standard protocol. The data is stored in the datalogger and can be downloaded to a portable PC on-site or remotely using a wireless cellular connection, satellite connection, or phone line.

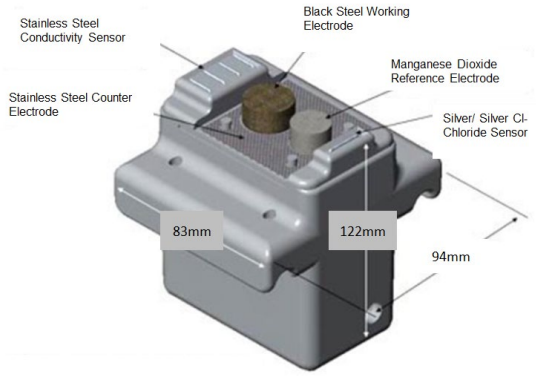

Figure 3.35: ECI-2 Embedded corrosion instrument

Smart concrete sensors: Wireless sensors developed by Giatec Scientific Inc. can be attached to the rebar by twisting two wires around the rebar prior to casting of concrete. Two types of sensors were installed:

- ***Smart rock2 sensor:*** This is a wireless sensor for concrete temperature and strength monitoring. The temperature and strength of the concrete can be viewed using the SmartRock2 mobile app.
- ***Blue rock sensor:*** This is a wireless sensor for monitoring relative humidity and temperature of concrete. The measurements can be viewed using the Blue Rock mobile app.

On September 19, 2017, two ECI-2 devices and ten wireless smart sensors were installed in a bridge deck for long-term corrosion monitoring (**Figure 3.36**). This bridge is in Columbia at the intersection of Leaphart Road and I-26. The two ECI-2 devices and the datalogger are powered by a rechargeable battery connected to a solar panel mounted on the bridge (**Figure 3.37**). LoggerNet software was used to create a program for the data logger and to collect data from the two ECI-2 devices. Five BlueRock and five Smart Rock 2 sensors were also installed to monitor the temperature, humidity, and strength of the concrete. **Figure 3.38** shows the location of each sensor.

Figure 3.36: ECI-2 and smart sensors during installation and prior to casting

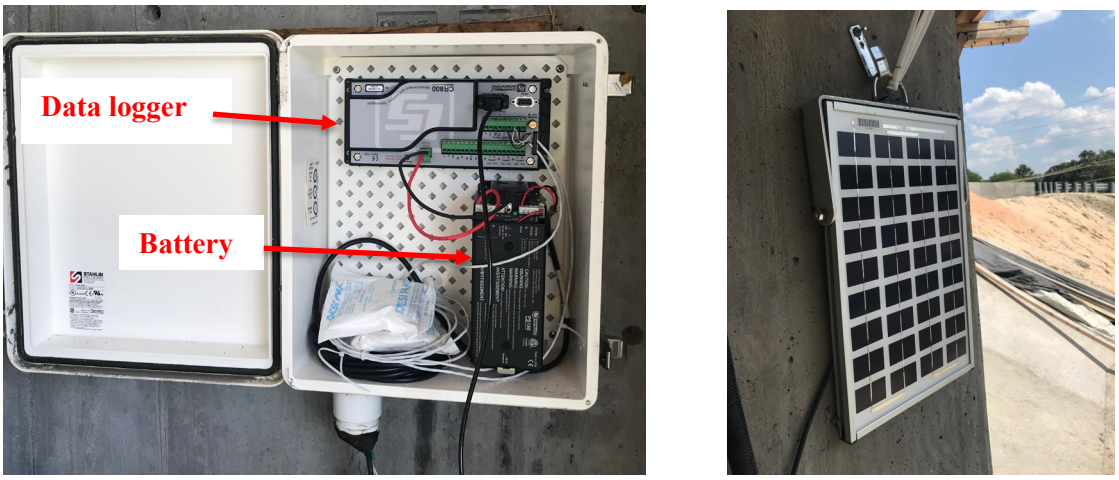

(a) battery and datalogger box (b) solar panel

Figure 3.37: Long term corrosion monitoring system

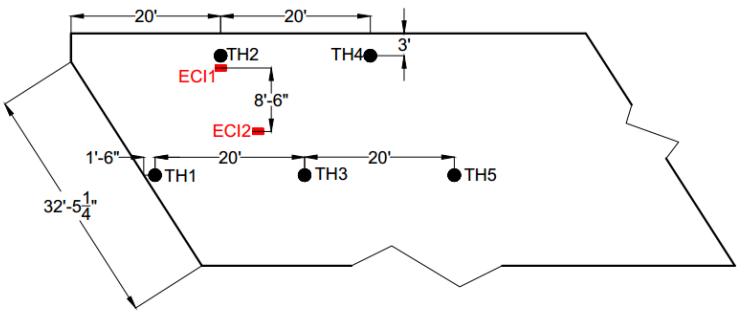

Figure 3.38: Location of ECI-2 and smart sensors in the deck

CHAPTER 4: FINDINGS AND DISCUSSION

This chapter presents the results of rapid evaluation methods including IR, GPR, HRV, DAR, and IR-UTD. The results of traditional evaluation methods such as visual inspection, chain dragging, chloride concentration testing, and coring, are compared with rapid evaluation methods. Results are presented separately for each bridge. For more details, see Appendix B (Nondestructive Evaluation of Two Bridge Deck Specimens), Appendix C (NDE Feasibility Deck Study-Phase I), Appendix D (NDE Feasibility Deck Study-Phase II), and Appendix E (ThermalStare IR-UTD Infrared Measurements).

4.1 S-34, Pond Branch Road over I-20 (good condition)

Results of evaluation methods and core locations for this bridge are presented in **Figure 4.1**. **Figure 4.1a** illustrates the HRV results which were utilized along with IR images to differentiate delaminated areas from surface features such as discoloration, oil stains, sand, and rust deposits. Minimal patching was observed from the HRV image. Infrared thermography results are presented in **Figure 4.1b**. The red hatched area shows a delaminated region, the black hatched area shows a patched region, and the green area shows spalling. The patched area was reported as 0.5 % of the entire deck area based on IR results. No spalling was observed for this bridge. Chain dragging and DAR results are presented in **Figure 4.1c.** Chain dragging was conducted between bents 1 and 2 and bents 4 and 5. The blue shaded areas show the delaminated region presented by chain dragging and the orange shaded areas depict the delaminated region presented by DAR. The summary result of IR-UTD is presented in **Figure 4.1d.**

There is very limited deep defect (yellow region) indicated in this bridge and most of the defects are related to shallow defects (red region) along the center line. The red areas indicate shallow depth defects or another characteristic such as water and moisture near the seams or joints. **Figures 4.1e and 41f** present results of the GPR investigation. **Figure 4.1e** is a contour map, which indicates three regions with different damage levels. The blue areas indicate regions with medium damage, pink regions severe damage, and white areas no damage. Cover depth contours are presented in **Figure 4.1f**. The average concrete cover was indicated as 2.7 in.

Chloride concentration testing and coring were conducted to supplement the rapid bridge evaluation methods. The profile of chloride concentration in terms of sample depth is presented in **Figure 4.2**. In this figure, the standard deviations of chloride concentration are indicated for regions with medium and severe damage except for the undamaged region (only one sample was taken). The average chloride concentration at the reinforcement level is also presented in **Figure 4.3**. The reinforcement level for each level of damage was considered based on the cover depth contour (**Figure 4.1f**). According to **Figure 4.3**, a correlation between chloride concentration and cover depth is observable. The chloride concentration at the reinforcement level increases as the cover depth decreases. Moreover, the chloride concentration for the severely damaged regions is higher, on average, than the other two regions, which supports the GPR results. However, the GPR contour for the medium and no damage regions do not correlate with the chloride results (**Figure 4.3**).

Chloride ranges were defined for the severe, medium, and no damage regions based on the chloride concentration test results for this bridge. The ranges of 0.1 to 0.16, 0.05 to 0.1, and 0 to 0.05 were

considered for severe, medium, and no damage, respectively. The accuracy percentage for GPR results was calculated using the powder samples taken, the average chloride concentration at the reinforcement level for each sample, and the defined chloride concentration ranges. The chloride concentration percentage for medium and no damage regions were not within the defined chloride concentration ranges. Therefore, the accuracy percentage for GPR was calculated two times; first using the powder samples of only the severe damage region and second for the powder samples of the three regions. 50% of the samples taken in the severely damaged region were within the defined range at the reinforcement level. The total accuracy percentage, considering all chloride samples taken from the three regions, is 33%.

Results of visual inspection for the extracted cores are shown in **Table 4.1**. Average diameter, length, weight, number of pieces, presence of reinforcement, visible cracking, and delamination are reported. The cores were taken by either BDI/Infrasense or U. South Carolina as indicated in the last column. Photographs of the cores for severe, medium, and no damage regions are shown in **Figures 4.4, 4.5 and 4.6**.

The following formulation was utilized for quantifying the accuracy of the different methods in terms of delamination and defects (Robison and Tanner, 2011):

$$Accuracy\ percentage = \frac{Number\ of\ cores\ that\ correctly\ predicted\ the\ condition}{Total\ number\ of\ cores} \quad (4.1)$$

Vehicle mounted infrared thermography (**Figure 4.1b**): 50% of the cores taken from the areas predicted to have delamination (red cross hatched areas) demonstrated signs of delamination. 90% of the cores taken from areas predicted to have no delamination (white areas) were intact.

DAR (**Figure 4.1c**): 100% of the cores taken from areas predicted to have delamination (orange-shaded regions) demonstrated signs of delamination. 90% of the cores taken from areas predicted to have no delamination (white areas) were intact.

Chain dragging (**Figure 4.1c**): 50% of the cores taken from areas predicted to have delamination (blue areas) demonstrated signs of delamination. Because chain dragging was only conducted between bents 1 and 2 and bents 4 and 5 with no cores taken between bents 4 and 5, the accuracy percentage calculation is limited to the region between bents 1 and 2 and the severely damaged regions.

IR-UTD (**Figure 4.1d)**: Regions with defects are shown as yellow and red shaded regions (deep and shallow defects, respectively). The yellow regions are the discrete delaminated areas and the red regions are thought to be due to moisture along a seam or construction joint. Both shallow and deep defects were considered. 50% of the cores extracted from red regions demonstrated signs of delamination. 100% of the cores extracted from regions indicating no defects (non-shaded regions) were intact.

Percent accuracy for all methods based on chloride concentration and visual condition are presented in **Figure 4.7**. Percent accuracy for GPR was calculated based on the samples with chloride concentrations within the highest defined range (0.10 to 0.16%). Chloride concentration for other samples do not follow the expected trend in the GPR results. The accuracy for chain

dragging was calculated based on the cores taken from the severely damaged regions, since chain dragging was not conducted in cored locations in the medium and no damage regions.

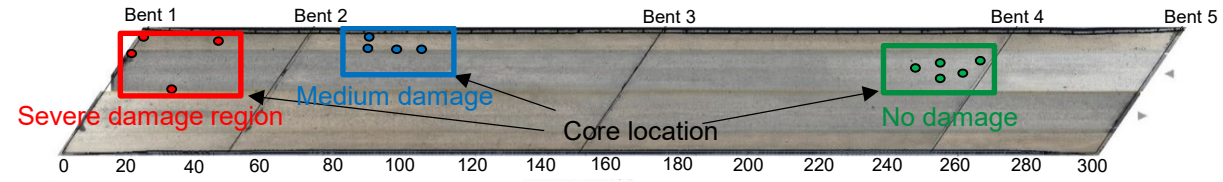

a) Vehicle mounted high resolution video

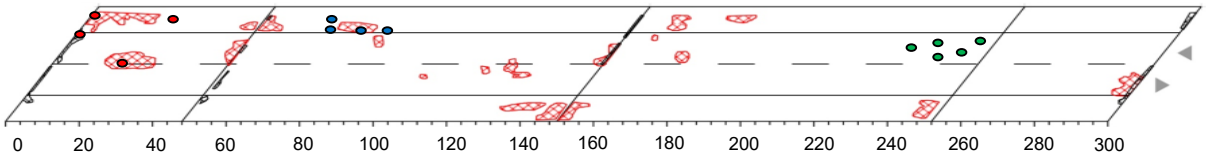

b) Vehicle mounted infrared thermography

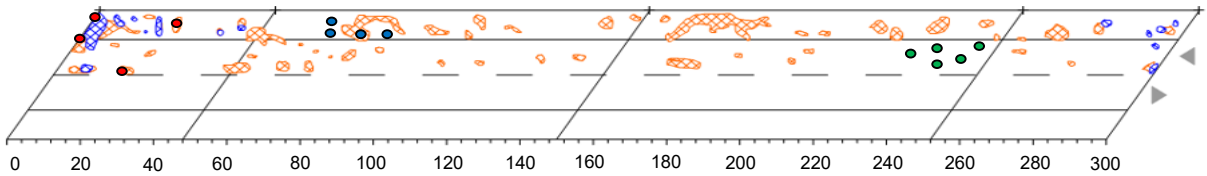

c) Chain dragging and DAR

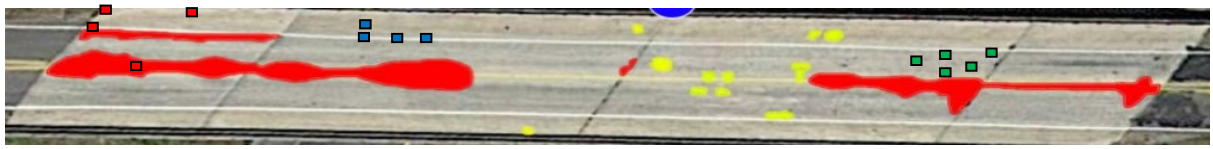

d) Pole mounted IR-UTD

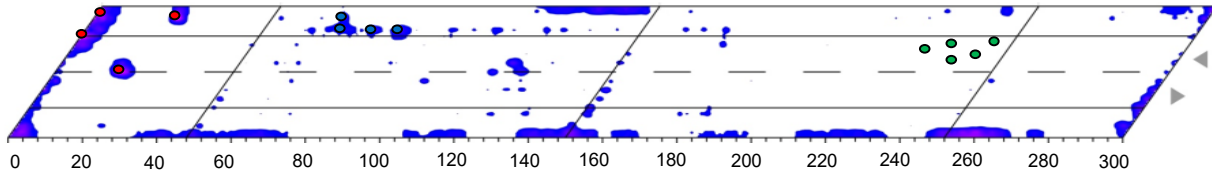

e) Vehicle mounted ground penetrating radar

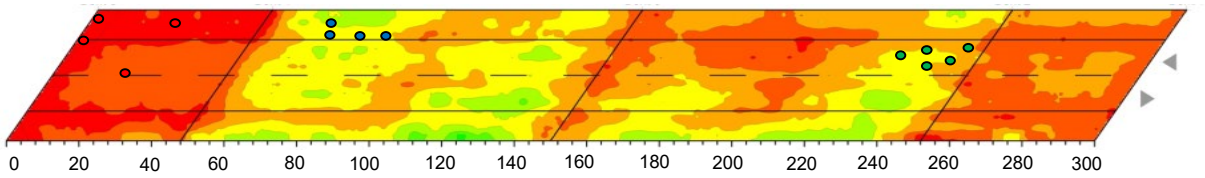

f) Concrete cover results (vehicle mounted GPR)

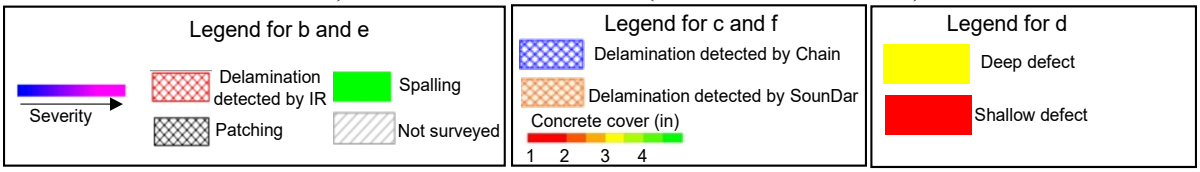

Figure 4.1: Evaluation method results, (S-34, Pond Branch Road over I-20, good condition; BDI/Infrasense Inc., 2017, ThermalStare, LLC., 2017) *(figure reproduced with permission)*

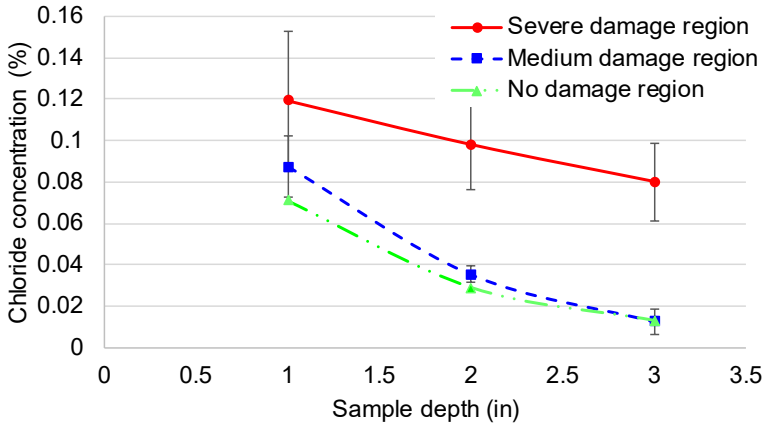

Figure 4.2: Chloride concentration results
(S-34, Pond Branch Road over I-20, good condition)

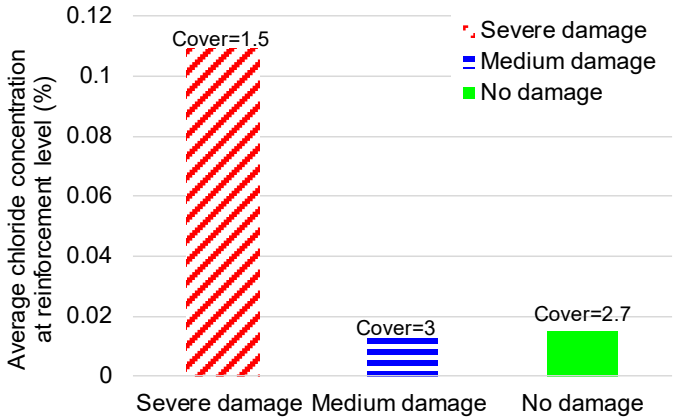

Figure 4.3: Average chloride concentration at reinforcement level
(S-34, Pond Branch Road over I-20, good condition)

Table 4.1: Characteristics of cores (S-34, Pond Branch Road over I-20, good condition)

Core	Diameter (in)	Length (in)	Weight (lb.)	Number of pieces	Rebar	Visible crack	Delamination	Taken by
S-34-S1	2.2	4.3	1.25	2	No	Yes	Yes	BDI
S-34-S2	2.2	2.0	0.60	2	No	Yes	Yes	BDI
S-34-S3	2.2	2.5	0.85	1	No	Yes	Yes	BDI
S-34-S4	2.3	1.3	0.40	7	Yes	Yes	Yes	BDI
S-34-M1	2.2	5.3	1.70	1	No	No	No	BDI
S-34-M2	2.2	5.3	1.65	1	No	No	No	BDI
S-34-M3	2.2	5.4	1.70	1	No	No	No	BDI
S-34-M4	2.2	5.9	1.90	1	No	No	No	BDI
S-34-N1	2.2	2.8	0.90	2	No	No	No	BDI
S-34-N2	2.3	4.0	1.30	1	No	No	No	BDI
S-34-N3	2.3	5.5	1.85	1	No	No	No	USC
S-34-N4	2.3	4.6	1.60	1	Yes	No	No	USC
S-34-N5	2.2	2.7	0.80	1	No	No	No	USC
S-34-N6	2.3	6.1	2.05	1	No	No	No	USC

a) S-34-S1

b) S-34-S2

c) S-34-S3

d) S-34-S4

Figure 4.4: Cores taken from 'severe damage' region (S-34, Pond Branch Road over I-20, good condition)

a) S-34-M1 **b) S-34-M2** **c) S-34-M3** **d) S-34-M4**

Figure 4.5: Cores taken from 'meduim damage' regions (S-34, Pond Branch Road over I-20, good condition)

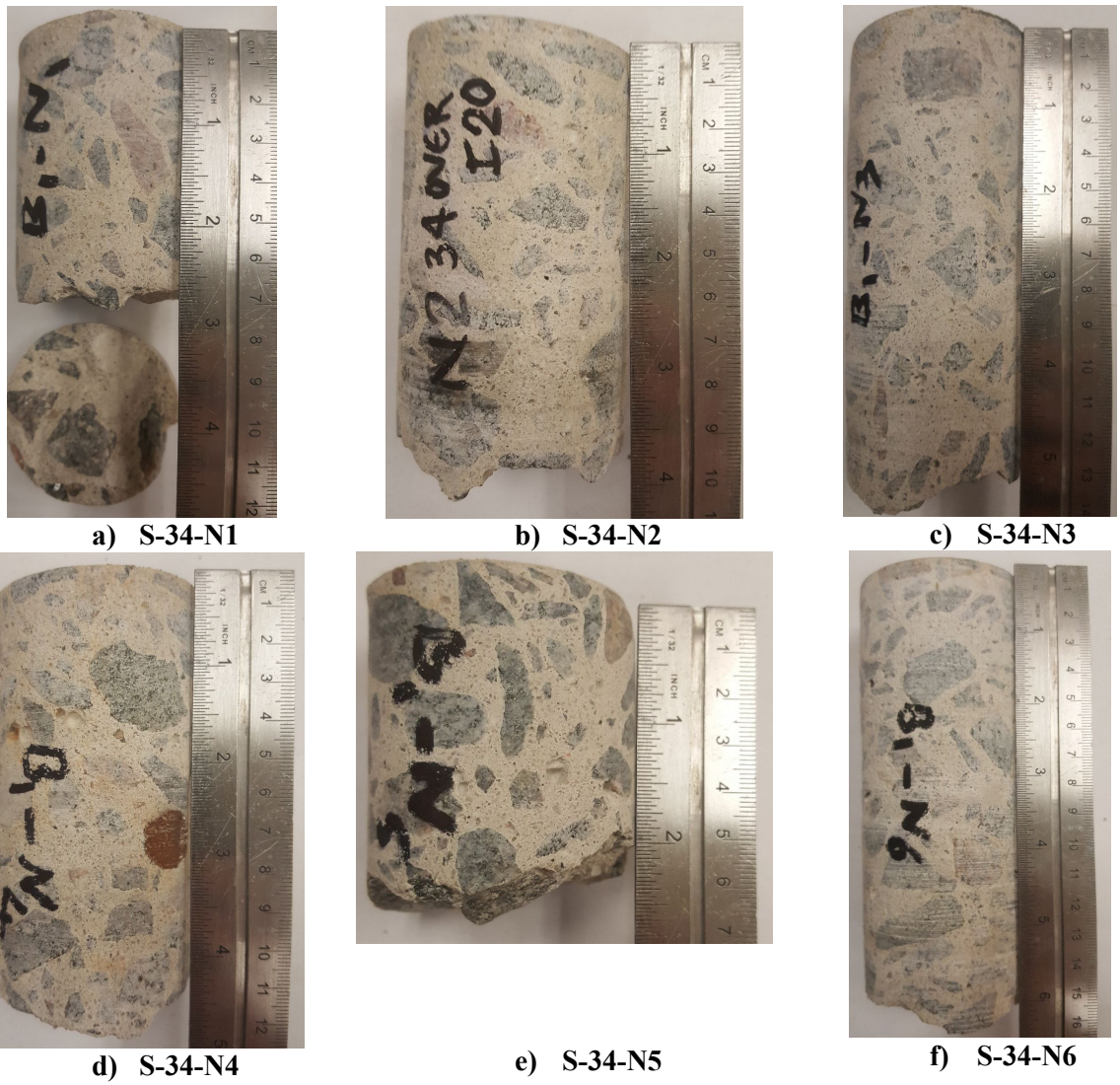

a) S-34-N1 b) S-34-N2 c) S-34-N3

d) S-34-N4 e) S-34-N5 f) S-34-N6

Figure 4.6: Cores taken from 'no damage' region (S-34, Pond Branch Road over I-20, good condition)

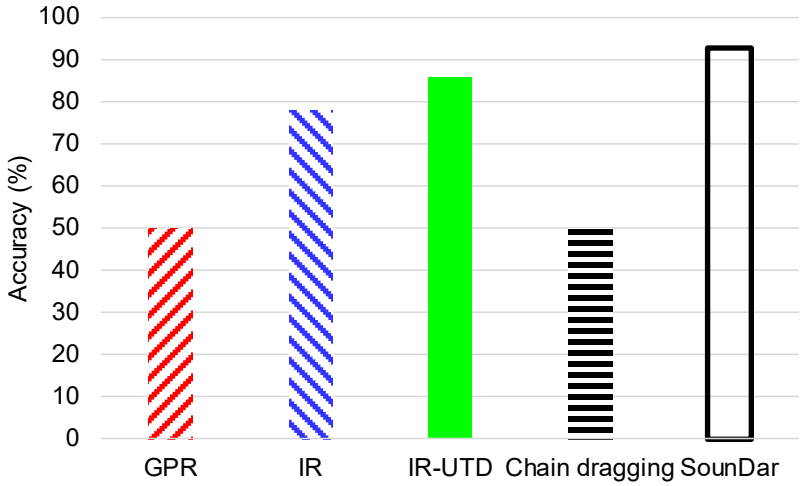

Figure 4.7: Accuracy of evaluaton methods
(S-34, Pond Branch Road over I-20, good condition)

Results of carbonation tests are presented in **Table 4.2**. The average depth of carbonation for several points around each core was calculated and reported. The largest and smallest depths are also reported. The last column (general comments) provides additional explanation regarding the test results. The carbonation depth for core S-34-M1 was not continuous around the core, but rather is limited to one or two core sides (limited carbonated region). The carbonated region was continuous in core S-34-M3. Most of the cores taken did not demonstrate signs of carbonation.

Table 4.2: Carbonation results (S-34, Pond Branch Road over I-20, good condition)

Core	Avg. depth (in)	Max depth (in)	Minimum depth (in)	General comments
S-34-S1	-	-	-	No carbonation
S-34-S1	-	-	-	No carbonation
S-34-S4	-	-	-	No carbonation
S-34-M1	0.08	0.12	0.04	Limited region
S-34-M2	-	-	-	No carbonation
S-34-M3	0.15	0.24	0.08	Continuous
S-34-M4	-	-	-	No carbonation
S-34-N1	-	-	-	No carbonation
S-34-N2	-	-	-	No carbonation
S-34-N3	-	-	-	No carbonation
S-34-N4	-	-	-	No carbonation
S-34-N5	0.18	0.20	0.16	Limited region
S-34-N6	-	-	-	No carbonation

Density, absorption, and volume of permeable pore space (voids) were calculated in general conformance with ASTM C642 (2006). Results are presented in **Table 4.3**. Only three cores met the conditions required per ASTM for the absorption test. A correlation exists between absorption (after immersion and boiling) and void percentage, where cores with a higher void percentage have

a higher absorption rate. The void percentage for the core taken from the region with medium damage (S-34-M4) demonstrated a higher value than the cores for the no damage region (S-34-N3 and S-34-N6). This may contribute to the higher chloride concentration for the region with medium damage (according to GPR contour) compared to the no damage region at the reinforcement level.

Table 4.3: Absorption and void test results (S-34, Pond Branch Road over I-20, good condition)

	Absorption after immersion (%)	Absorption after immersion and boiling (%)	Bulk density, dry (lb./ft^3)	Voids (%)
S-34-M4	4.98	6.33	136	13.7
S-34-N3	4.11	4.69	141	10.6
S-34-N6	4.07	4.93	141	11.1

4.2 S-106, Mineral Springs Road over I-20 (poor condition)

The results of rapid and traditional methods for the bridge deck located at S-106, Mineral Springs Road over I-20, are presented in **Figure 4.8**. **Figure 4.8a** shows HRV results indicating several patched locations between bents 1 and 2. Vehicle mounted infrared thermography results are presented in **Figure 4.8b**, with the area of patching (red hatched area) reported as 11.1% of the deck area. Minimal spalling is observed in this bridge (green regions, **Figure 4.8b**). Based on vehicle mounted IR, 6.7% of the bridge deck predicted to be delaminated. Chain dragging and DAR results are indicated in **Figure 4.8c.** Chain dragging was conducted between bents 3 and 4. The blue shaded areas show delaminated regions indicated through chain dragging and the orange shaded area depicts delaminated regions indicated through DAR. IR-UTD scanning was not conducted for this bridge deck. **Figures 4.8d** and **4.8e** present the vehicle mounted GPR results. **Figure 4.8d** is a contour map indicating three regions with different damage levels. The blue regions indicate regions with medium damage, pink regions severe damage, and white regions indicate no damage. Cover depth contours are presented in **Figure 4.8e**. The average cover for this bridge deck is 2.2 inches, which is lower than for bridge decks at S-34 Pond Branch Road over I-20 and US-21 Wilson Blvd over I-20.

Chloride concentration testing and coring were conducted to aid in assessment of the evaluation methods. The profile of chloride concentration in terms of sample depth is presented in **Figure 4.9** as the average chloride concentration for each region (severe, medium, and no damage regions based on GPR results) along with the associated standard deviation. The average chloride concentration at the reinforcement level and the average concrete cover for the locations, where the powder samples were taken, are presented in **Figure 4.10**. The reinforcement level for each damage region was selected based on the cover depth contour (**Figure 4.8e**). The samples taken from the region with the lowest concrete cover have the largest chloride concentration at the reinforcement level, and the samples taken from the region with the largest concrete cover demonstrated the lowest chloride concentration at the reinforcement level, although they were in the region indicating medium damage. The measured chloride concentrations were generally small. The chloride concentration level for regions with severe damage at reinforcement level was, on average, more than the other regions.

To calculate the accuracy of GPR based on chloride concentration ranges were defined for the three regions. The ranges were selected based on the test results of this bridge for regions with severe, medium, and no damage (0.045 to 0.070, 0.022 to 0.045, and 0 to 0.022, respectively). The accuracy percentages were calculated according to the powder samples taken from different regions, average chloride concentration at the reinforcement level, and the chloride concentration ranges. 100% of the samples taken from the severely damaged region are within the defined range at the reinforcement level. 75% of the samples taken from the region with medium damage were within the defined chloride concentration range, and 0% of the samples taken from the no damage region were within the defined range. The total percentage of accuracy, based on samples taken in the three regions, was 58%.

Visual inspection results for the cores are presented in **Table 4.4**. Average diameter, length, weight, number of pieces, presence of rebar, visible cracking, and delamination are reported. The last column indicates whether the core was extracted by BDI or U. South Carolina. Pictures of cores for severe, medium, and no damage are illustrated in **Figures 4.11, 4.12 and 4.13,** respectively. Equation (4) was utilized for quantifying the accuracy of the bridge evaluation methods in terms of delamination and defects.

Vehicle mounted infrared thermography (**Figure 4.8b**): Delamination was observed in none (0%) of the cores extracted from areas predicted to have delamination (red shaded region). Delamination was not observed in any cores extracted from areas predicted to have no delamination (white areas).

DAR (**Figure 4.8c**): Delamination was observed in 80% of the cores extracted from areas predicted to have delamination (orange shaded regions). Delamination was not observed in any cores extracted from areas predicted to have no delamination (white areas).

Chain dragging: This method was only conducted between bents 3 and 4 where no cores were extracted (**Figure 4.8c**). Therefore, calculating the accuracy percentage is not feasible.

Percent accuracy was calculated according to chloride concentration and visual assessment of the cores (**Figure 4.14**). Accuracy for vehicle mounted GPR was calculated based on the chloride concentrations within the highest defined range (0.045 to 0.070) as other samples did not follow the expected trend for the medium and no damage regions. IR-UTD was not conducted on this bridge.

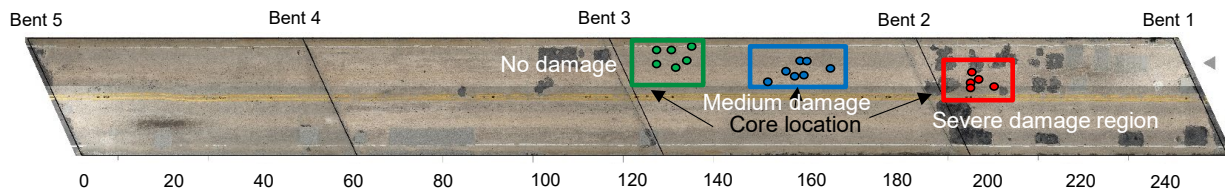

a) Vehicle mounted high resolution video

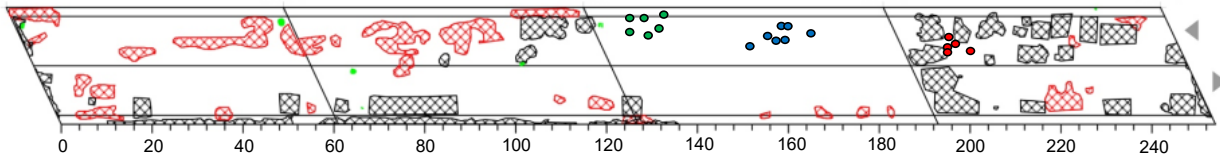

b) Vehicle mounted infrared thermography

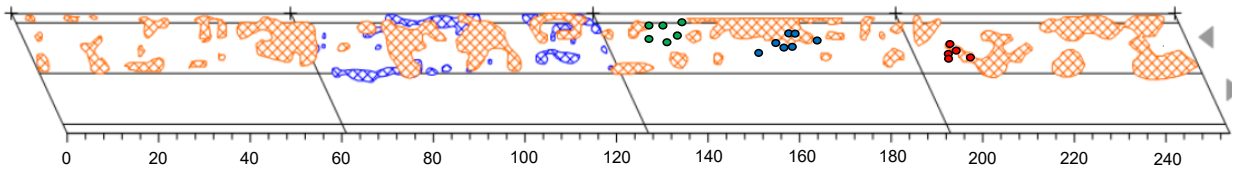

c) Chain dragging and DAR

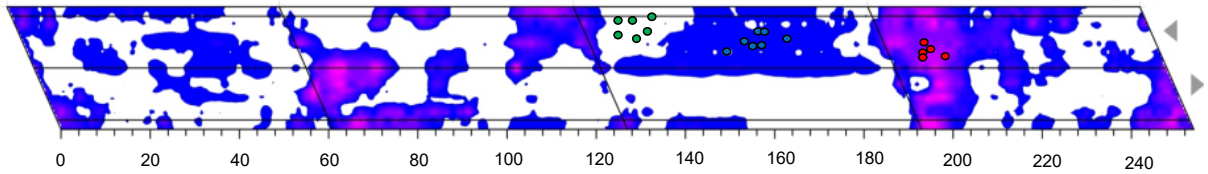

d) Vehicle mounted ground penetrating radar

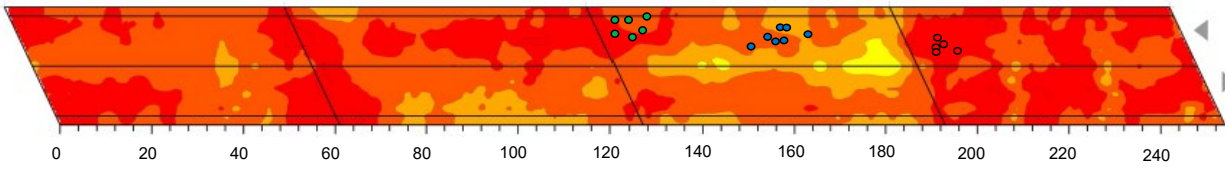

e) Concrete cover results (Vehicle mounted GPR)

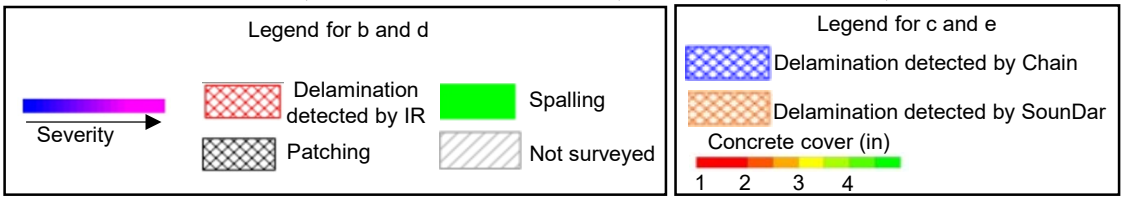

Figure 4.8: Evaluation method results, (S-106, Mineral Springs Road over I-20, poor condition) (BDI/Infrasense Inc., 2017) *(figure reproduced with permission)*

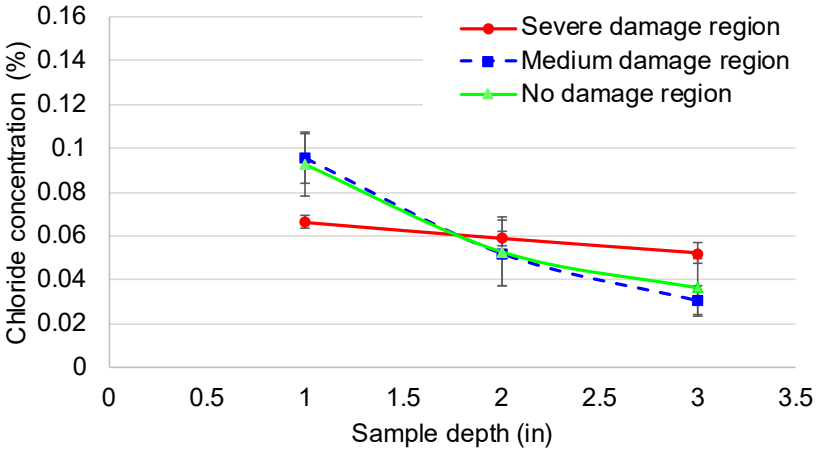

Figure 4.9: Chloride concentration results
(S-106, Mineral Springs Road over I-20, poor condition)

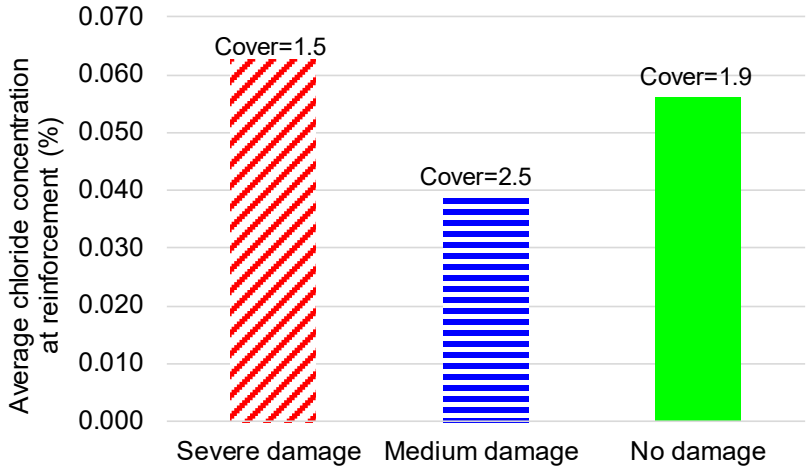

Figure 4.10: Average chloride concentration at reinforcement level
(S-106, Mineral Springs Road over I-20, poor condition)

Table 4.4: Characteristics of cores (S-106, Mineral Springs Road over I-20, poor condition)

Core	Diameter (in)	Length (in)	Weight (lb.)	Number of pieces	Rebar	Visible crack	Delamination	Taken by
S-106-S1	2.24	5.46	1.85	2	Yes	No	Yes	BDI
S-106-S2	2.25	5.71	1.90	1	No	No	No	BDI
S-106-S3	2.24	4.98	1.65	1	No	No	No	BDI
S-106-S4	2.25	4.91	1.60	2	No	No	Yes	BDI
S-106-S5	2.30	2.89	0.95	2	No	No	Yes	BDI
S-106-M1	2.30	3.57	1.20	1	No	No	Yes	BDI
S-106-M2	2.31	4.63	1.35	1	No	No	No	BDI
S-106-M3	2.31	4.90	1.60	1	No	No	No	BDI
S-106-M4	2.30	3.14	1.00	1	No	No	Yes	BDI
S-106-M5	2.31	4.41	1.45	1	No	No	No	BDI
S-106-M6	2.31	4.78	1.65	1	No	No	No	USC
S-106-M7	2.30	5.24	1.80	1	No	No	No	USC
S-106-N1	2.31	4.61	1.40	1	No	No	No	BDI
S-106-N2	2.31	4.78	1.65	1	No	No	No	BDI
S-106-N3	2.31	4.83	1.55	1	No	No	No	BDI
S-106-N4	2.31	4.44	1.55	1	No	No	No	BDI
S-106-N5	2.31	4.19	1.40	1	No	No	No	USC
S-106-N6	2.31	5.69	1.90	1	No	No	No	USC

a) S-106-S1

b) S-106-S2

c) S-106-S3

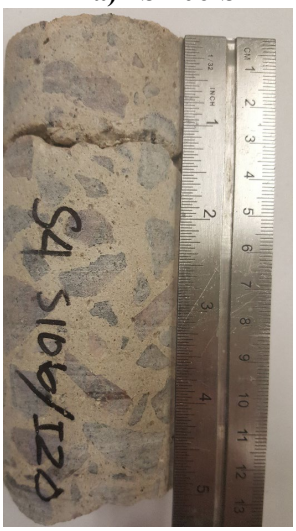

d) S-106-S4

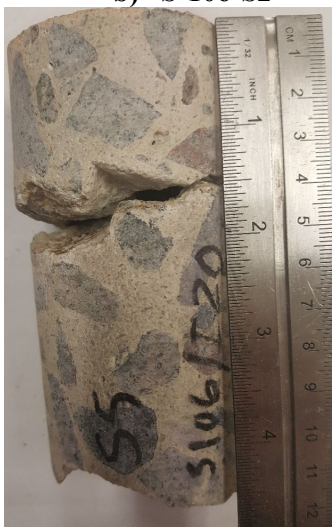

e) S-106-S5

Figure 4.11: Cores taken from 'severe damage' region (S-106, Mineral Springs Road over I-20, poor condition)

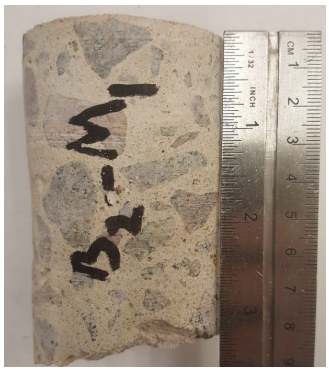

a) S-106-M1

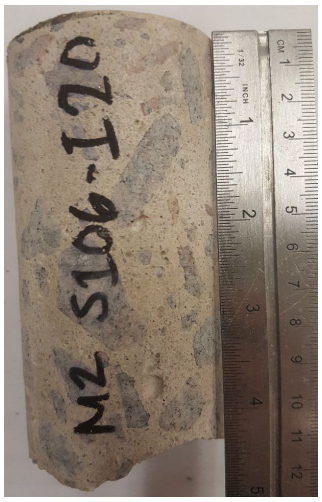

b) S-106-M2

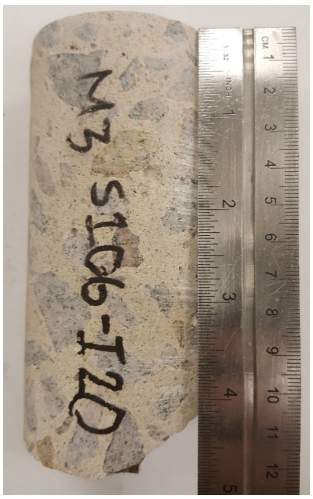

c) S-106-M3

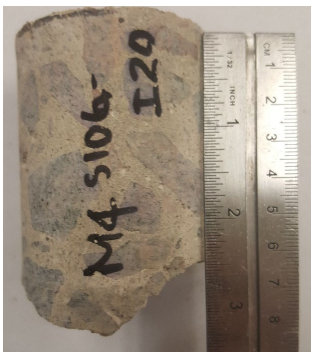

d) S-106-M4

e) S-106-M5

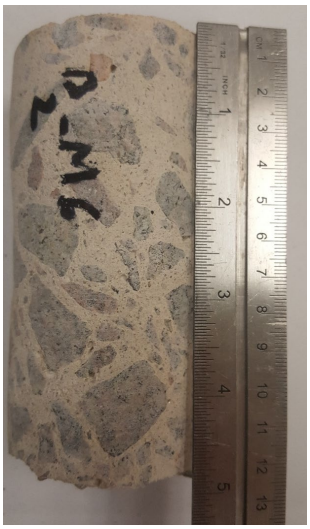

f) S-106-M6

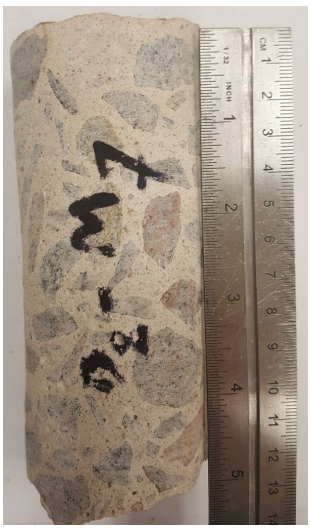

g) S-106-M7

Figure 4.12: Cores taken from 'meduim damage' region (S-106, Mineral Springs Road over I-20, poor condition)

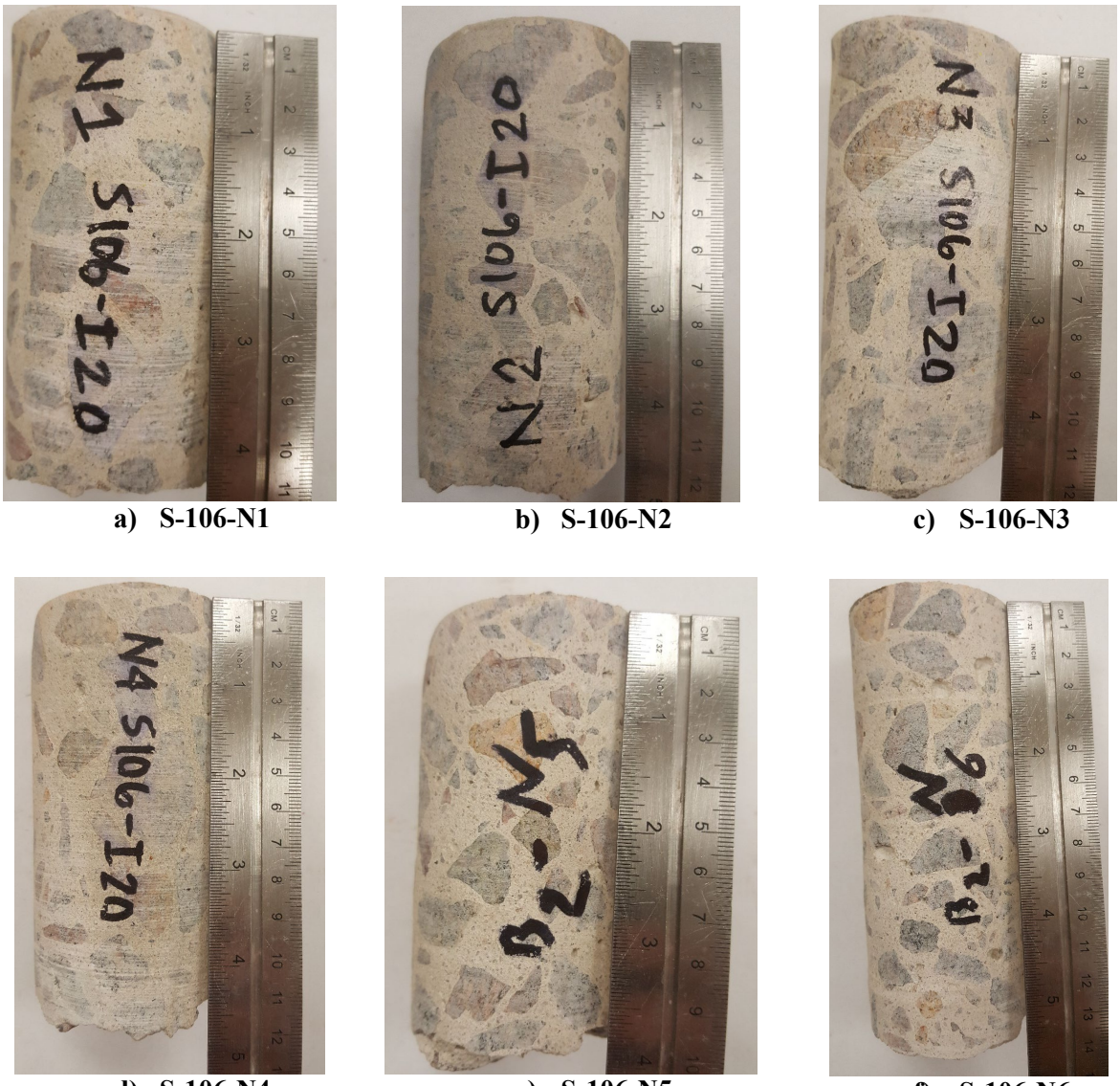

a) S-106-N1 b) S-106-N2 c) S-106-N3

d) S-106-N4 e) S-106-N5 f) S-106-N6

Figure 4.13: Cores taken from 'no damage' region
(S-106, Mineral Springs Road over I-20, poor condition)

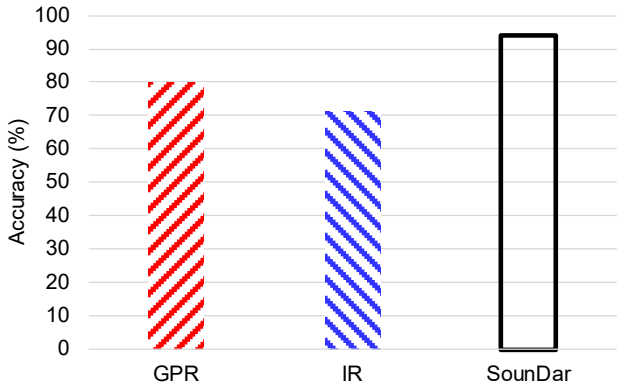

Figure 4.14: Accuracy of evaluaton methods
(S-106, Mineral Springs Road over I-20, poor condition)

Carbonation test results are presented in **Table 4.5**. Average depth of carbonation for several points around the cores is reported as carbonated depth was not constant. The largest and smallest carbonated depths are also reported. The carbonation depth for cores S-106-S1 and S-106-S2 was not continuous around the core. The carbonated region was continuous in the other cores. One core (S-106-S3) did not demonstrate signs of carbonation.

Table 4.5: Characteristics of cores (S-106, Mineral Springs Road over I-20, poor condition)

Core	Avg. depth (in)	Maximum depth (in)	Minimum depth (in)	General comments
S-106-S1	0.27	0.59	0.079	Limited carbonation
S-106-S2	0.13	0.20	0.079	Limited carbonation
S-106-S3	-	-	-	No carbonation
S-106-S5	0.16	0.63	0.059	Continuous carbonation
S-106-M1	0.22	0.32	0.079	Continuous carbonation
S-106-M2	0.26	0.39	0.12	Continuous carbonation
S-106-M3	0.31	0.63	0.079	Continuous carbonation
S-106-M4	0.28	0.51	0.12	Continuous carbonation
S-106-M5	0.27	0.35	0.12	Continuous carbonation
S-106-M6	0.35	0.61	0.20	Continuous carbonation
S-106-M7	0.30	0.55	0.12	Continuous carbonation
S-106-N1	0.40	0.67	0.12	Continuous carbonation
S-106-N2	0.25	0.47	0.12	Continuous carbonation
S-106-N3	0.28	0.79	0.12	Continuous carbonation
S-106-N4	0.24	0.51	0.079	Continuous carbonation
S-106-N5	0.28	0.51	0.079	Continuous carbonation
S-106-N6	0.22	0.59	0.079	Continuous carbonation

Density, absorption, and volume of permeable pore space (voids) were calculated in general conformance with ASTM C642 (2006). Results are presented in **Table 4.6**. Three cores met the conditions required for the absorption test per ASTM. Core S-106-M7 had the lowest absorption

and void percentage, which may help to explain the low chloride concentration associated with the medium damage region (vehicle mounted GPR). Core S-106-N6 had the highest absorption and void percentage. This may be one cause for the higher chloride concentration in the no damage region when compared to the medium damage region.

Table 4.6: Absorption and void test results (S-106, Mineral Springs Road over I-20, poor condition)

	Absorption after immersion (%)	Absorption after immersion and boiling (%)	Bulk density, dry (lb./ft3)	Voids (%)
S-106-S2	4.71	5.16	140	11.6
S-106-M7	3.81	4.86	140	10.9
S-106-N6	4.59	5.49	139	12.2

4.3 US-21, Wilson Boulevard over I-20 (poor condition)

Results for the bridge deck located at US-21, Wilson Blvd over I-20 are presented in **Figure 4.15**. The vehicle mounted HRV results (**Figure 4.15a)** indicate several patched locations, especially between bents 3 and 4 and bents 4 and 5. Vehicle mounted infrared thermography results are presented in **Figure 4.15b**, with the red hatched area indicating a delaminated region and the black hatched area indicating a patched area (reported to be 20.7% of the deck area). Minimal spalling was observed. 3.4% of the bridge deck was indicated as delamination based on vehicle mounted IR. Chain dragging and DAR results are shown in **Figure 4.15c.** Chain dragging was conducted between bents 2 and 3. The blue shaded areas show delaminated regions presented by chain dragging and the orange shaded area depicts delaminated regions indicated through DAR. Results of pole mounted IR-UTD are presented in **Figure 4.15d**, indicating several large patched regions (green). Next to the patches, discrete delaminated regions can be observed (yellow). Large delaminated regions were indicated between bents 2 and 3. **Figures 4.15e and 4.15f** present vehicle mounted GPR results. **Figure 4.15e** indicates three regions with different damage levels. The blue areas show medium damage regions, pink indicates areas with severe damage, and white indicates no damage. Cover depth is presented in **Figure 4.15f**, with average cover of 1.7 inches, which is the shallowest cover depth among the evaluated bridges.

Chloride concentration testing and coring were conducted to aid in assessing the accuracy of the evaluation methods. The chloride concentration profiles in terms of sample depth are presented in **Figure 4.16** with associated standard deviations. Average chloride concentrations at the reinforcement level and average concrete cover for the locations where the powder samples were taken are presented in **Figure 4.17**. The reinforcement level for each region was selected based on the cover depth contour (**Figure 4.15f**). Chloride concentrations for this bridge deck are low. The chloride concentration for severely damaged regions is higher on average than the two other regions. However, the GPR contour for medium and no damage regions does not correlate to chloride concentrations at the reinforcement level (**Figure 4.17**). Although concrete cover for the medium damage region is less than for the no damage region, the chloride concentration for the former is less than the no damage region at the reinforcement level. This may be associated with the fact that medium damage regions have been repaired and patched. Therefore, the medium damage regions have material which is more resistant to chloride penetration. To calculate the

accuracy of the GPR based on the chloride concentrations, three chloride concentration ranges were defined. The ranges of 0.12 to 0.18, 0.06 to 0.12, 0.00 to 0.06 were selected. Accuracy percentages were calculated according to the powder samples taken, the average chloride concentration at the reinforcement level for each sample, and the defined chloride concentration ranges. 50% of the samples taken in the severely damaged region were within the defined range at the reinforcement level. None (0%) of the samples taken from the region with medium damage were within the defined chloride concentration range, and 25% of the samples taken from the no damage region were within the defined range. Percent accuracy overall was 25% based on vehicle mounted GPR.

Visual inspection results for the cores is presented in **Table 4.7**. Average diameter, length, weight, number of pieces, presence of rebar, visible cracking, and delamination are reported. The cores were taken by either BDI or U. South Carolina as indicated in the last column. Photographs of cores for severe, medium, and no damage regions are shown in **Figures 4.18, 4.19 and 4.20**, respectively. Equation (4) was used for quantifying the accuracy of the different methods in terms of delamination and defects.

Vehicle mounted infrared thermography (**Figure 4.15b**): Delamination was observed in 67% of the cores extracted from areas indicating delamination (red shaded areas), and all cores extracted (100%) from the areas indicating no delamination were intact.

DAR (**Figure 4.15c**): Delamination was observed in 88% of the cores extracted from areas indicating delamination (orange shaded regions), and all cores extracted (100%) from areas indicating no delamination were intact (white areas).

Chain dragging (**Figure 4.15c**): Delamination was observed in all (100%) of the cores extracted from areas indicating delamination. Because chain dragging was only conducted between bents 2 and 3 accuracy is limited to this region.

Pole mounted IR-UTD: Regions with indications of defects are shown as yellow and red shaded regions (deep and shallow) in **Figure 4.15d**. Both shallow and deep defects were considered in the calculation of accuracy. Delamination was observed in 88% of the cores extracted from the yellow regions. 63% of the cores extracted from the no color regions were intact.

Percent accuracy for all evaluation methods was calculated according to the chloride concentrations and the visual condition of the cores (**Figure 4.21**). Accuracy for vehicle mounted GPR was calculated based on samples with chloride concentration within the highest defined range (0.12 to 0.18) because the samples did not follow expected trends in the medium and undamaged regions. The accuracy of chain dragging was calculated based on the cores taken between bents 2 and 3.

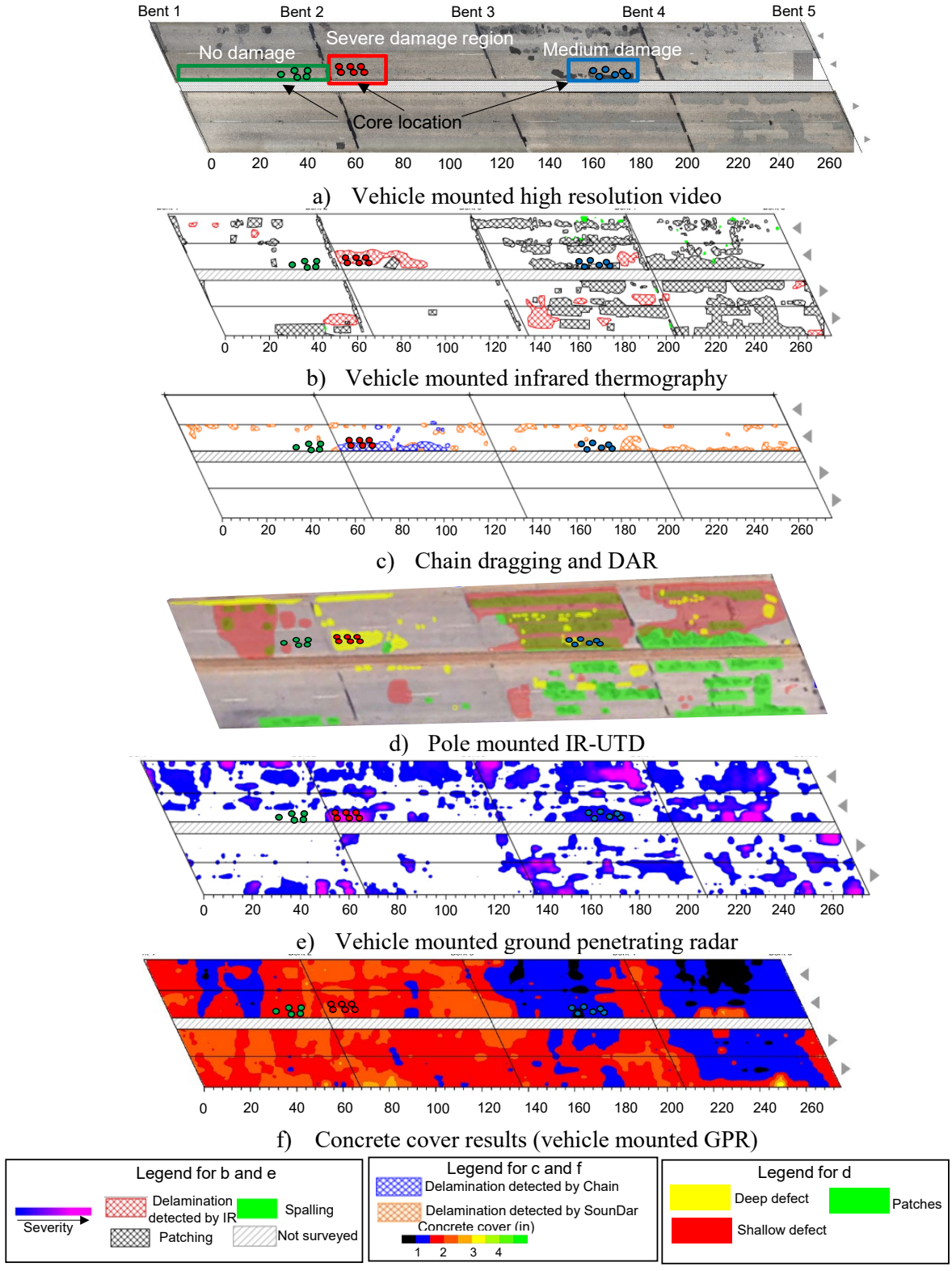

Figure 4.15: Evaluation method results, (US-21, Wilson Blvd over I-20, poor condition; BDI and Infrasense Inc., 2017, ThermalStare, LLC., 2017) *(figure reproduced with permission)*

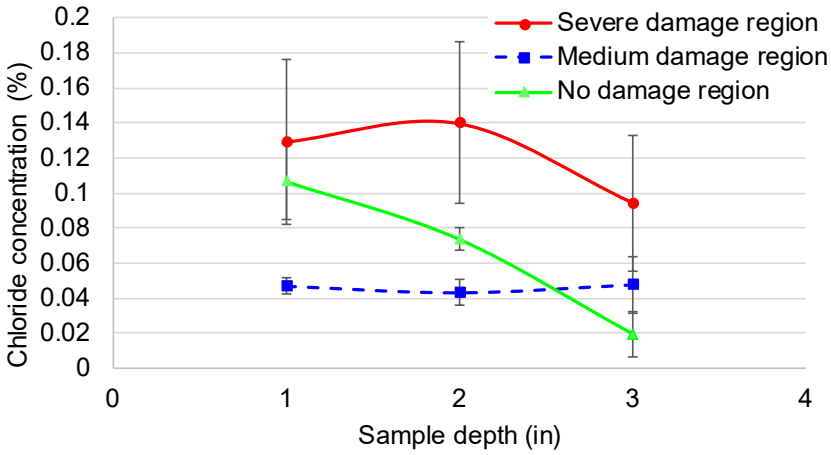

Figure 4.16: Chloride concentration results (US-21, Wilson Blvd over I-20, poor condition)

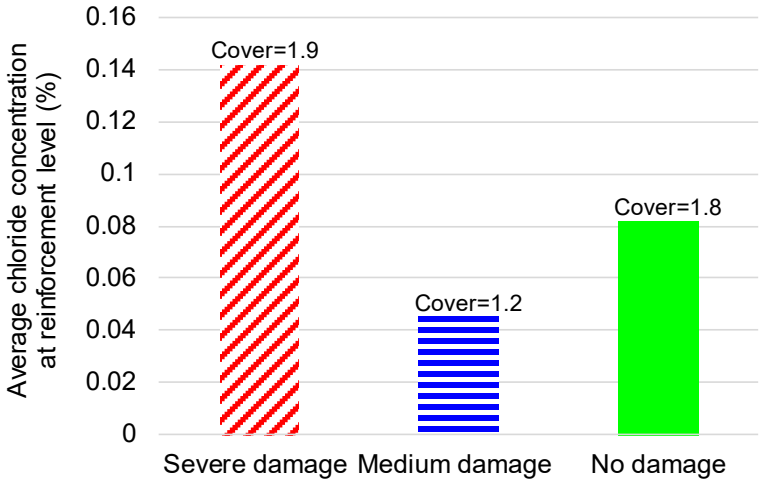

Figure 4.17: Average chloride concentration at level of reinforcement (US-21, Wilson Blvd over I-20, poor condition)

Table 4.7: Carbonation test results (US-21, Wilson Blvd over I-20, poor condition)

Core	Diameter (in)	Length (in)	Weight (lb.)	Number of pieces	Rebar	Visible crack	Delamination	Taken by
US-21-S1	2.72	4.70	2.15	2	No	Yes	Yes	BDI
US-21-S2	2.72	2.30	1.00	3	Yes	No	Yes	BDI
US-21-S3	2.72	2.32	1.05	5	Yes	Yes	Yes	BDI
US-21-S4	2.70	5.13	2.50	2	Yes	Yes	Yes	BDI
US-21-S5	2.31	2.23	0.95	2	Yes	No	Yes	USC
US-21-S6	2.31	4.94	1.95	2	Yes	No	Yes	USC
US-21-M1	2.72	4.28	2.20	1	No	No	No	BDI
US-21-M2	2.72	3.83	1.80	2	No	Yes	Yes	BDI
US-21-M3	2.72	4.69	2.30	1	No	Yes	No	BDI
US-21-M4	2.71	3.78	1.85	3	Yes	Yes	Yes	BDI
US-21-M5	2.72	4.22	2.10	1	No	No	No	BDI
US-21-M6	2.28	3.77	1.60	1	No	Yes	Yes	USC
US-21-N1	2.73	3.55	1.85	1	Yes	No	No	BDI
US-21-N2	2.73	4.36	2.10	1	No	No	No	BDI
US-21-N3	2.72	3.92	1.95	1	No	No	No	BDI
US-21-N4	2.31	4.52	1.75	1	Yes	No	No	USC
US-21-N5	2.31	4.11	1.70	1	Yes	No	No	USC

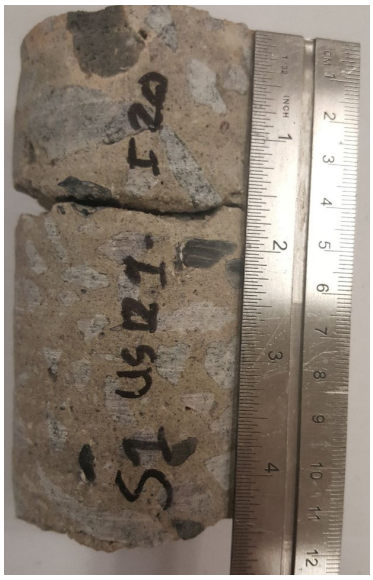

a) US-21-S1

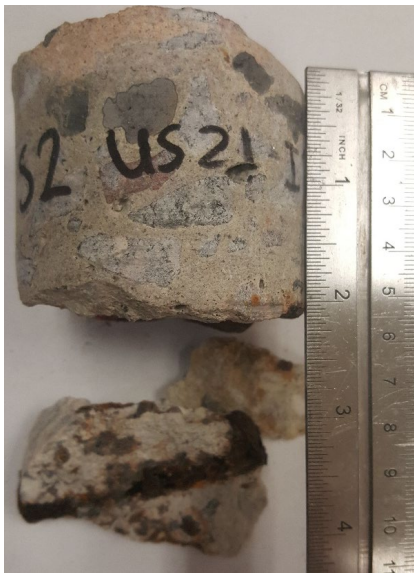

b) US-21-S2

c) US-21-S3

d) US-21-S4

e) US-21-S5

f) US-21-S6

Figure 4.18: Cores taken from 'severe damage' region (US-21, Wilson Blvd over I-20, poor condition)

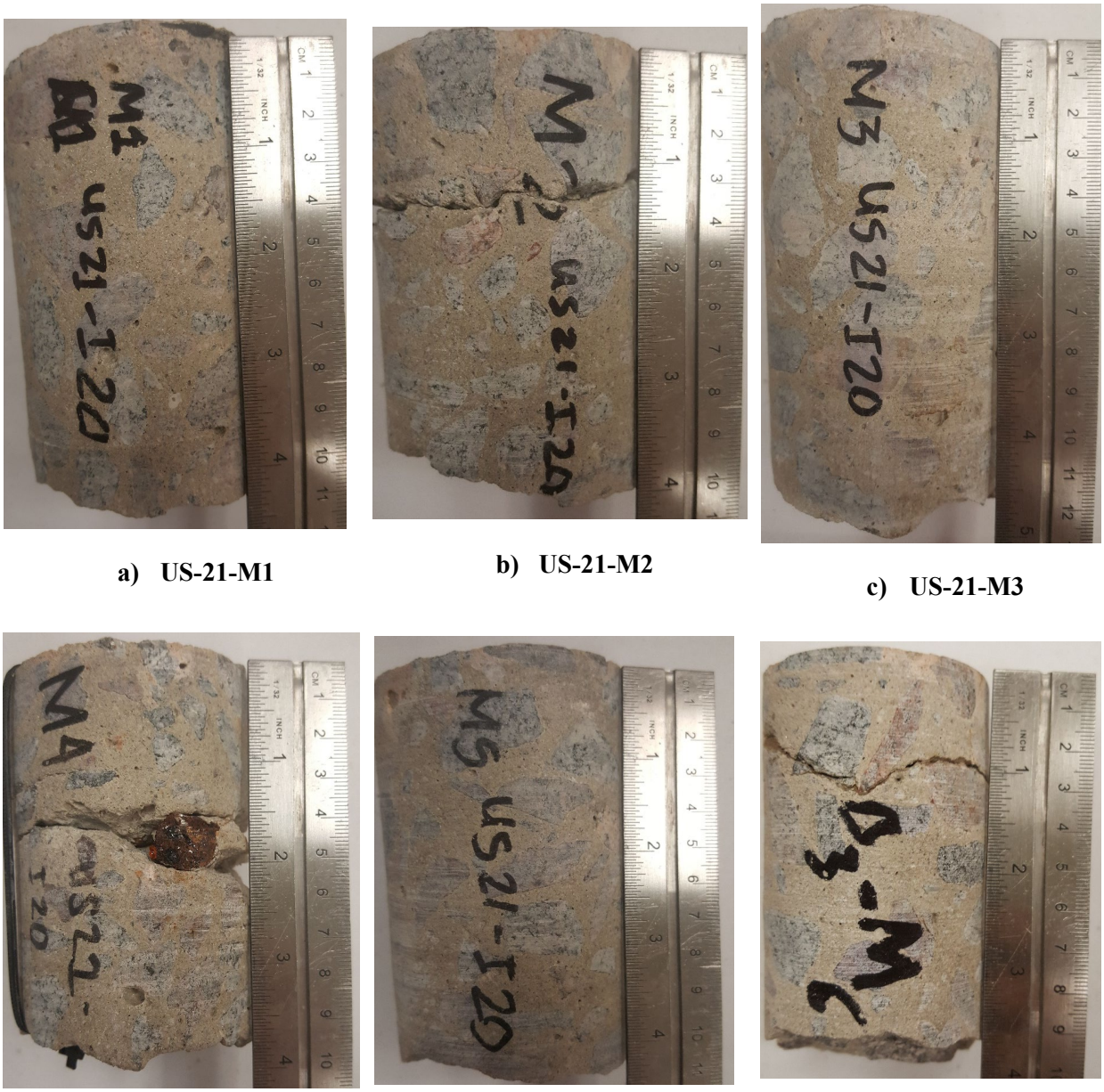

a) US-21-M1

b) US-21-M2

c) US-21-M3

d) US-21-M4

e) US-21-M5

f) US-21-M6

Figure 4.19: Cores taken from 'medium damage' region (US-21, Wilson Blvd over I-20, poor condition)

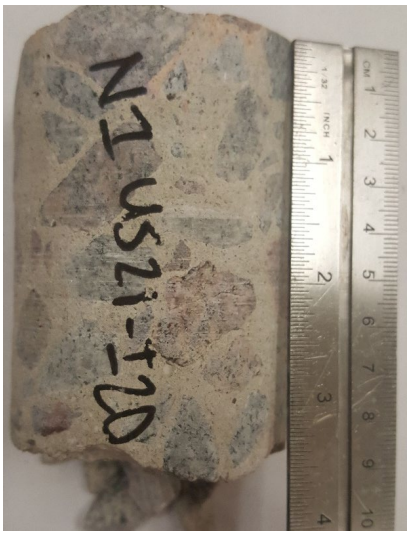

a) US-21-N1

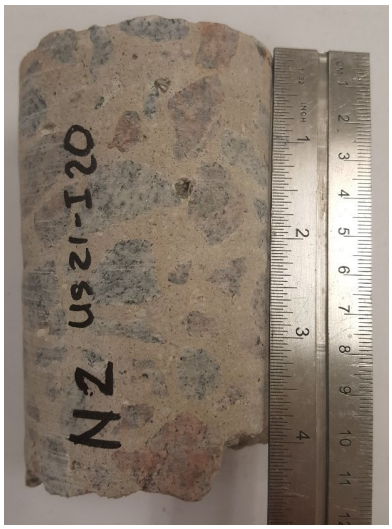

b) US-21-N2

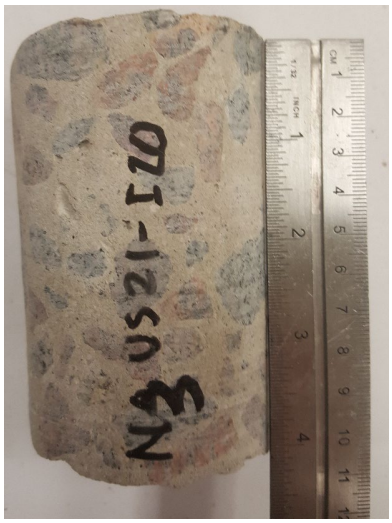

c) US-21-N3

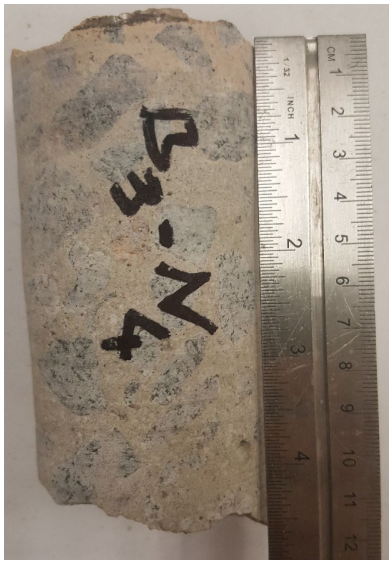

d) US-21-N4

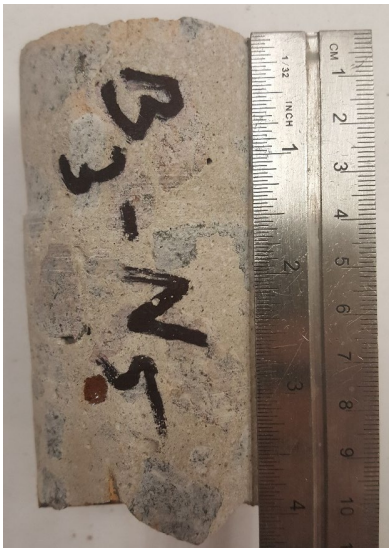

e) US-21-N5

Figure 4.20: Cores taken from 'no damage' region (US-21, Wilson Blvd over I-20, poor condition)

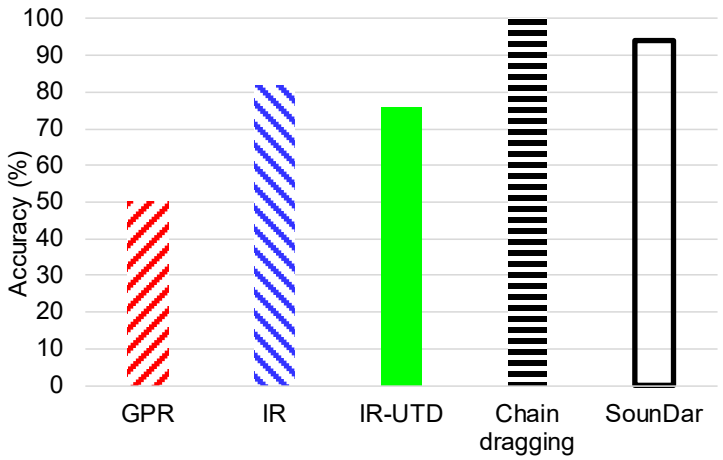

Figure 4.21: Accuracy of evaluaton methods (S-34, Pond Branch Road over I-20, poor condition)

Carbonation tests are presented in **Table 4.8**. Average depths of carbonation were calculated and reported for several points around the cores since the carbonated depth was not constant. Carbonation depth for core US-21-M4 was not continuous around the core but is limited to one or two core sides. The carbonated region was continuous in the other cores and most cores had indications of carbonation.

Table 4.8: Carbonation test results (US-21, Wilson Blvd over I-20, poor condition)

Core	Avg. depth (in)	Max depth (in)	Minimum depth (in)	General comments
US-21-S1	0.25	0.39	0.12	Continuous carbonation
US-21-S3	0.17	0.35	0.059	Continuous carbonation
US-21-S5	0.31	0.51	0.12	Continuous carbonation
US-21-S6	0.28	0.53	0.098	Continuous carbonation
US-21-M1	-	-	-	No carbonation
US-21-M2	-	-	-	No carbonation
US-21-M3	-	-	-	No carbonation
US-21-M4	0.25	0.37	0.098	Limited carbonation
US-21-M6	0.50	0.53	0.47	Continuous carbonation
US-21-N1	0.31	0.47	0.12	Continuous carbonation
US-21-N3	0.22	0.47	0.079	Continuous carbonation
US-21-N4	0.41	0.55	0.20	Continuous carbonation

Density, absorption, and volume of permeable pore space (voids) were calculated in general conformance with ASTM C642 (2006) (**Table 4.9**). Three cores met the conditions for the absorption test per ASTM. Cores US-21-M1 and US-21-M3 had lower void percentages than US-21-N3. The void percentage for US-21-M3 is in the same range as US-21-N3. The core US-21-M3 had a visible crack which may affect its absorption and void percentage. The higher value of absorption for the core located in the no damage region (US-21-N3) may be one potential

explanation for the higher chloride concentration in the no damage region compared to the medium damage region.

Table 4.9: Absorption and void test of US-21, Wilson Blvd over I-20

	Absorption after immersion (%)	Absorption after immersion and boiling (%)	Bulk density, dry (lb./ft3)	Voids (%)
US-21-M1	4.31	4.64	141	10.5
US-21-M3	4.67	5.02	139	11.2
US-21-N3	4.59	5.00	142	11.4

4.4 SC 555, Farrow Road over I-77 (medium condition)

Results for the bridge deck located at Farrow road over I-77 are presented in **Figures 4.22 and 4.23**. This bridge had an overlay performed by SCDOT in 2017 during the time of vehicle mounted scanning. **Figure 4.22** is related to the northbound lane and **Figure 4.23** is related to the southbound lane. **Figures 4.22a** and **4.23a** illustrate vehicle mounted HRV results. There were several locations of patching between bents 2 and 3 and bent 2 and the south abutment in the northbound lanes and between bents 2 and 3 and bents 3 and 4 in the southbound lanes. Results of vehicle mounted infrared thermography are presented in **Figures 4.22b** and **4.23b**. The red hatched area shows delaminated regions and the black hatched area shows regions of patching. Minimal spalling was observed. The patching areas as detected by vehicle mounted IR were reported as 9.4% and 21.8% of the northbound and southbound lanes, respectively. Furthermore, 17% of the northbound and 8.6% of the southbound lanes were assessed as delaminated regions by vehicle mounted IR. Chain dragging, DAR, and IR-UTD were not conducted on this bridge deck because the deck was replaced by an overlay. **Figures 4.22c and 4.22d** are related to vehicle mounted GPR results for the northbound lanes and **Figures 4.23c and 4.23d** illustrate vehicle mounted GPR results for the southbound lanes. **Figures 4.22c** and **4.23c** are contour maps indicating three regions with differing levels of damage. The blue regions correspond to medium damage, pink to severe damage, and regions correspond to regions with no damage. Cover depth contours are presented in **Figures 4.22d** and **4.23d**. Average covers are 2.5 and 2.6 inches for the northbound and southbound lanes, respectively.

Because the bridge was modified by an overlay during the project, concrete core samples and chloride powder samples were not taken. Therefore, accuracy of the methods was not assessed.

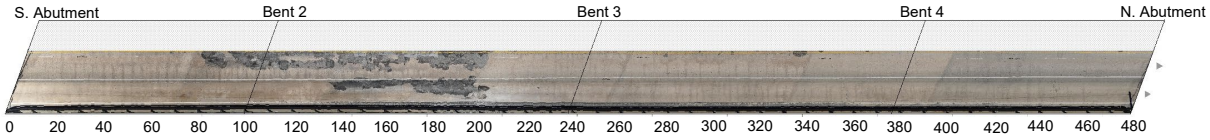

a) Vehicle mounted high resolution video

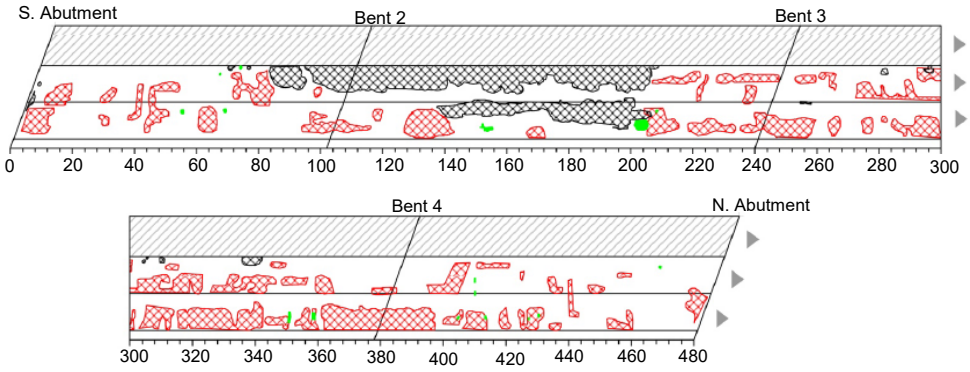

b) Vehicle mounted infrared thermography

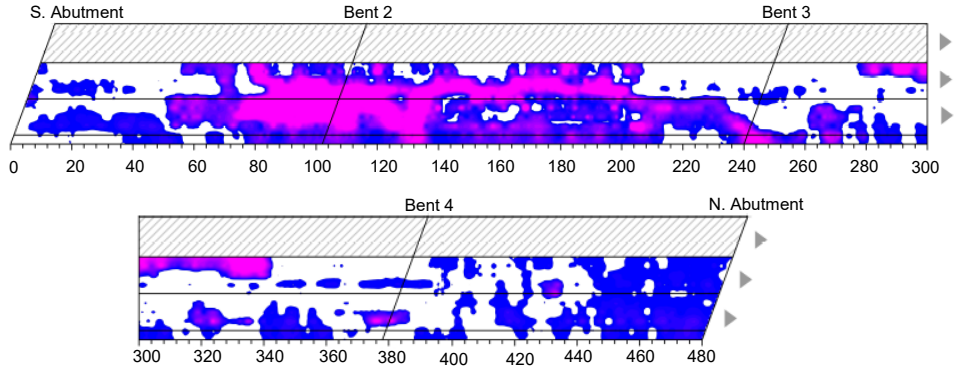

c) Vehicle mounted ground penetrating radar

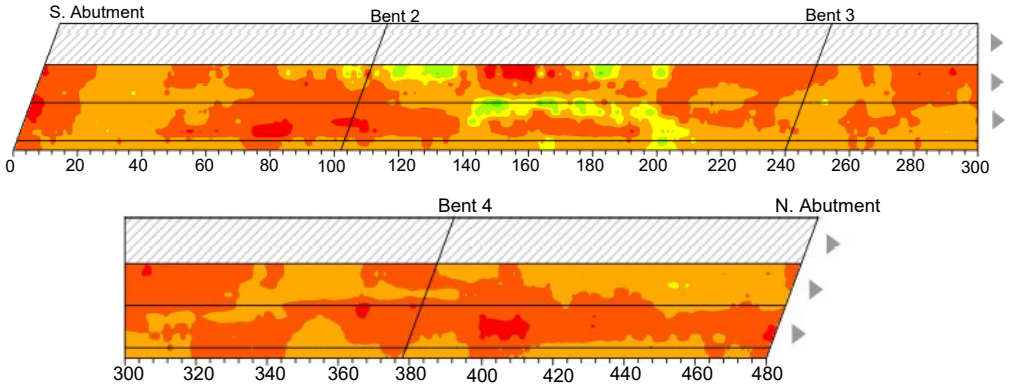

d) Concrete cover results (vehicle mounted GPR)

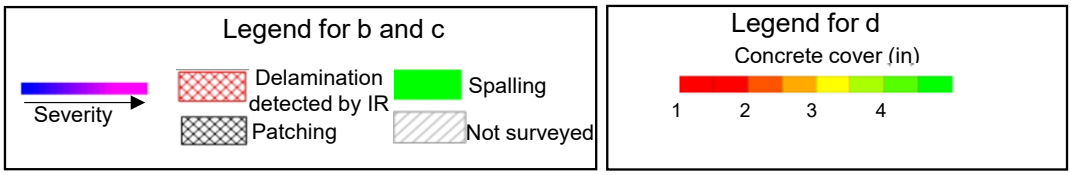

Figure 4.22: Evaluation method results (SC 555, Farrow road over I-77, Northbound, medium condition; BDI/Infrasense Inc., 2017)

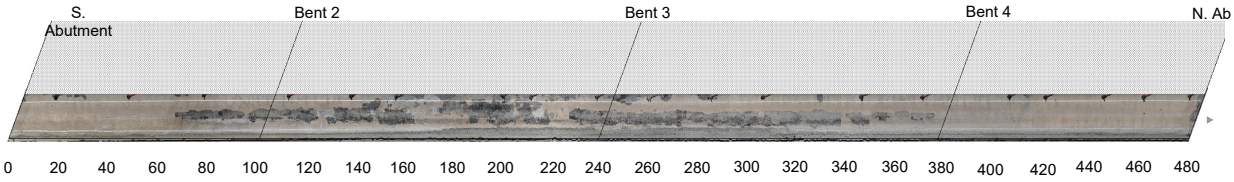

a) Vehicle mounted high resolution video

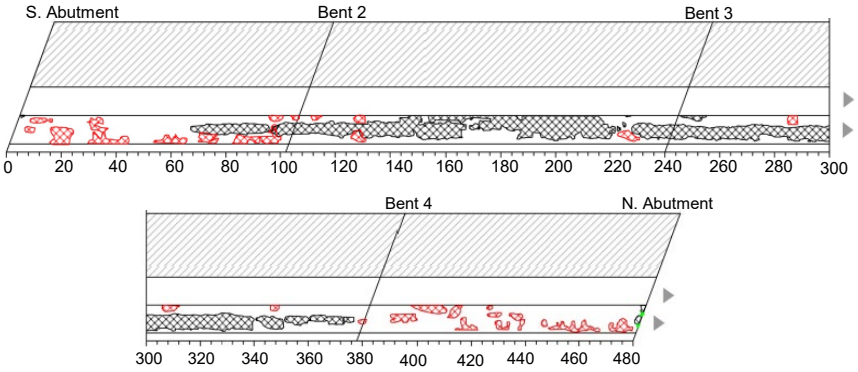

b) Vehicle mounted infrared thermography

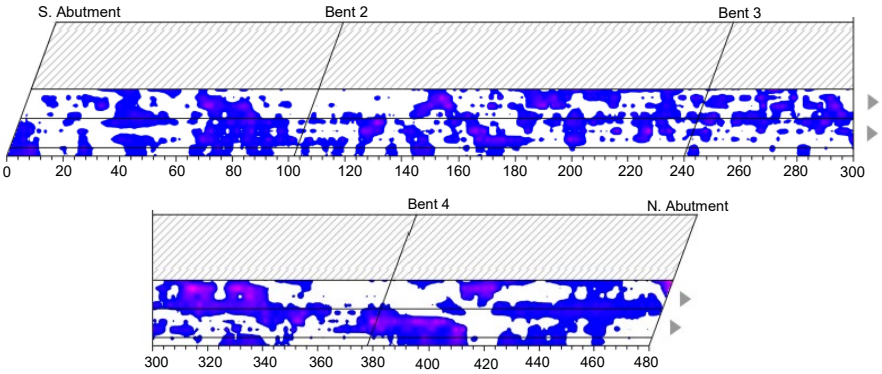

c) Vehicle mounted ground penetrating radar

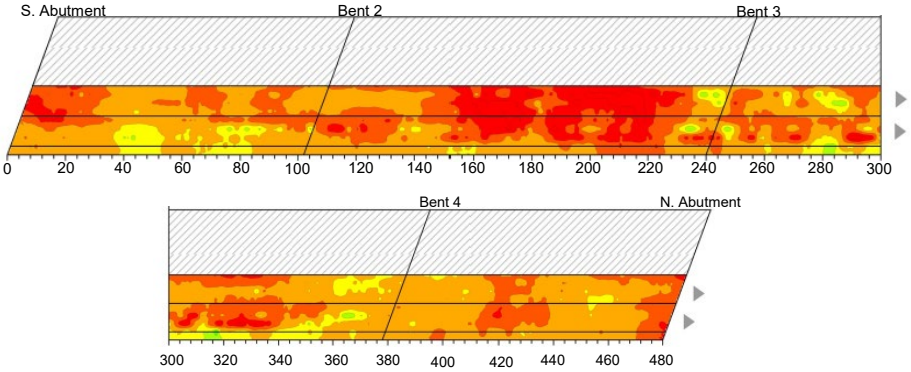

d) Concrete cover results (vehicle mounted GPR)

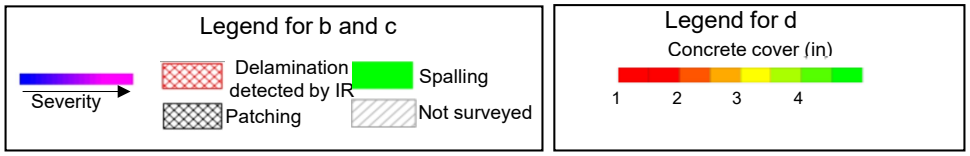

Figure 4.23: Evaluation method results (SC 555, Farrow road over I-77, Southbound, medium condition; BDI/Infrasense Inc., 2017)

4.5 Laboratory Deck Specimens

4.5.1 Preliminary scanning

On July 19, 2016, BDI and Infrasense performed visual inspection, GPR, HCP, IR, and IE testing on two bridge deck specimens. A 1 ft. x 1 ft. grid was established on the top surface of the specimens. A summary of the tests is presented below, and a more detailed analysis may be found in Appendix B.

Ground Penetrating Radar (GPR): GPR measurements (shown in **Figure 4.24**) indicated relatively low levels of corrosion in both slabs.

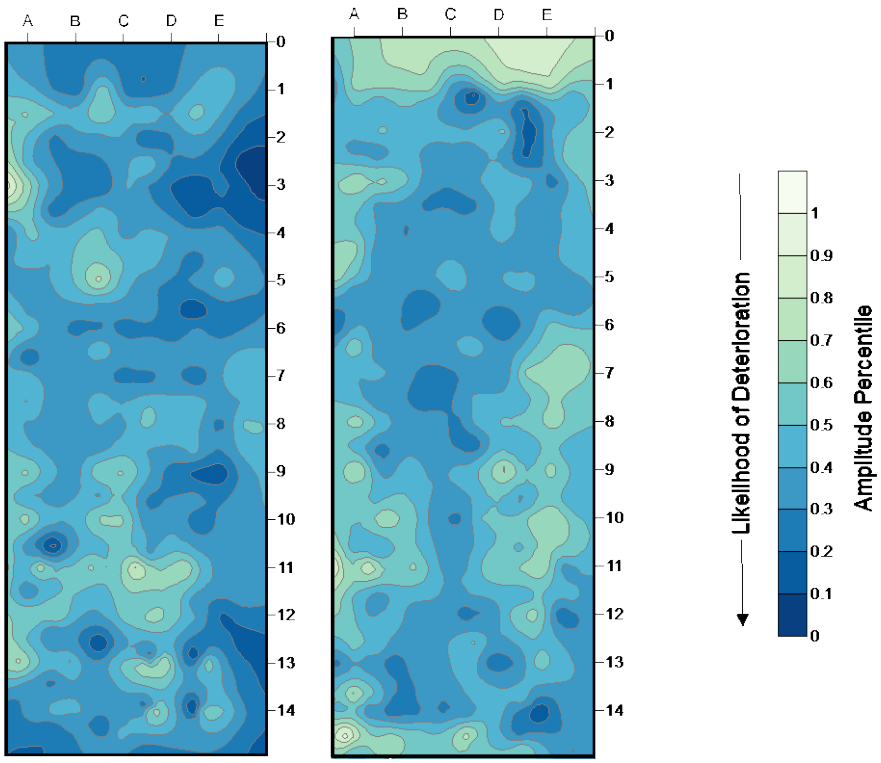

Figure 4.24: GPR deterioration map for slab 1 (left) and slab 2 (right), (BDI/Infrasense Inc., 2016) (*figure reproduced with permission*)

Half-Cell Potential (HCP): HCP measurements indicate the probability of corrosion in accordance with the values presented in **Table 2.1**. **Figure 4.25** presents a graphical representation of the areas corresponding to varying levels of corrosive activity as indicated by their HCP measurement values and **Table 2.1**. Little to no active corrosion was observed in the specimens, and the areas that did show active corrosion potential are localized.

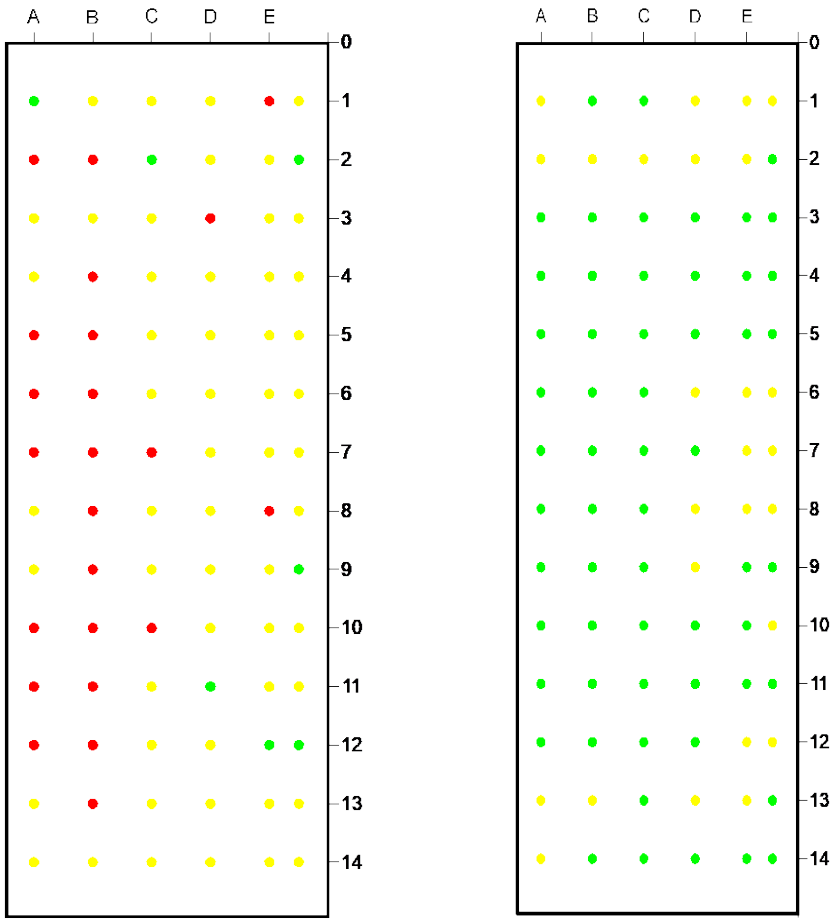

Figure 4.25: Half-Cell Potential Measurements for slab 1 (left) and slab 2 (right) (BDI/Infrasense Inc., 2016) *(figure reproduced with permission)*

Impact Echo (IE): IE is associated with resonant frequencies corresponding to the thickness of the deck slab. If the slab is intact, the thickness data is clear and should correspond with the expected slab thickness. If the slab is delaminated, the thickness data is unclear and will not correspond to the thickness of the slab. IE results are presented in **Figure 4.26**. As shown in this figure, most of the data points correspond to the expected thickness (green dots-sound concrete), where the other points show a different thickness (red/yellow-delaminated). Moreover, analysis resulted in several test points with values larger than the thickness of the slab (especially for slab 2). These values correspond to a very low frequency measurement. In these instances, Equation 2.1 does not hold true as the dominant frequency measured is no longer that of the elastic wave reverberating through the thickness of the slab. Instead, the frequency measured is synonymous with the flexural mode of a thin layer (delamination or debonding) near the surface. For this reason, these values should be interpreted as a shallow delamination or debonding rather than a much thicker slab.

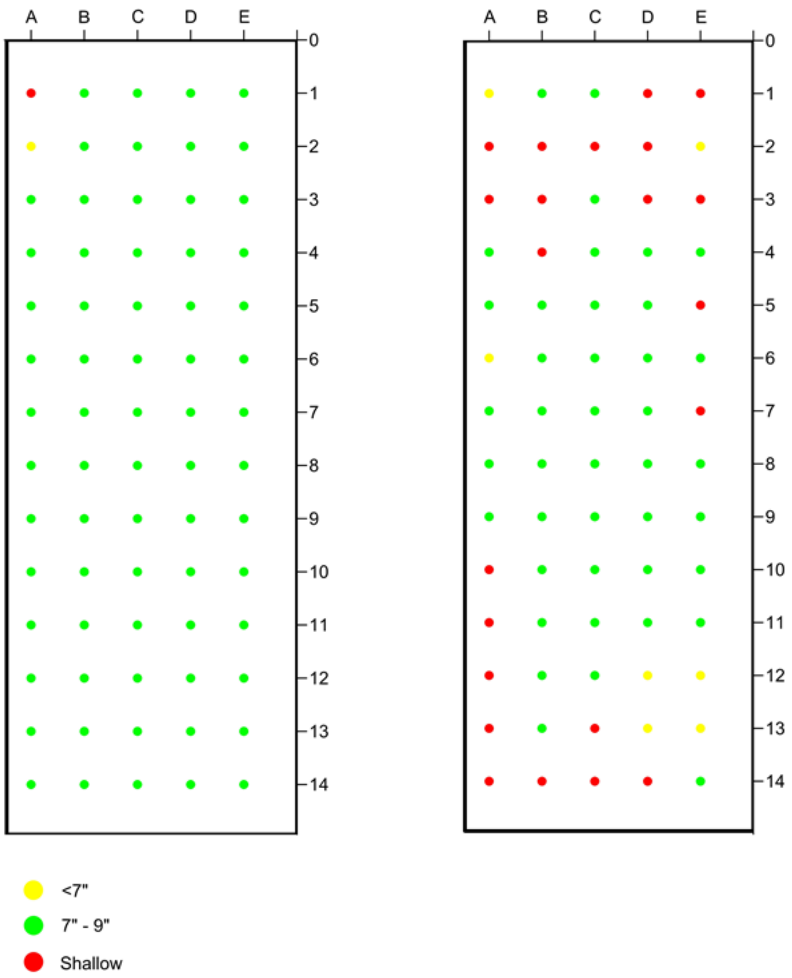

Figure 4.26: Impact Echo (IE) results for slab 1 (left) and slab 2 (right) (BDI/Infrasense Inc., 2016) *(figure reproduced with permission)*

Infrared Thermography (IR): IR testing data was reviewed simultaneously with the HRV data to differentiate delaminated areas from surface features (discoloration, oil stains, sand, and rust deposits, etc.) that appear in the infrared spectrum but are unrelated to subsurface conditions. **Figures 4.27 and 4.28** show the infrared and visual data for slabs 1 and 2, respectively. The images show that most, if not all, of the thermal anomalies have a corresponding condition on the visual images (e.g. debris, remaining binder, staining). The darker the color of the deck surface, the higher the emissivity and corresponding surface temperature. Therefore, areas of the slabs where the binder/overlay were not fully removed are relatively higher temperature than areas of bare concrete.

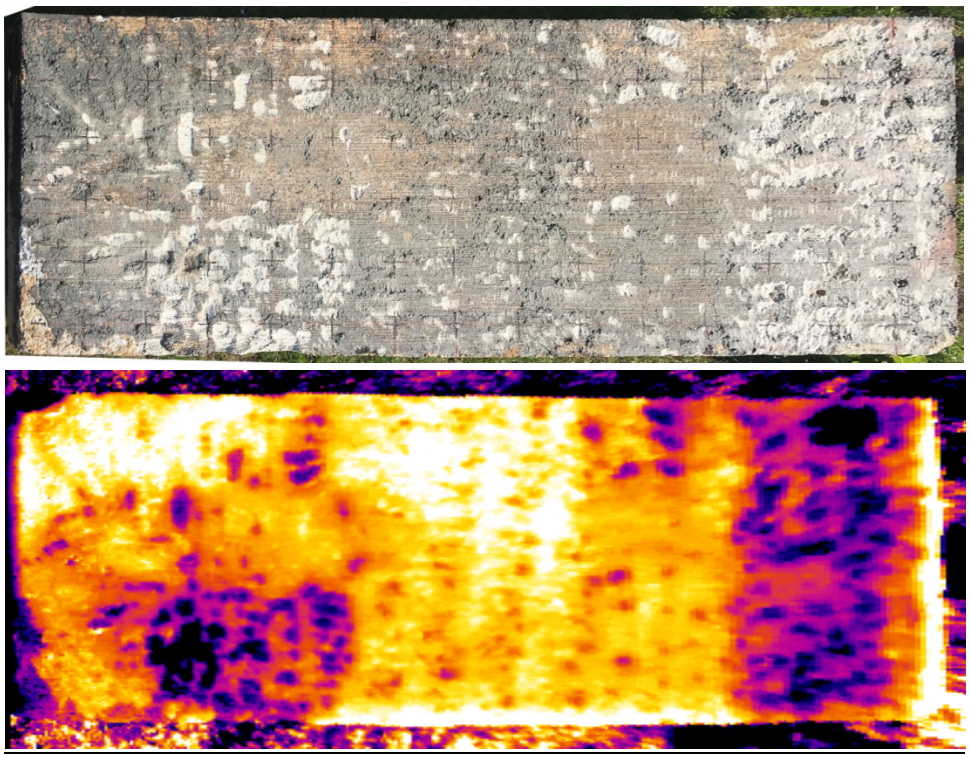

Figure 4.27: Infrared thermography results for slab 1 (BDI/Infrasense Inc., 2016)
(figure reproduced with permission)

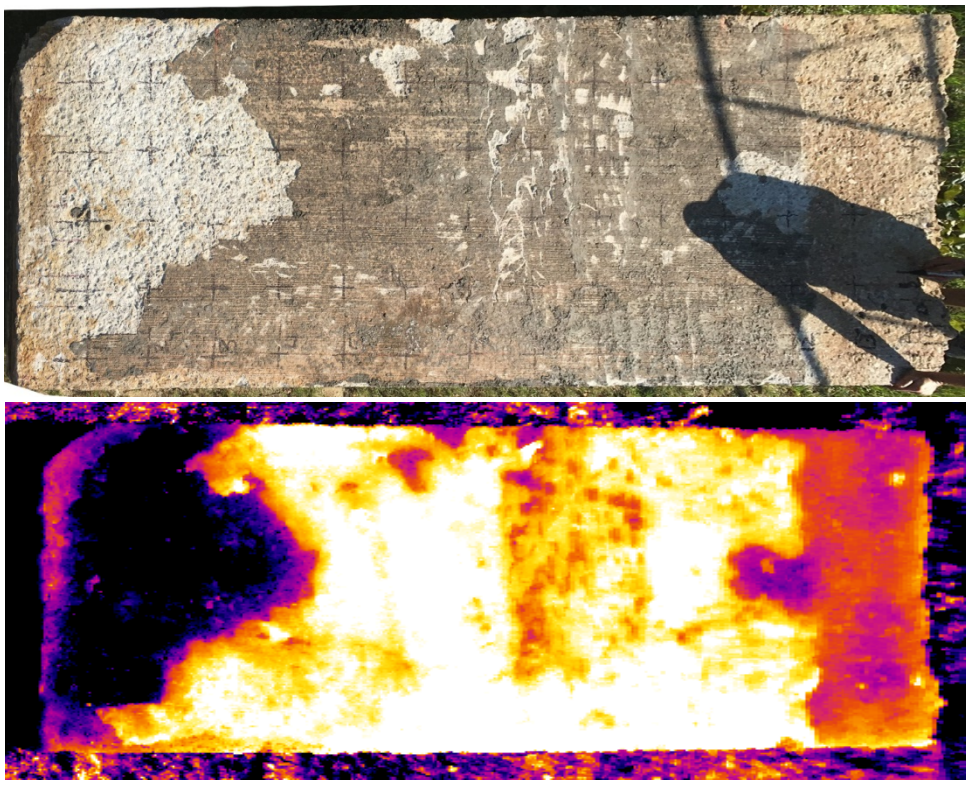

Figure 4.28: Infrared thermography results for slab 2 (BDI/Infrasense Inc., 2016)
(figure reproduced with permission)

4.5.2 Accelerated corrosion results for deck specimens

HCP measurements taken before starting the conditioning period indicated a passive state of reinforcement. 3% NaCl solution was then placed in the openings and half-cell potential measurements were recorded weekly beginning December 16, 2016. **Figure 4.29** to **Figure 4.36** show half-cell potential and linear polarization resistance (Rp) as functions of time for all locations (**Figure 3.30**). A drop in both potential and resistance indicate signs of corrosion. It can be noticed that after approximately 45 days of exposure to chlorides HCP values were lower than -0.35V (indicated as the corrosion threshold) at all eight locations. At the end of the wet/dry cycles (after nine months of conditioning), HCP readings were more negative than -0.50 V, indicating that severe corrosion was probable at all eight locations.

Polarization resistance (Rp) can be defined as the ratio between applied voltage and the step of current when the metal is slightly polarized (Andrade and Alonso, 2004). Due to the instantaneous nature of Rp measurements trends in the data set are more important than the measurement taken on any day. Therefore, a statistical method was used to exclude outliers with high and low values. The data with a trend line is presented in **Figure 4.29** to **Figure 4.36**. The trend line for Rp values at location 1 shows a different trend because this location has a problem with leakage and the sealing material reached as far as the reinforcing bar, leading to difficulty attaching the wire clip to the reinforcing bar. After 45-90 days of the wet/dry cycle, the Rp values agree with HCP values as they both decreased at all locations except location 1.

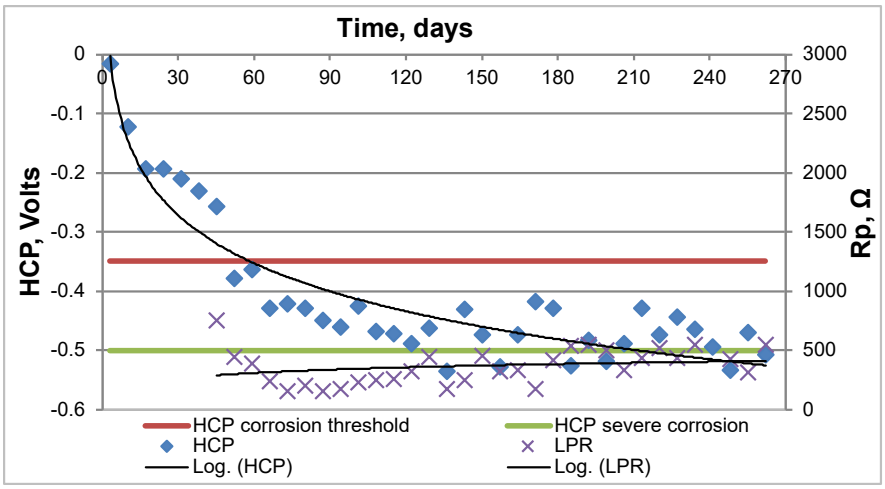

Figure 4.29: Electrochemical measurements – location 1

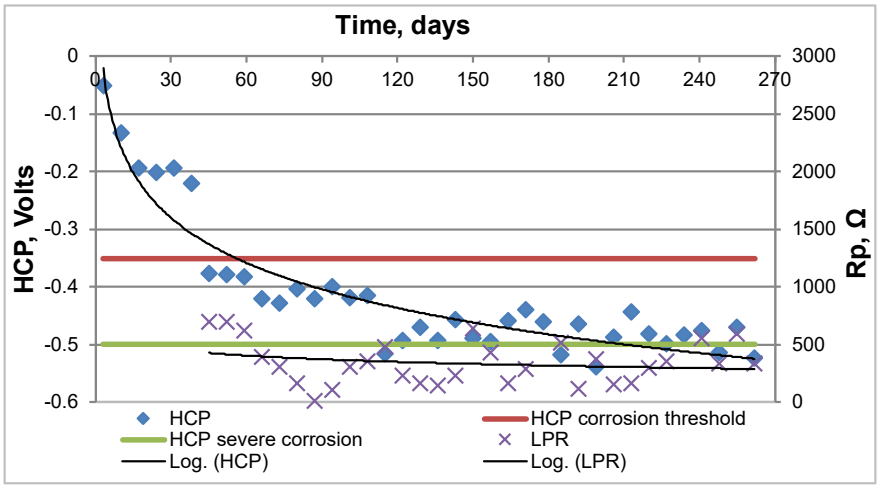

Figure 4.30: Electrochemical measurements – location 2

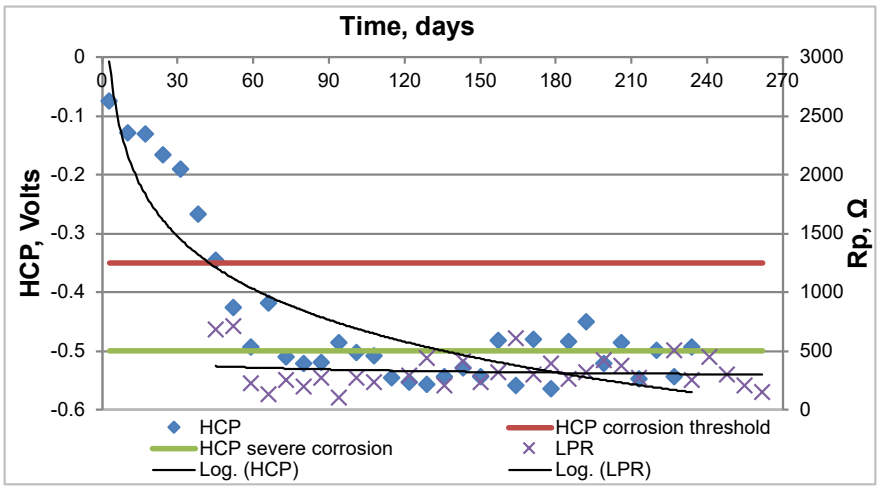

Figure 4.31: Electrochemical measurements – location 3

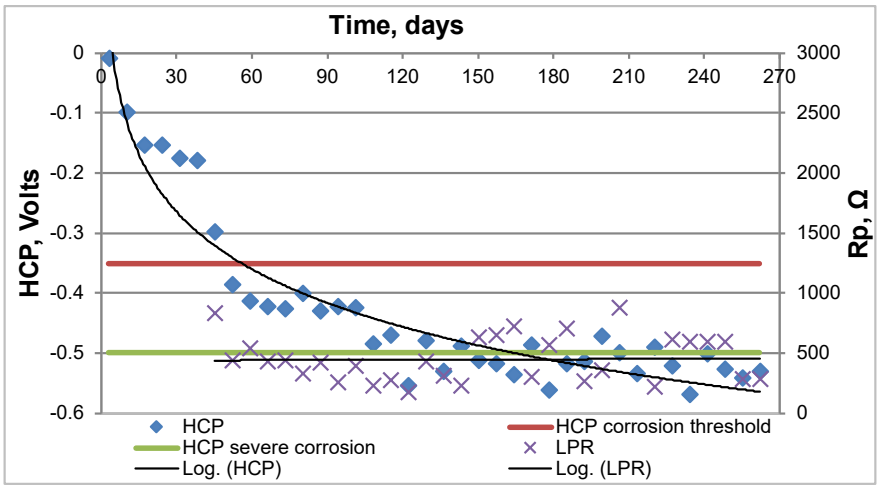

Figure 4.32: Electrochemical measurements – location 4

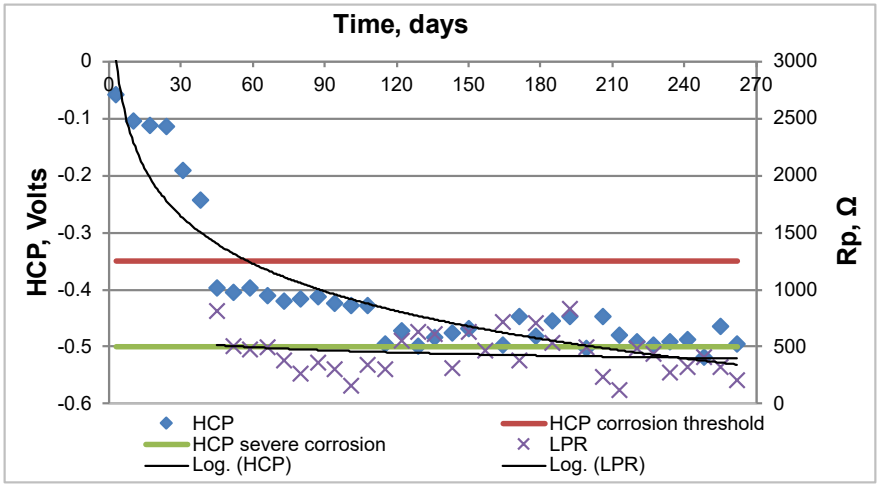

Figure 4.33: Electrochemical measurements – location 5

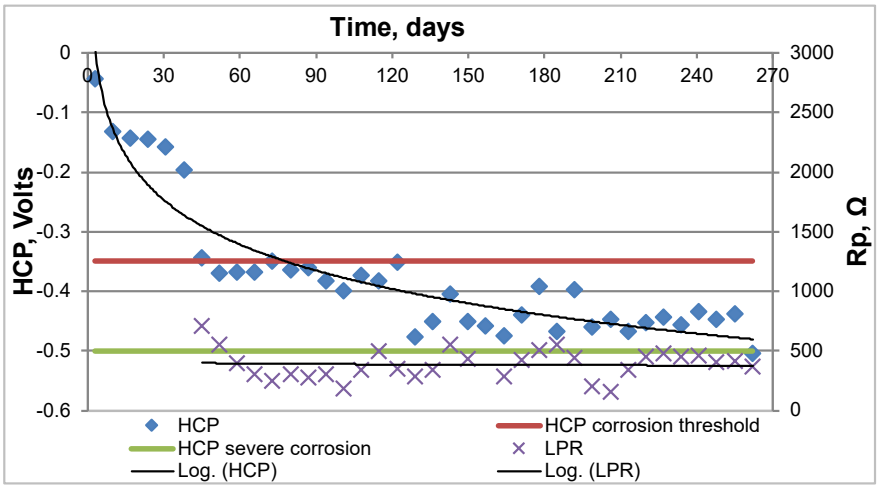

Figure 4.34: Electrochemical measurements – location 6

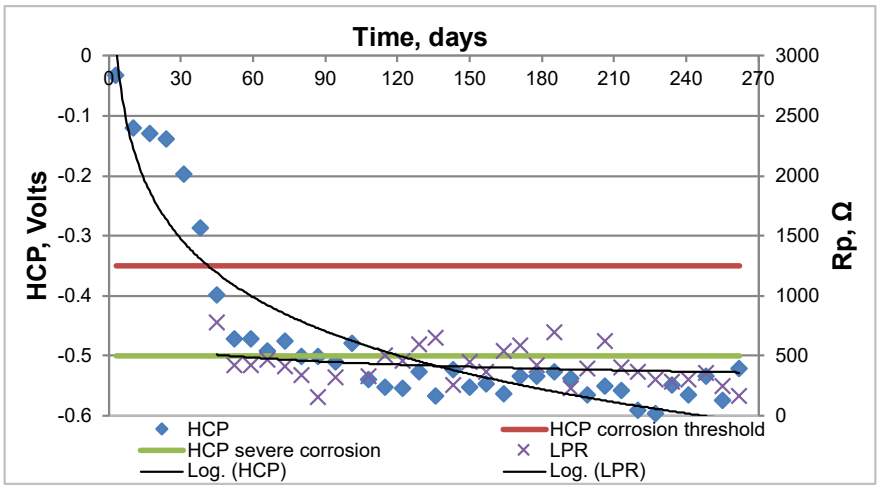

Figure 4.35: Electrochemical measurements – location 7

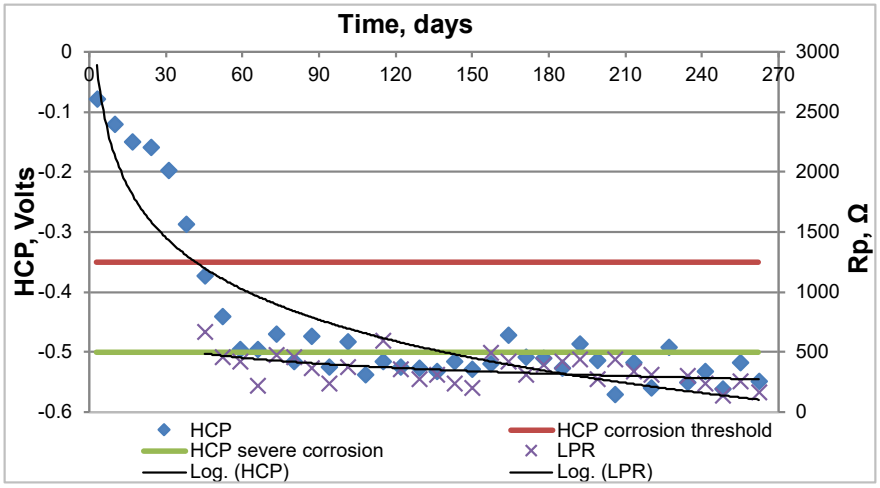

Figure 4.36: Electrochemical measurements – location 8

Average current corrosion density and average corrosion rate of the reinforcing bar at the eight locations are presented in **Tables 4.10** and **4.11**. The corrosion rate for all locations is within a high range indicating a high level of corrosion activity. These results agree with the HCP results where HCP measurements indicate high probability of corrosion (potential more negative than -0.5 Volts).

Table 4.10: Corrosion current density and corrosion rate results

location	Average í corr (μA/ cm²)	Average CR (μm/year)
1	1.20	13.9
2	1.38	16.1
3	1.37	15.9
4	0.98	11.4
5	1.01	11.8
6	1.06	12.3
7	1.02	11.8
8	1.18	13.7
Average	1.15	13.4

Table 4.11: Corrosion rate values related to significance in terms of service life (Abdelrahman, 2016)

Corrosion Rate (mm/year)	Corrosion Level
≤ 0.001	Negligible
0.001-0.005	Low
0.005-0.010	Moderate
> 0.01	High

UPV and IE measurements were conducted starting in January of 2017 and were repeated every two months to enable comparisons between wave velocity over time at 21 selected points (see **Figure 3.33)**. Wave velocity measurements during the testing period using IE are shown in **Figure 4.37** and UPV results are shown in **Figure 4.38**. UPV measurements ranged from 9,528 ft./sec. to 11,701 ft./sec. (2,904 to 3,566 m/sec.) with an average velocity of 10,535 ft. /sec. (3,211 m/sec.). Wave velocity measurements using impact echo (IE) ranged from 10,460 ft./sec. to 12,213 ft./sec. (3,188 to 3,723 m/sec.) with an average of 11,176 ft./sec. (3,406 m/sec.).

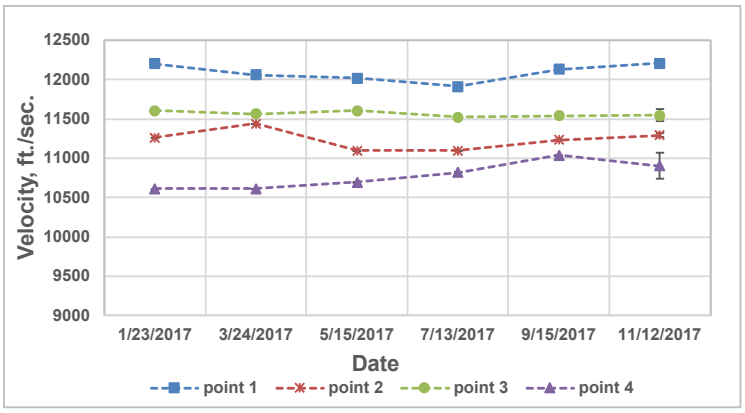

(a) Points 1-4

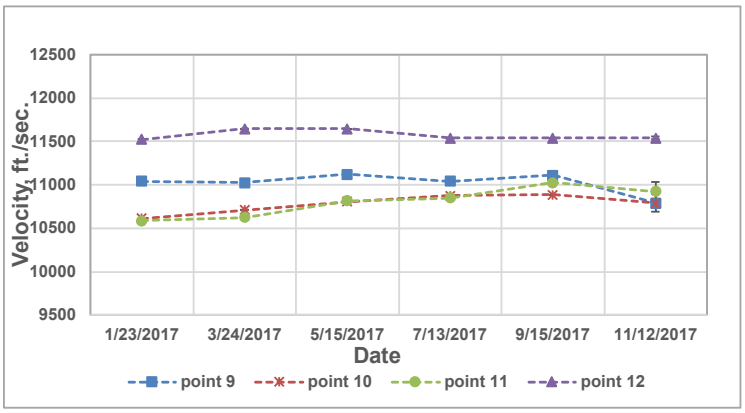

(b) Points 9-12

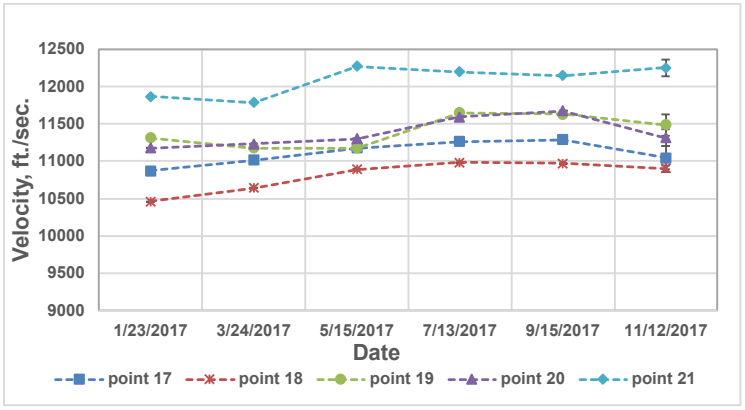

c) Points 17-21

Figure 4.37: IE wave velocity results

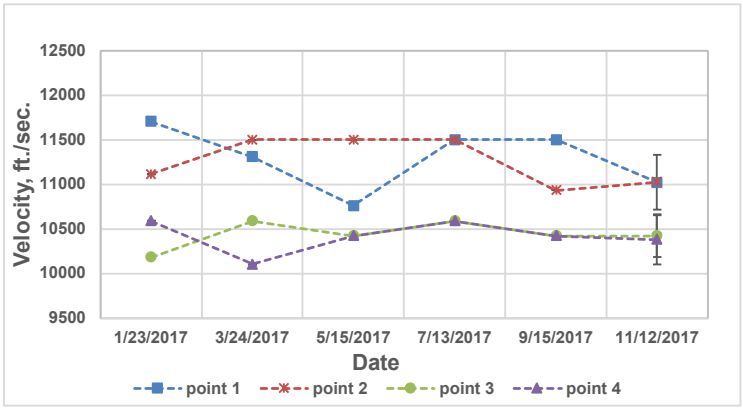

(a) Points 1-4

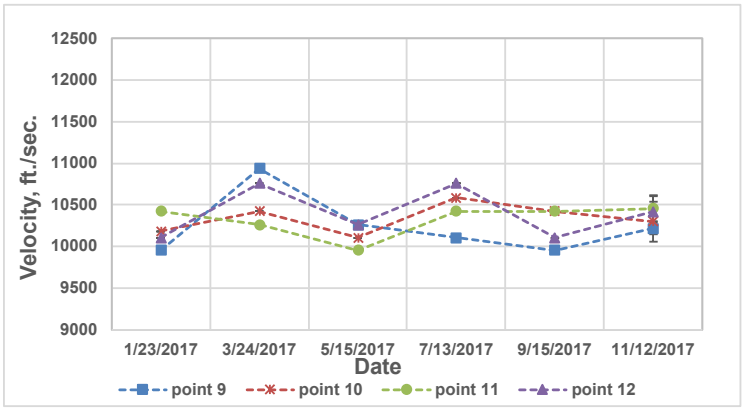

(b) Points 9-12

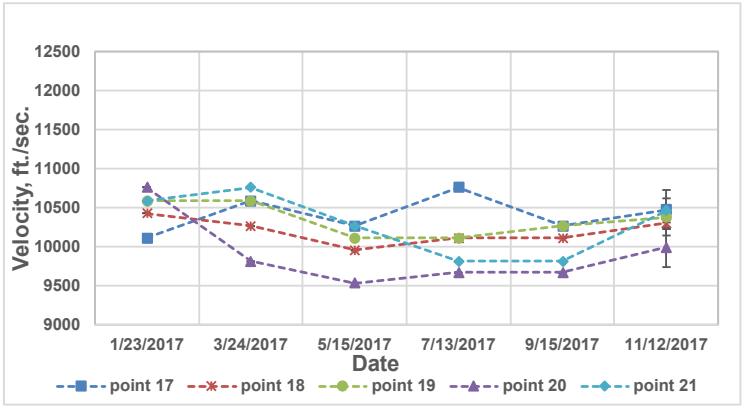

c) Points 17-21

Figure 4.38: UPV wave velocity results

It is apparent that the wave velocity measurements fluctuate. The maximum coefficient of variation (COV) based on the average values of the UPV readings was between 2.5 to 4.0% for points 1, 5, 7, 9, 16, 17, 18, 19, 20, and 21; while the maximum COV for the IE readings was 1.5% for points 4, 5, 6 and 2.0% for points 17, 18, 19, 20, and 21, with other points having lesser values. Gassman

and Tawheed (2004) recommended an acceptable variation of the wave velocity in concrete to be approximately 2.0 to 2.5%. The 3% variation for point 1 may be attributed to the presence of sealing material and the finishing layer on that area which may cause signal distortion; the area of points 17 through 21 may have experienced some damage as the traces of salt can be prominently seen on the concrete deck surface; while there is no sign of damage on the area associated with points 4, 5, 6, and 7. The variation of all other points indicates that no significant damage occurred during the conditioning period and concrete integrity was unaffected by the accelerated corrosion process for that particular time. The small variation of the wave velocity measurements can be attributed to many factors including the concrete slab having areas with a rough surface and suffering from a significant gradation of the coarse aggregates, resulting in difficulty attaching the transducer to the concrete surface. Other factors are the different energy of the impact source at each time of testing and variability associated with attaching the transducer and the impact source at the same location each time.

4.6 Preliminary Results from Leaphart Bridge over I-26

Five parameters are measured by the embedded ECI-2 instruments including linear polarization resistance (LPR), open circuit potential (OCP), chloride ion concentration (Cl-), resistivity, and temperature. Each of the parameters is linked to the corrosivity of the concrete. By using multiple inputs, the robustness of the decision system is increased, as the likelihood that all four parameters will become uncorrelated to corrosivity under the same conditions is minimized (Virginia Technologies, Inc., 2014). **Figure 4.39** shows the results recorded from the ECI-2 sensor for eight months. Results of each parameter are discussed below.

Temperature: The temperature versus time relation is shown in **Figure 4.39**a. The benefit of using this parameter is that the change in the temperature influences polarization resistance (R_P) and corrosion potential (E_{corr}). Corrosion rates of materials increase as the temperature increases, since chemical reactions occur at higher rates with increased temperature.

Chloride level: The chloride level versus time relation is shown in **Figure 4.39**b. The decreasing chloride level at the beginning is due to high moisture content after casting and during the curing period. It then increases and stabilizes after 120 days. More information about this parameter is available in chapter three.

Open circuit potential or Corrosion potential: The OCP/E_{corr} versus time relation is shown in **Figure 4.39**c. This relationship is often used as an indication of corrosion risk. As seen in the beginning of this plot, highly corrosive data is observed during the curing period due to high moisture content and then it stabilizes after 120 days. Based on ASTM C876 (2015), **Table 2.1**, more negative than 0.35 Volts indicates high corrosion risk (90% probability). These ranges are based on experience of corrosion in chloride contaminated concrete bridge decks, but when carbonation is the cause of corrosion or cathodic processes are modified, the range of the corrosion potential may be different (Virginia Technologies, Inc., 2014). No sign of corrosion is observed based on these ranges.

Concrete resistivity: Concrete resistivity versus time is shown in **Figure 4.39**d. During concrete casting and curing the plot shows low and fluctuating values of resistivity due to high moisture content, then after 120 days stabilizes. The resistivity of concrete may vary over a wide range,

from 10^1 to 10^6 Ω m. The resistivity increases as the concrete cures. No sign of corrosion is observed based on the limits show in **Table 4.12** (Song and Saraswathy, 2007).

Table 4.12: Concrete resistivity limits

Resistivity (Ohm-cm)	Corrosion risk
Greater than 20,000	Negligible
10,000 to 20,000	Low
5,000 to 10,000	High
Less than 5,000	Very high

Polarization resistance: Linear polarization resistance versus time is shown in **Figure 4.39**e. As expected, high values of Rp are observed for the first eight months which indicates that the steel reinforcement is in a passive state. For steel in concrete, the transition from the passive state to an actively corroding state is accompanied by a substantial change in the polarization resistance as shown in **Table 4.13**.

Table 4.13: Typical R_p values

Specific polarization resistance (Rp) kΩ.cm2	Steel reinforcement condition
>500	Passive state
~50 or larger	Passive state (current not well contained)
< 10 (if < 2 heavily corroding)	Active state (corroding)

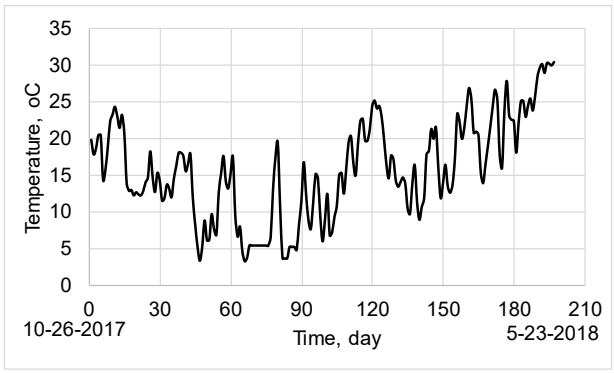

(a) Temperature

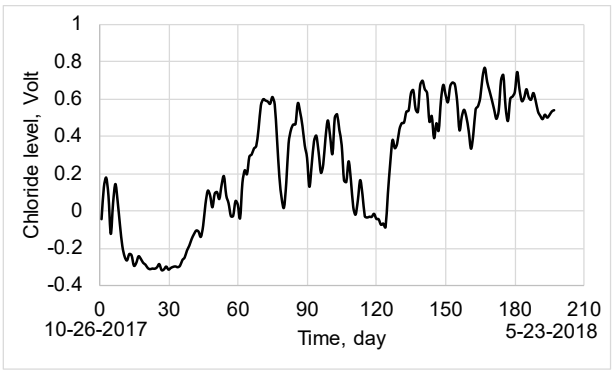

(b) Chloride level

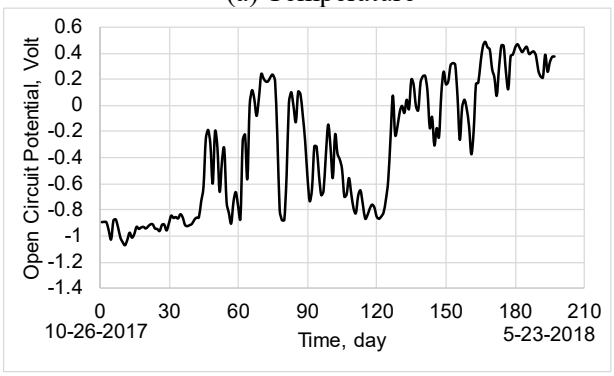

I Open circuit potential

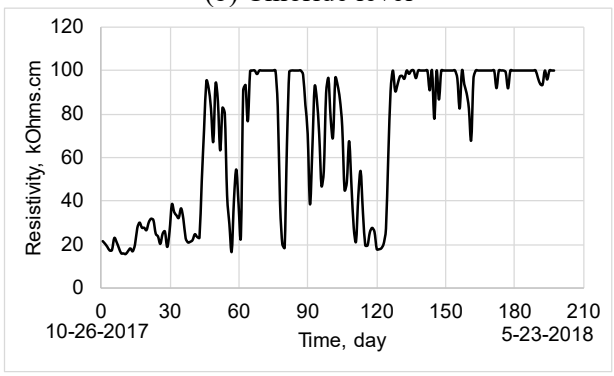

(d) Resistivity

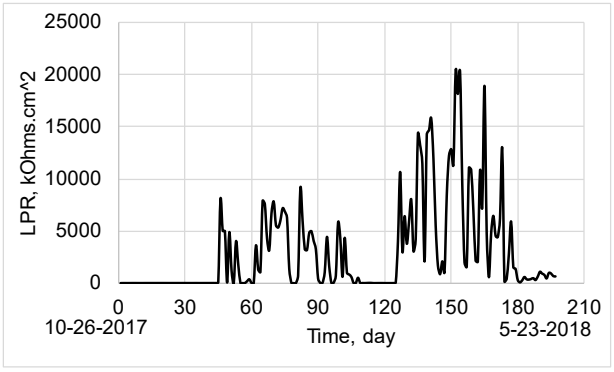

I Linear polarization resistance

Figure 4.39: Embedded corrosion monitoring results

CHAPTER 5: LIFE CYCLE COST ANALYSIS

5.1 Introduction

Rapid evaluation methods such as GPR, IR, HRV and DAR have been developed for rapid bridge deck assessment. As discussed in chapter 1, the traditional chain dragging method requires traffic control and more man power than the rapid evaluation methods. Previous studies (Yehia et al., 2008; Scott et al., 2003) have indicated that rapid evaluation methods outperform traditional methods in terms of accuracy. For these reasons, some transportation agencies have begun to investigate the cost-benefit of utilizing rapid evaluation methods. Of interest to these agencies is whether it is more cost effective to utilize one or more of the rapid bridge deck evaluation methods than chain dragging.

This study seeks to answer the above question for the SCDOT by performing two analyses: 1) Performance assessment of chain dragging versus three rapid evaluation methods (truck-mounted, DAR, and pole-mounted), and 2) Life cycle cost (LCC) comparison between chain dragging and the three rapid evaluation methods. The truck-mounted method consisted of GPR, IR and HRV, and the pole-mounted method consisted of IR and HRV. The performance of each bridge deck evaluation method was assessed based on four metrics: accuracy in detecting delamination, time to perform the evaluation, ease of data interpretation, and cost.

The cost effectiveness of a method was assessed by computing the LCC of a bridge deck for a 55-year analysis period. The LCC is the summation of initial construction cost, bridge deck evaluation cost, bridge deck repair cost and user cost minus the salvage value. The LCC was estimated using the RealCost tool developed by the Federal Highway Administration (FHWA). This tool was developed to support the life-cycle cost analysis (LCCA) of pavement projects (FHWA, 2004). However, it has been applied to other types of projects such as sustainability rating of civil infrastructure projects (Clevenges et al., 2013). **Figure 5.1** shows a screenshot of RealCost's Switchboard which facilitates the data input process. The data can also be entered directly on the spreadsheets as shown in **Figure 5.2**.

Like other LCCA methods, RealCost uses economic principles to compare the LCC of competing construction or rehabilitation alternatives for a single project. RealCost provides two types of LCC: deterministic and probabilistic. The deterministic cost uses the discrete input values the users provided based on historical data and engineering judgement. The probabilistic cost accounts for the uncertainty and variation associated with the input values. In probabilistic analysis, the input variables are described by a probability distribution function that conveys the range of likely inputs. Given the probability distribution parameters specified by the user, RealCost uses Monte Carlo simulation to generate random values from the specified probability distributions and provides a range of potential LCC.

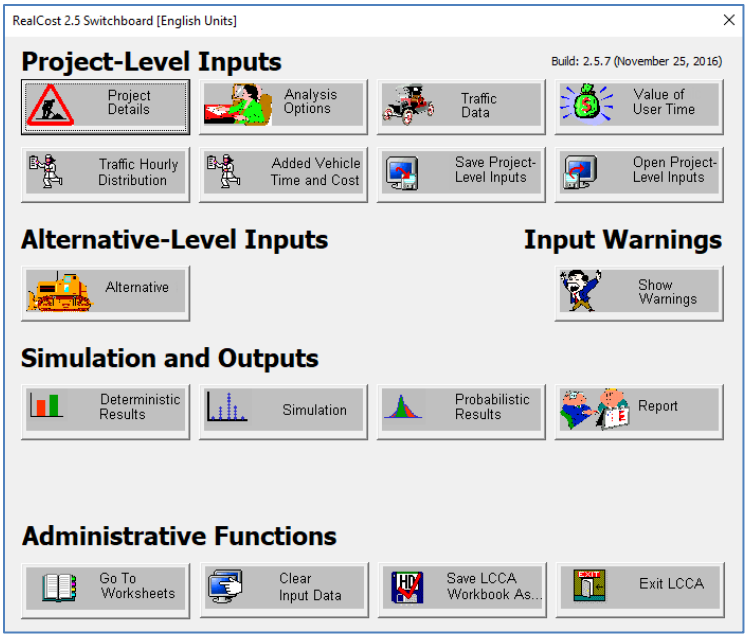

Figure 5.1: RealCost's Switchboard for data entry

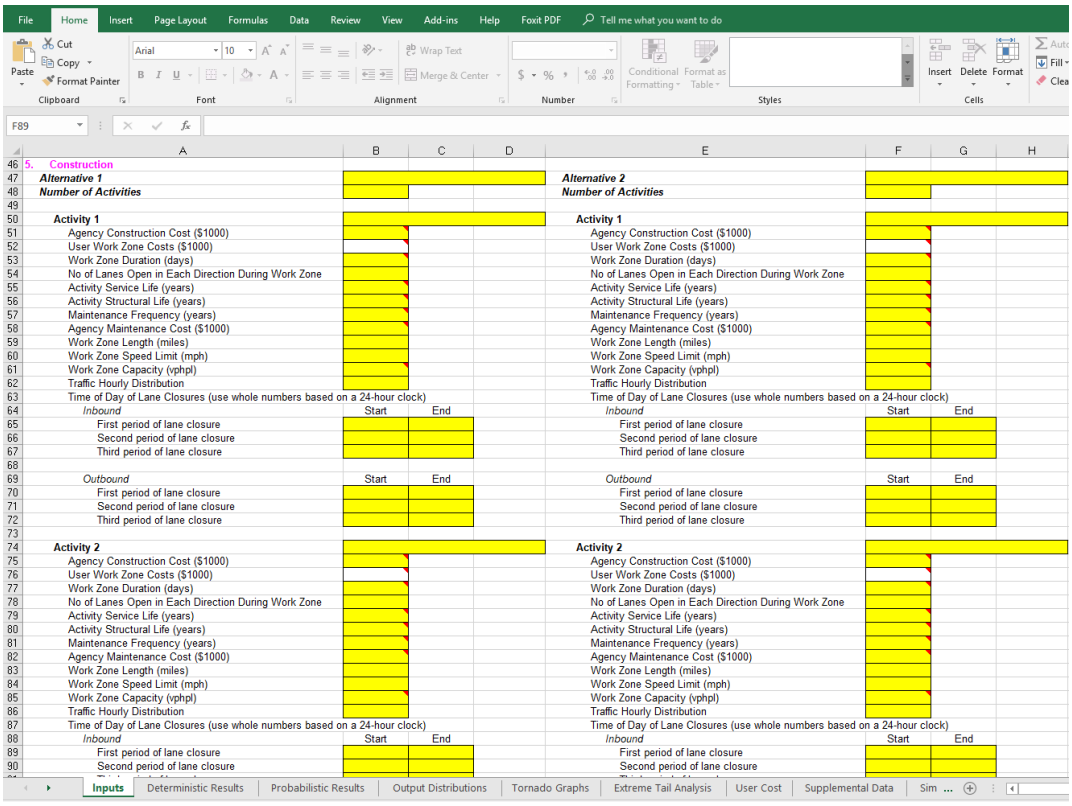

Figure 5.2: Spreadsheet for RealCost data entry

5.2 Performance Assessment of Bridge Deck Evaluation Methods

As mentioned in section 5.1, the performance of each bridge deck evaluation method was assessed based on four metrics: accuracy in detecting delamination, time to perform the evaluation, ease of data interpretation, and cost. Each metric was given a score between 0 and 1, where 1 represents the best performance. Additionally, a weight factor was assigned to each metric based on our understanding of its importance to the SCDOT. Given the score for each metric and weight factor, the overall grade for each bridge deck evaluation method was computed using the weighted average method. **Table 5.1** shows the scores, weight factors, and overall grade for each bridge deck evaluation method. As shown, DAR is ranked best and chain dragging is ranked worst among the methods evaluated for detecting delamination. This ranking reflects the fact that chain dragging was found to detect delamination with 70% accuracy, truck-mounted with 77% accuracy, pole-mounted with 81% accuracy, and DAR with 94% accuracy. These accuracy values are used in section 5.3 to determine the percentage of delamination detected by each evaluation method.

Table 5.1: Performance assessment and ranking of bridge deck evaluation methods

Evaluation method	Deterioration type	Accuracy	Time	Ease of data interpretation	Cost	Overall grade	Rank
		WF=0.47	WF=0.23	WF=0.12	WF=0.18		
Deck acoustic response	Delamination	0.94	0.85	0.85	0.9	0.90	1
Vehicle mounted	Delamination	0.77	0.95	0.8	0.95	0.85	2
Pole mounted	Delamination	0.81	0.8	0.75	0.7	0.78	3
Vehicle mounted	Chlorides	0.55	0.95	0.65	0.95	0.72	4
Chain dragging	Delamination	0.7	0.5	0.95	0.85	0.71	5

WF= Weight Factor

5.3 Life-Cycle Cost Analysis

As shown in **Figures 5.1** and **5.2**, RealCost allows the user to compare the LCC between any two alternatives. For each alternative, the user can specify multiple activities that represent the initial construction and subsequent maintenance activities performed on the bridge deck during the analysis period. In this study, the LCC difference between chain dragging and vehicle mounted; chain dragging and DAR; and chain dragging and pole mounted evaluation were analyzed. For each comparison it was assumed that the first bridge deck evaluation is performed 15 years after the initial construction, and the subsequent bridge deck evaluations are performed every 10 years thereafter. Given an analysis period of 55 years, a total of five bridge deck evaluations were considered in the analysis. As mentioned, the LCC is the summation of initial construction cost, bridge deck evaluation cost, bridge deck repair cost, and user cost minus the salvage value. The summation of initial construction cost, bridge deck evaluation cost, and bridge deck repair cost is called agency cost. The following explains how these costs were determined.

The initial construction cost of a bridge deck was estimated as per “structures design guidelines” (SDG, 2007). For a 15,000 sq. ft. bridge deck, the initial construction cost was estimated to be $405,000. The bridge deck evaluation cost of chain dragging and the three rapid evaluation methods were provided by the SCDOT and Bridge Diagnostics Inc., respectively. Note that for chain dragging, the evaluation cost was given for a 10,000 sq. ft. bridge deck. For rapid evaluation

methods, the cost was estimated for each bridge deck based on the total cost and number of bridge decks the contractor performed in a day. In this analysis, a 15,000 sq. ft. bridge deck is considered; hence, the chain dragging evaluation cost was scaled up accordingly. **Table 5.2** shows the cost of the bridge deck evaluation by methods.

It was assumed that after each bridge deck evaluation, SCDOT will repair the detected damaged sections. The bridge deck repair cost was estimated using a bridge deck delamination prediction model (Equation 5.1) developed by Taylor et al. (2016). This model predicts the percentage of delamination at any given year after the initial bridge deck construction. To reflect the accuracy of each evaluation method in detecting delamination as discussed in Section 5.2, the percentage of delamination detected by each method was estimated by multiplying the delamination percentage predicted by the model (Equation 5.1) by the accuracy of the corresponding evaluation method. The bridge deck repair cost for different repair types were provided by the SCDOT and is shown in **Table 5.3.**

$$D = (0.98 \cdot e^{0.079 \cdot A} - 0.98) \tag{5.1}$$

where,

D – Percentage of delamination in the bridge deck A years after initial construction
A – Age of deck

Table 5.2: Cost of bridge deck evaluation methods

Method	Cost
Traditional (chain dragging)	$2,300 (for a 15,000 sq. ft bridge deck)
Vehicle mounted	700 ($/bridge deck)
Pole mounted	9,000 ($/bridge deck)
Deck acoustic response	1,300 ($/bridge deck)

Table 5.3: Cost of repairing bridge deck

Type of repair	Cost ($/sq. ft.)
Minor (less than 15% patching)	89
Major (15% - 30% patching)	78
Rehabilitation (greater than 30% patching)	67
Replacement of the deck (hydro demolition and latex mod. concrete)	56

User cost includes the expenditures incurred by the traveling public such as delays and related vehicle operating cost. The costs shown in the tables to follow include traffic control during evaluation, repair and initial construction. RealCost calculates the user cost from user inputs such as length of work zone, duration of the work, speed limit within the work zone, number of lanes open during work, value of time, and traffic data. The value of time was provided by the SCDOT and is shown in **Table 5.4**. The traffic data such as annual average daily traffic (AADT), percentage of heavy vehicle and annual traffic growth (**Table 5.5)** were obtained from the SCDOT website (SCDOT, 2018). The free flow capacity, queue dissipation capacity, maximum AADT, and maximum queue length were calculated based on RealCost's suggested procedures (FHWA, 2004).

Table 5.4: Value of time

Vehicle type	Value of time ($/hour)
Passenger car	50
Single unit trucks	65
Combination trucks	80

Table 5.5: Traffic data

Description	Value
AADT at the beginning of the analysis period (total for both directions)	2,600
Single unit trucks as percentage of AADT	7
Combination trucks as percentage of AADT	8
Annual growth rate of traffic (%)	1.2
Speed limit under normal operating conditions (mph)	65
Lanes open in each direction under normal conditions	2
Free flow capacity (vehicle per hour per lane)	2,047
Queue dissipation capacity (vehicle per hour per lane)	1,500
Maximum AADT (total for both directions)	40,955
Maximum queue length (miles)	7
Rural or Urban hourly traffic distribution	Urban

Salvage value is the value of the bridge deck based on its remaining service life at the end of the analysis period (Huang et al., 2004). This was calculated by multiplying the initial construction cost of the bridge deck by the percentage of "sound" deck (i.e., non-damaged and useable portions) at the end of the analysis period. **Figure 5.3** shows how the accuracy of an evaluation method affects the percentage of remaining sound deck throughout the analysis period. The upward jumps in years of 15, 25, 35, and 45 indicate an increase in the percentage of sound deck due to the repair work that was performed after the evaluation. The repair work that was done in year 55 is not shown in **Figure 5.3**. From **Figure 5.3**, it can be observed that the more accurate the evaluation method the higher the percentage of remaining sound deck at the end of the analysis period (55 years). It can be inferred from this finding that using a more accurate evaluation method will yield a higher salvage value.

To compare the LCC between two competing methods, the LCC of each method was converted to the net present value (NPV). That is, all future costs (evaluation, repair and user) for the entire analysis period were converted to the present value (year of initial construction of the bridge deck). The NPV was computed using the discount rate (i.e., the interest by which the future cost is discounted to the present value) specified by the user as shown in Equation 5.2.

$$LCC = I - S(i, n_N) + \sum_{k=1}^{N} M_k \left[\frac{1}{(1+i)^{n_k}} \right] \tag{5.2}$$

where,

I = Initial construction cost of the bridge deck
$S(i, n_N)$ = Salvage value that is discounted to the year of initial construction of the bridge deck
M = Maintenance, repair and user cost

i = Discount rate
n = Year of expenditure
k = Number of activities

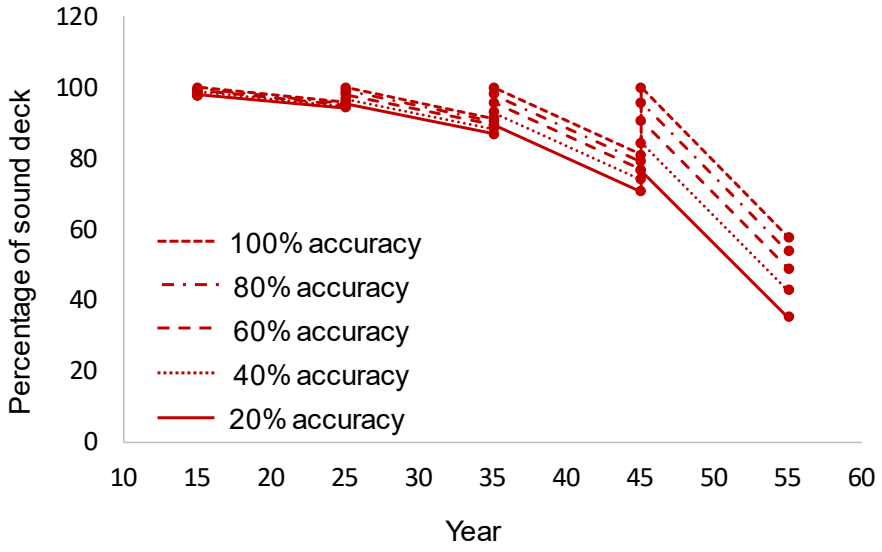

Figure 5.3: Effect of evaluation method accuracy on percentage of remaining sound deck

In addition to the above details, several other parameters were assumed for the LCC comparison. These include:

- Traffic hourly distribution follows the default values provided by RealCost.
- Added time and vehicle stopping costs in South Carolina are the same as those provided by RealCost.
- Each repaired portion will deteriorate at the rate yielded by Equation 5.1.
- The probability distribution function for all input variables was assumed to be uniform. The minimum and maximum values of the uniform distribution were assumed to be 10% less and more than the deterministic values, respectively.
- The discount rate is 4%.
- 100% of the detected delamination will be repaired after each evaluation.
- 20 bridges can be evaluated in a day using the vehicle mounted method.
- 10 bridges can be evaluated in a day using the DAR method.
- Two bridges can be evaluated in a day using the pole mounted method.

5.4 Results and Discussion

5.4.1 Deterministic analysis results

Table 5.6 shows the LCC comparison between chain dragging and the vehicle mounted method. The results indicate that the vehicle mounted method is more cost-effective than chain dragging. **Table 5.7** shows the LCC comparison between chain dragging and the DAR method. The results indicate that chain dragging is more cost-effective than DAR. Lastly, **Table 5.8** shows the LCC

comparison between chain dragging and the pole mounted method. The results indicate that chain dragging is more cost effective than the pole mounted method. These comparisons are based on detection of delaminations (as opposed to chlorides). It should be noted that the user cost for chain dragging is higher than the other three methods; the reason why the other three methods have the same user cost is because they do not require traffic control during the bridge deck evaluation. The total LCC for all methods is within the same range (LCC for any method is within five percent of any other method).

Table 5.6: Comparison of deterministic LCC between chain dragging and vehicle mounted methods

Method	Chain dragging	Vehicle mounted
Agency cost	$449,760	$451,320
User cost	$28,620	$23,180
Total LCC	$478,380	$474,500

Table 5.7: Comparison of deterministic LCC between chain dragging and DAR methods

Method	Chain dragging	DAR
Agency cost	$449,760	$460,880
User cost	$28,620	$23,180
Total LCC	$478,380	$484,060

Table 5.8: Comparison of deterministic LCC between chain dragging and pole mounted methods

Method	Chain dragging	Pole mounted
Agency cost	$449,760	$467,490
User cost	$28,620	$23,180
Total LCC	$478,380	$490,670

5.4.2 Probabilistic analysis results

Table 5.9 shows the LCC comparison between chain dragging and the vehicle mounted method. The results indicate that the vehicle mounted method is more cost-effective than chain dragging; its min/max values are lower and so is its range. **Table 5.10** shows the LCC comparison between chain dragging and the DAR method. The results indicate that chain dragging is more cost-effective than DAR; its min/max values are lower and so is its range. Lastly, **Table 5.11** shows the LCC comparison between chain dragging and the pole mounted method. The results indicate that chain dragging is more cost-effective than the pole mounted method; its min/max values are lower and so is its range. These comparisons are again based on detection of delaminations (as opposed to chlorides). The results of the total LCC are again within the same range.

Table 5.9: Comparison of probabilistic LCC between chain dragging and vehicle mounted methods

Method	Chain dragging		Vehicle mounted	
	Minimum	Maximum	Minimum	Maximum
Agency cost	$393,240	$513,760	$397,850	$516,600
User cost	$26,210	$32,110	$21,170	$25,130
Total LCC	$419,450	$545,870	$419,020	$541,730

Table 5.10: Comparison of probabilistic LCC between chain dragging and DAR methods

Method	Chain dragging		DAR	
	Minimum	Maximum	Minimum	Maximum
Agency cost	$393,240	$513,760	$399,880	$527,700
User cost	$26,210	$32,110	$21,170	$25,130
Total LCC	$419,450	$545,870	$421,050	$552,830

Table 5.11: Comparison of probabilistic LCC between chain dragging and pole mounted methods

Method	Chain dragging		Pole mounted	
	Minimum	Maximum	Minimum	Maximum
Agency cost	$393,240	$513,760	$443,960	$505,730
User cost	$26,210	$32,110	$21,170	$25,130
Total LCC	$419,450	$545,870	$465,130	$560,860

5.5 Conclusions

In this study, the life-cycle cost of chain dragging was compared against three rapid evaluation methods (vehicle mounted, deck acoustic response, and pole mounted). Both the deterministic and probabilistic costs indicate that the vehicle mounted method is the most cost-effective among the four. The costs of all four methods were within a similar range.

CHAPTER 6: CONCLUSIONS AND RECOMMENDATIONS

6.1 Conclusions

Bridge decks with differing damage levels were investigated using rapid bridge deck evaluation methods (i.e. ground penetrating radar, conventional and ultra-time domain infrared sensing, high resolution video, deck acoustic response) to assess the efficacy of such methods for concrete bridge decks in South Carolina. It is envisioned that such methods may be used in the future either in place of, or in addition to, traditional evaluation methods of bridge deck evaluation (i.e. coring, chloride concentration testing, and chain dragging).

The rapid evaluation methods investigated varied in terms of cost, need for traffic control and type of traffic control, and interpretation of results. To address accuracy, results gathered from each of the rapid evaluation methods were compared to results gained by sampling (referred to as 'ground truth' comparison, in this case gained through coring and/or chloride concentration testing). Coring and chloride concentration testing were not conducted on the bridge deck located at SC 555, Farrow Road over I-77, as this bridge had an overlay performed by SCDOT during the project period.

Conclusions related to the rapid evaluation methods (vehicle mounted, pole mounted, and deck acoustic response) are as follows:

1. Deck acoustic response (DAR) had the highest accuracy for detection of delamination.
2. Vehicle mounted IR and pole mounted IR-UTD showed promising results for detection of delamination.
3. Contour plots attained through vehicle mounted GPR did not generally correlate with detection of delamination. However, the most extreme contours (bright pink regions) did provide reasonable correlation with delamination. Because GPR is sensitive to moisture conditions and chlorides in the bridge deck, GPR is thought to be sensitive to conditions causing future degradation.
4. Each of the methods appears to be sensitive to threshold settings. Therefore, as experience is gained it is expected that accuracy may improve.

In addition to the field studies, a bridge deck specimen was subjected to an accelerated corrosion environment in a laboratory setting. Conclusions are as follows:

1. Half-cell potential results indicate that corrosion initiated after 45 days of conditioning. A high level of corrosion probability was attained at the end of the test period.
2. The average loss due to corrosion (in terms of diameter) based on linear polarization resistance was estimated to be 10 μm. The value required for crack initiation based on cover to diameter (c/ø) ratio is estimated to be 28 μm.
3. Impact echo and ultrasonic pulse velocity were used to detect a damaged area with 4% wave velocity variation and clear evidence of damage. The small variation in wave velocity is consistent with minor damage occurring during the conditioning period.
4. The testing period significantly accelerated the corrosion process but was not severe enough to initiate cracking of the concrete cover.

To better understand the conditions that lead to degradation of bridge decks in South Carolina, instrumentation was installed in the deck of the Leaphart Bridge over I-26. Initial readings are within the expected range of behavior. It is recommended that the readings be continued by SCDOT for a period of ten years. At the conclusion of this monitoring period, the need for continued monitoring should be re-evaluated.

The life-cycle cost of chain dragging was compared to that of three rapid evaluation methods (vehicle mounted, deck acoustic response, and pole mounted). Both the deterministic and probabilistic costs indicate that the vehicle mounted method is the most cost-effective method among the four. However, the life-cycle costs associated with all four methods were within the same range.

6.2 Recommendations and Future Research

Because the rapid evaluation methods investigated differ in terms of traffic control requirements and degradation mechanisms, recommendations are dependent on perceived needs of the SCDOT and are divided into two broad categories. The first category is referred to a local evaluation, which is taken to mean either a single bridge or a relatively small number of bridges (i.e. ten or less) in a relatively well confined geographic region (i.e. within a 20 mile radius of one another). The second category is referred to as evaluation for asset management, which is taken to mean a relatively large number of bridges in a less well confined geographic region (i.e. bridge locations extending beyond a 20 mile radius of one another).

Local evaluation: For local bridge deck evaluation that is focused on the detection of delaminated regions, deck acoustic response (DAR) demonstrated the most accurate results among the rapid methods and would therefore serve as a reasonable replacement for chain dragging. The advantage of DAR over chain dragging is the speed of evaluation (operating at approximately 10 mph). However, this method does require rolling traffic control. The pole mounted method also provided reasonable results for local evaluation focused on delaminations and is worthy of consideration. The pole-mounted method, however, requires significant time for evaluation (in the range of one day per bridge deck) and therefore is not well-suited for evaluating large numbers of bridges in a short time period.

Asset management: For asset management that is focused on the detection of delaminated regions, deck acoustic response is not well-suited due to the speed of evaluation. Rather, vehicle mounted infrared sensing proved to the most feasible means of evaluation as traffic control is not required. In addition to infrared sensing the vehicle mounted method investigated also provided contours based on ground penetrating radar. In the extreme contour regions of GPR mapping reasonable correlations with delamination were found. GPR is thought to be sensitive to the conditions leading to degradation (i.e. moisture and chlorides) and therefore this method can potentially be used to provide insight into future deck degradation which is an added benefit with the vehicle mounted scanning approach. Another advantage of GPR was the ability to assess concrete cover which is also useful for prediction of future degradation.

Future research: In most cases the rapid evaluation methods produced contour plots with little interpretation of results. Therefore, it was left up to the user to determine which types of contours

were of interest and for what purpose. Future research should focus on automated interpretation of contour plots (computer vision) for the different rapid evaluation methodologies.

The causes of degradation in South Carolina concrete bridge decks are not clear. Relatively low quality, permeable concrete was observed in cores removed from portions of the decks indicating a potential material selection issue. The most notable example of poor quality materials was US-21, Wilson Blvd over I-20. To better understand the causes of concrete bridge decks in South Carolina, future research should include in-depth studies of bridge decks for which the history of materials and construction methods are well understood. These studies should be conducted in parallel with visual observation of bridge deck construction methods and material sampling in combination with embedded sensor networks that are amenable to the detection of the conditions leading to degradation. One network of interest may include embedded acoustic emission sensors, as these types of sensors are very sensitive to the detection of early micro-cracking in reinforced concrete and related systems (Abdelrahman et al., 2018; Assi et al., 2018).

6.3 Implementation

Life cycle cost analysis indicates that most of the rapid evaluation methods investigated (e.g. vehicle mounted, deck acoustic response, and pole mounted) have similar cost when compared to chain dragging. Chain dragging is effective for the detection of delamination, however, it does not directly address moisture intrusion or the presence of chlorides in concrete bridge decks. Chain dragging requires traffic control, making it costly and potentially less safe than the more rapid methods of evaluation. Recommendations for implementation should consider the relative importance of safety, cost, and accuracy for the two cases described above – local evaluation and asset management.

Local evaluation: Among the rapid evaluation methods investigated, deck acoustic response appears to hold the most promise for detection of delaminated regions. This method should be implemented in a follow on study in combination with chain dragging for a subset of bridge decks in poor, medium and good condition to enable additional comparisons between the two methods. The number of bridge decks for this study will depend upon SCDOT resources and interest. A minimum number suggested is three decks of each condition (i.e. poor, medium, and good) resulting in a total of nine bridge decks. If the outcome of this follow on comparative study is positive, deck acoustic response may be considered by SCDOT as a replacement for chain dragging.

For cases where traffic control is difficult to obtain, the vehicle mounted method of evaluation may be considered over deck acoustic response. The pole mounted method may also be considered in instances where traffic control is not required for this method, such as bridge decks with large shoulders or pedestrian lanes.

Asset management: Vehicle mounted evaluation is the only rapid evaluation method investigated the did not require any form of traffic control. Due to this aspect, vehicle mounted evaluation should be implemented in a follow on study like the study described above for local evaluation (e.g. at least nine bridge decks should be included in the follow on study). If the outcome of the follow on study is positive, then vehicle mounted evaluation may be considered by SCDOT as a new method for the very rapid assessment and resulting management of the concrete bridge deck

inventory in South Carolina. Deck acoustic response and the pole mounted method were not as well suited to asset management, because these methods did not include information gained through GPR (in the configurations investigated), which appears to be an include information relating to the conditions causing future degradation, and the speed of evaluation is considerably less for these methods.

Rapid evaluation methods investigated are in relatively early stages of technical implementation. Therefore, it is expected that costs associated with all rapid evaluation methods will continue to decrease over time. These methods require specialized equipment and appear to be sensitive to user defined parameters (i.e. threshold settings) as well as proprietary algorithms for data interpretation. Therefore, in the near term it is recommended that service providers be retained by SCDOT to perform the evaluations and to deliver the results. The results are likely to require some level of interpretation on the part of the SCDOT and therefore it is recommended that the same individuals within SCDOT perform these interpretations until confidence is gained with the methods. In the future, it may be feasible and cost effective for SCDOT to lease or purchase rapid evaluation systems and to perform the evaluation in house. Training provided by the service providers would be useful to enable this transition.

REFERENCES

Abdelrahman, M., *Evaluation of Concrete Degradation using Acoustic Emission: Data Filtering and Damage Detection*. Doctoral dissertation, University of South Carolina, pp. 1-189, 2016.

Abdelrahman, M., ElBatanouny, M., Dixon, K., Serrato, M., and Ziehl, P., *Remote Monitoring and Evaluation of Damage at a Decommissioned Nuclear Facility Using Acoustic Emission*, Journal of Applied Sciences, 8(9), pp. 1-28 pp., 2018.

Andrade, C., and Alonso, C., *Test Methods for On-Site Corrosion Rate Measurement of Steel Reinforcement in Concrete by Means of the Polarization Resistance Method*. Materials and Structures, 37(9), pp. 623-643, 2004.

Arrow, K. J., Cropper, M. L., Eads, G. C., Hahn, R. W., Lave, L. B., Noll, R. G., and Stavins, R., *Benefit-Cost Analysis in Environmental, Health, and Safety Regulation*. Washington, DC: American Enterprise Institute, pp. 1-17, 1996.

Assi, L., Soltangharaei, V., Anay, R., Ziehl, P., and Matta, F., *Investigation of Portland Cement Paste Hydration using Acoustic Emission*, Journal of Cement and Concrete Research, Vol. 103, pp. 216-225., 2018.

ASTM C1383-15, *Standard Test Method for Measuring the P-Wave Speed and the Thickness of Concrete Plates Using the Impact-Echo Method*, Available: https://www.astm.org/Standards/C1383.htm. 2015.

ASTM C597-16, *Standard Test Method for Pulse Velocity Through Concrete*, Available: https://www.astm.org/Standards/C597.htm.

ASTM C642, *Standard Test Method for Density, Absorption, and Voids in Hardened Concrete*, Available: https://www.astm.org/DATABASE.CART/HISTORICAL/C642-06.htm. 2006.

ASTM C876-15, *Standard Test Method for Corrosion Potentials of Uncoated Reinforcing Steel in Concrete*, Available: https://www.astm.org/Standards/C876.htm, 2015.

ASTM D4580-12, *Standard Practice for Measuring Delaminations in Concrete Bridge Decks by Sounding*, West Conshohocken, PA, ASTM International, 2012.

ASTM D4788-03, *Standard Test Method for Detecting Delaminations in Bridge Decks Using Infrared Thermography*, Available: https://www.astm.org/Standards/D4788.htm. 2013.

ASTM D6087-08, *Standard Test Method for Evaluating Asphalt-Covered Concrete Bridge Decks Using Ground Penetrating Radar*, Available: https://www.astm.org/Standards/D6087.htm, 2015.

BDI and Infrasense Inc., *Feasibility Study: Nondestructive Evaluation of Bridge Decks*. Phase I Report, pp. 1-31, 2017.

BDI and Infrasense Inc., *Feasibility Study: Nondestructive Evaluation of Bridge Decks*. Phase II Report, pp. 1-14, 2018.

BDI and Infrasense Inc., *Nondestructive Evaluation of Two Bridge Deck Specimen*. Report, pp. 1-21, 2016.

Clevenger, C. M., Ozbek, M. E., and Simpson, S., *Review of Sustainability Rating Systems used for Infrastructure Projects,* 49th ASC Annual International Conference Proceedings, pp. 10–13, 2013.

Farrag, S., Yehia, S., and Qaddoumi, N., *Investigation of Mix Variation Effect on Defect Detection Ability using Infrared Thermography as a Nondestructive Evaluation Tech* Data Physics Corporation, *SignalCalc - Ace, Dynamic Signal Analyzers*, Available: http://www.dataphysics.com/products-and-solutions/dynamic-signal-analyzers-signalcalc/signalcalc-ace.html, [Accessed: 20-Oct-2017].

Farrag, S., Yehia, S., and Qaddoumi, N., *Investigation of Mix Variation Effect on Defect Detection Ability using Infrared Thermography as a Nondestructive Evaluation Technique*, Journal of Bridge Engineering, 21(3), pp. 04015055-1 to 04015055-15, 2015.

FHWA., *Life Cycle Cost Analysis 'RealCost' User Manual Real Cost*, Federal Highway Administration, 400 Seventh Street, Washington, DC 20590, V.2.1. Available: https://www.fhwa.dot.gov /infrastructure/asstmgmt/lccasoft.cfm, 2004.

Gassman, S., and Tawhed, W., *Nondestructive Assessment of Damage in Concrete Bridge Decks*, ASCE Journal of Performance of Constructed Facilities, 18(4), pp. 220-231, 2004.

Germann Instruments. Inc., *Pundit Manual*, pp. 105-108, Available: http://www.germann.org/TestSystems/PUNDIT/PUNDIT.pdf.

Graybeal, B., Rolander, D., Phares, B., Moore, M., and Washer, G., *Reliability and Accuracy of In-Depth Inspection of Highway Bridges*, Transportation Research Record: Journal of the Transportation Research Board, (1749), pp. 93-99, 2011.

Gucunski, N., Iman, A., Romero, F., *Nondestructive Testing to Identify Concrete Bridge Deck Deterioration*, Transportation Research Board, SHRP 2 REPORT S2-R06A-RR-1, 85 pp., 2013.

Gucunski, N., Romero, F. A., Shokouhi, P., and Makresias, J., *Complementary Impact Echo and Ground Penetrating Radar Evaluation of Bridge Decks on I-84 Interchange in Connecticut*, Earthquake Engineering and Soil Dynamics, pp. 1-10, 2005.

Hsiao, C., Cheng, C., Liou, T., and Juang, Y., *Detecting Flaws in Concrete Blocks using the Impact-Echo Method*, NDT & E International, 41(2), pp. 98-107, 2008.

Huang, Y. H., Adams, T. M., and Pincheira, J. A., *Analysis of Life-Cycle Maintenance Strategies for Concrete Bridge Decks*, ASCE Journal of Bridge Engineering, 9(3), pp. 250–258, 2004.

Huston, D., Gucunski, N., Maher, A., Cui, J., Burns, D., and Jalinoos, F., *Bridge Deck Condition Assessment with Electromagnetic*, Proceedings of the 6th International Workshop on Structural Health Monitoring (Acoustic and Automated Methods), 2007.

Infrasense, *GPR Bridge Deck Condition Evaluation*, Available: http://www.infrasense.com/gpr-bridge-deck, [Accessed: 03-Oct-2017].

Infrasense, Inc., *Bridge Deck Condition Survey Using Ground Penetrating Radar (GPR) on the I-295 Corridor*, Portland, Maine, Final Report, Available: https://www.maine.gov/mdot/contractors/projects/2011/017929.00-portland/dr017929.00.pdf

James Instruments, *C-CL-3000 Chlorimeter Operator's Manual*, pp. 1-2, 2018.

Jaquez, C., *Analysis of Accelerated Corrosion Experiment on Reinforced Concrete Slabs Using Half-Cell Potential Measurements*. Doctoral Dissertation, University of Massachusetts, Lowell, 223 pp., 2013.

Meola, C., and Carlomagno, G., *Recent Advances in the use of Infrared Thermography*, Measurement Science and Technology, 15(9), pp. R27-R58, 2004.

Montgomery S., *Development of a Chloride Concentration Sampling Protocol for Concrete Bridge Decks*, M.S. thesis, Department of Civil and Environmental Engineering, Brigham Young University, Provo, Utah, 2014.

Moore, M., Phares, B. M., Graybeal, B., Rolander, D., and Washer, G., *Reliability of Visual Inspection for Highway Bridges*, Volume I (No. FHWA-RD-01-020), 2001.

New York State Department of Transportation, NYDOT, *Bridge Deck Evaluation Manual*, 1992.

NRMCA, *Delamination of Troweled Concrete Surfaces*. Available: https://www.nrmca.org/aboutconcrete/cips/20p.pdf, pp. 1-2, 2004.

O'Reilly, M., Darwin, D., Browning, J., and Locke Jr, C. E., *Evaluation of Multiple Corrosion Protection Systems for Reinforced Concrete Bridge Decks*, University of Kansas Center for Research, Inc., 487 pp. 2011.

Parrillo, R., Roberts, R., and Haggan, A., *Bridge Deck Condition Assessment using Ground Penetrating Radar*, Proceedings of the ECNDT, Berlin, Germany, pp. 25-29, 2006.

Penetradar Corporation, *Ground Penetrating Radar used for Detecting Deterioration and Voids & Determining Pavement Layer Thickness and Moisture Content*. Available: www. Penetradar.com [Accessed: 03-Sep-2017].

Petro, J. T. Jr., and Kim, J., *Detection of Delamination in Concrete using Ultrasonic Pulse Velocity Test*, Construction and Building Materials, 26(1), pp. 574-582, 2012.

RILEM RECOMMENDATIONS, CPC-18, *Measurement of Hardened Concrete Carbonation Depth*, Materials and Structures, 21(6), pp. 453-455, 1988.

Robison, T. W., and Tanner, J. E., *Bridge Deck Evaluation using Non-Destructive Test Methods*, FHWA-WY-10/07F. Available: http://www.dot.state.wy.us/files/live/sites/wydot/files/shared/Planning/Research/RS04209_1007F.pdf, pp. 1-192, 2011.

Scott, M., Rezaizadeh, A., Delahaza, A., Santos, C. G., Moore, M., Graybeal, B., and Washer, G., *A Comparison of Nondestructive Evaluation Methods for Bridge Deck Assessment*, NDT and E, International, 36(4), pp. 245–255, 2003.

SDG 9 BDR Bridge Cost Estimating General. Available: http://www.fdot.gov/structures/StructuresManual/2007July/DesignGuidelines/SDG9.1General.htm. [Accessed: 15-May-2018].

Sketchley, A., *Condition Assessment of Reinforced Concrete Bridge Decks as Conductive Media using GPR*, M.S. Thesis, Dalhousie University, pp. 1-110, 2014.

Sneed, L. Anderson, N. and Torgashov E., *Nondestructive Evaluation of MoDOT Bridge Decks – Pilot Study*, Final Report prepared for the Missouri Department of Transportation, 178 pp., 2014.

Song, H., and Saraswathy, V., *Corrosion Monitoring of Reinforced Concrete Structures - A Review*, International Journal of Electrochemical Science, 2, pp. 1-28, 2007.

South Carolina Department of Transportation (SCDOT). For additional information see https://www.scdot.org/. [Accessed: 26-Jul-2018].

Sun, H., Zhu, J., & Ham, S., *Acoustic Evaluation of Concrete Delaminations using Ball-Chain Impact Excitation*, The Journal of the Acoustical Society of America, 141(5), pp. EL477-EL481, 2017.

Taylor B. R., Qiao, Y., Bowman, M. D., and S. Labi., *The Economic Impact of Implementing Nondestructive Testing of Reinforced Concrete Bridge Decks in Indiana*, Joint Transportation Research Program Publication No. FHWA/IN/JTRP-2016/20, West Lafayette, Indiana: Purdue University, 2016.

ThermalStare, LLC., *Infrared Measurements: IR-UTD Data Summary*, Report, pp. 1-60, 2017.

Vélez, W., Matta, F., and Ziehl, P., *Acoustic Emission Intensity Analysis of Corrosion in Prestressed Concrete Piles*. In AIP Conference Proceedings, Vol. 1581, No. 1, pp. 888-894. AIP. 2014.

Virginia Technologies, Inc., *Embedded Corrosion Instrument Model ECI-2 Product Manual*, pp. 1-16, 2013.

Washer, G., Trial, M., Jungnitsch, A., and Nelson, S., *Field Testing of Hand-Held Infrared Thermography*, Phase II TPF-5(247) Interim Report, pp. 1-94, 2015.

Yehia, S., Abudayyeh, O., Abdel-Qader, I., and Zalt, A., *Ground-Penetrating Radar, Chain Drag, and Ground Truth: Correlation of Bridge Deck Assessment Data*. Transp. Res. Rec. J. Transp. Res. Board, no. 2044, pp. 39–50, 2008.